

Electronic Thesis and Dissertation Repository

---

4-29-2015 12:00 AM

## MIR156 Participates in Iron Homeostasis Through Targeting SPL9/SPL15 in Arabidopsis Thaliana

Ying Wang, *The University of Western Ontario*

Supervisor: Abdelali Hannoufa, *The University of Western Ontario*

Joint Supervisor: Denis Maxwell, *The University of Western Ontario*

A thesis submitted in partial fulfillment of the requirements for the Master of Science degree in Biology

© Ying Wang 2015

Follow this and additional works at: <https://ir.lib.uwo.ca/etd>



Part of the [Molecular Genetics Commons](#)

---

### Recommended Citation

Wang, Ying, "MIR156 Participates in Iron Homeostasis Through Targeting SPL9/SPL15 in Arabidopsis Thaliana" (2015). *Electronic Thesis and Dissertation Repository*. 2838.

<https://ir.lib.uwo.ca/etd/2838>

This Dissertation/Thesis is brought to you for free and open access by Scholarship@Western. It has been accepted for inclusion in Electronic Thesis and Dissertation Repository by an authorized administrator of Scholarship@Western. For more information, please contact [wlsadmin@uwo.ca](mailto:wlsadmin@uwo.ca).

**MIR156 PARTICIPATES IN IRON HOMEOSTASIS THROUGH TARGETING  
*SPL9/SPL15* IN *ARABIDOPSIS THALIANA***

(Thesis format: Monograph)

by

Ying Wang

Graduate Program in Biology

A thesis submitted in partial fulfillment  
of the requirements for the degree of  
Masters of Science

The School of Graduate and Postdoctoral Studies  
The University of Western Ontario  
London, Ontario, Canada

© Ying Wang 2015

## Abstract

Plants growing under iron deficiency suffer from multiple physiological defects. Although the effects of microRNA156 (miR156) on multiple aspects of plant development have been investigated, a possible role of miR156 in plant iron homeostasis has not been shown. By employing next-generation RNA-sequencing, the current research demonstrated that multiple iron homeostasis-related genes, including ones coding for Ferritins, group Ib bHLH transcription factors, and key enzymes involved in iron uptake, were differentially expressed in *Arabidopsis thaliana* plants overexpressing miR156. Overexpression of miR156 also enhanced *Arabidopsis* growth under iron-deficiency. In addition, expression analysis revealed that miR156 is a positive regulator of *FIT* and *PYE* genes partially through targeting *SPL9* and *SPL15*. By using Chromatin Immuno-Precipitation qPCR assay, *SPL9* and *SPL15* were found to have strong binding capability to the promoters of *PYE* and *FIT*. Taken together, my data suggest that miR156 is a positive regulator of iron homeostasis through targeting *SPL9* and *SPL15* in *Arabidopsis*.

**Keywords:** miR156, SQUAMOSA PROMPTER BINDING-like protein (SPL), iron homeostasis.

## **Acknowledgements**

I would like to give my sincere thanks to Dr. Abdelali Hannoufa, my supervisor, who provided me this excellent research opportunity in his group. I really appreciate him for his invaluable guidance, insightful advice, and for most, his enormous patience from the beginning of my project to the thesis writing.

My deepest appreciation goes to my co-supervisor, Dr. Denis Maxwell, for his kind support on my project. I am grateful for his wise comments which helped me improve my presentation and writing. Also, my thanks go to my advisory committee members, Dr. Sangeeta Dhaubhadel and Dr. Susanne Kohalmi, for their support and kind help during my study.

Special thanks to our technician, Lisa Amyot, for her technical support and suggestions through my stay at Agriculture and Agri-Food Canada. Also, I appreciate help from my friends and lab members from Dr. Hannoufa's and Dr. Yuhai Cui's labs. All the informative discussions and arguments motivated me during my project. I also appreciate help from staff members at Western University and Agriculture and Agri-Food Canada.

Last but not the least, I wish to express my deepest gratitude to my family: my parents who have always believed in me and provided unconditional support; my wife who has given me encouragement and love throughout my personal and academic life; as well as the new comer, my son, who teaches me what responsibility is, and makes my life joyful.

# Table of Contents

<b>Abstract.....</b>	<b>ii</b>
<b>Acknowledgements .....</b>	<b>iii</b>
<b>Table of Contents .....</b>	<b>iv</b>
<b>List of Tables .....</b>	<b>viii</b>
<b>List of Figures.....</b>	<b>ix</b>
<b>List of Appendices.....</b>	<b>xi</b>
<b>List of Abbreviations .....</b>	<b>xii</b>
<b>Chapter I. Introduction .....</b>	<b>1</b>
1.1 The importance of iron for living organisms .....	2
1.2 Iron homeostasis in plants.....	3
1.3 Molecular regulation of iron homeostasis in Arabidopsis .....	5
1.4 Plant microRNAs .....	8
1.5 Characterization of miR156/SPL regulatory network in plants .....	10
1.6 SQUAMOSA PROMOTER BINDING-like proteins .....	14
1.7 Proposed research .....	15
<b>Chapter II. Materials and Methods .....</b>	<b>17</b>
2.1 Plant materials and growth conditions .....	17
2.2 Isolation and quality control of total RNA from Arabidopsis.....	18
2.3 Illumina next-generation RNA-sequencing .....	19
2.4 cDNA synthesis and qRT-PCR.....	20
2.5 Extract genomic DNA from Arabidopsis.....	20

2.6 Generation of <i>pSPL:SPL-GFP</i> fusion constructs by Gateway cloning .....	21
2.7 Preparing competent cells .....	23
2.8 Transformation of competent bacterial cells.....	24
2.9 Arabidopsis transformation.....	25
2.10 Determination of iron content in rosette leaves .....	25
2.11 Root acidification assay .....	25
2.12 Ferric (Fe <sup>3+</sup> ) iron reduction assay .....	26
2.13 Chromatin Immuno-Precipitation (ChIP)-qPCR assay.....	26
2.14 Gene Ontology (GO) Parametric Analysis of Gene Set Enrichment (PAGE) analysis .....	28
2.15 Confocal microscopy .....	29
2.16 Statistical analyses .....	29
<b>Chapter III. Results .....</b>	<b>30</b>
3.1 Overexpression of miR156 resulted in extensive changes in the global gene expression pattern .....	30
3.1.1 RNA sample preparation and quality control for Illumina sequencing .....	30
3.1.2 General results of NG-RNA-SEQ.....	30
3.1.3 Validation of NG-RNA-SEQ results by qRT-PCR.....	32
3.1.4 Transcriptomics of <i>35S:miR156</i> plants .....	32
3.1.5 Differential repression of <i>SPL</i> genes by miR156 in leaves and roots.....	39
3.2 Iron homeostasis related genes are affected by overexpression of miR156 .....	42
3.3 MiR156 participates in iron homeostasis in Arabidopsis .....	42
3.3.1 Iron content of rosette leaves is not affected by overexpression of miR156 .....	44
3.3.2 Improved growth of <i>35S:miR156</i> plants under iron-deficiency condition.....	44
3.3.3 MiR156 has no effect on rhizosphere acidification .....	47

3.3.4 MiR156 affects iron reduction partially through targeting <i>SPL9</i> and <i>SPL15</i> .....	47
3.4 MiR156 regulates iron homeostasis-related genes through <i>SPL9</i> and <i>SPL15</i> .....	49
3.4.1 <i>FIT</i> and <i>PYE</i> were transiently up-regulated in the roots of <i>spl9/spl15</i> and <i>35S:miR156</i> plants under iron deficiency compared with WT plants .....	49
3.4.2 MiR156 has different effects on the expression patterns of <i>bHLH38</i> , <i>bHLH39</i> , <i>bHLH100</i> , and <i>bHLH101</i> under short term iron deficiency .....	52
3.4.3 MiR156 transiently upregulates iron uptake genes .....	54
3.5 <i>SPL9</i> and <i>SPL15</i> bind to the promoters of <i>FIT</i> and <i>PYE</i> genes .....	54
<b>Chapter IV. Discussion .....</b>	<b>60</b>
4.1 Research overview .....	60
4.2 Overexpression of miR156 impacts global gene expression .....	60
4.3 Overexpression of miR156 affects multiple iron homeostasis genes .....	62
4.4 MiR156 affects plant growth under iron deficiency but not iron contents .....	63
4.5 Overexpression of miR156 affects ferric reduction but not rhizosphere acidification .....	64
4.6 MiR156 up-regulates iron homeostasis genes under iron deficiency .....	65
4.7 Cross talk between phytohormone, miR156, and iron homeostasis .....	68
<b>Chapter V. Conclusions .....</b>	<b>72</b>
<b>References .....</b>	<b>74</b>
<b>Appendices .....</b>	<b>91</b>
Appendix A. Recipe for ½ MS medium. ....	91
Appendix B. Primers used in this study .....	92
Appendix C. Recipe for Lysogeny broth (LB) medium .....	100
Appendix D. Recipe for buffers used in ChIP assay .....	101

Appendix E. List of differentially expressed genes derived from NG-RNA-SEQ .....	102
Appendix F. The location of putative SPL binding sites in FIT promoter and the primers used in ChIP-qPCR assay.....	107
Appendix G. The location of putative SPL binding sites in PYE promoter and the primers used in ChIP-qPCR assay.....	108
<b>Curriculum Vitae .....</b>	<b>109</b>

## List of Tables

<b>Table 1.</b> Genes were detected in both roots and rosette leaves that have more than 2-fold changes on expression level.....	36
<b>Table 2.</b> Expression pattern of <i>SPL</i> genes in rosette leaves .....	40
<b>Table 3.</b> Expression pattern of <i>SPL</i> genes in roots.....	41

## List of Figures

<b>Figure 1.</b> Iron uptake mechanism in Arabidopsis. ....	4
<b>Figure 2.</b> A model depicting the molecular mechanism of the iron homeostasis regulatory pathway in <i>Arabidopsis thaliana</i> . ....	7
<b>Figure 3.</b> An overview of miRNA biogenesis in plants. ....	9
<b>Figure 4.</b> The miR156-SPL regulatory network in <i>Arabidopsis thaliana</i> . ....	12
<b>Figure 5.</b> A simplified Gateway cloning procedure for generating <i>pSPL:SPL-GFP</i> fusion constructs. ....	22
<b>Figure 6.</b> Examination of RNA quality using Bioanalyzer. ....	31
<b>Figure 7.</b> Venn diagram of differentially expressed genes derived from NG-RNA-SEQ. ....	33
<b>Figure 8.</b> qRT-PCR using 40 randomly selected differentially expressed genes. ....	34
<b>Figure 9.</b> Parametric Analysis of Gene Set Enrichment (PAGE) analysis of differentially expressed genes in rosette leaf (A) and root (B). ....	35
<b>Figure 10.</b> Multiple iron homeostasis-related genes were affected by overexpression of miR156. ....	43
<b>Figure 11.</b> Measurement of iron content in Arabidopsis rosette leaves. ....	45
<b>Figure 12.</b> Growth of WT, <i>spl9/spl15</i> and <i>35S:miR156</i> plants under iron deficiency. ..	46
<b>Figure 13.</b> Acidification of rhizosphere in WT, <i>spl9/spl15</i> , and <i>35S:miR156</i> plants under normal Fe condition (A) and iron-deficiency condition (B). ....	48
<b>Figure 14.</b> Ferric reduction in WT, <i>spl9/spl15</i> , and <i>35S:miR156</i> roots. ....	50
<b>Figure 15.</b> Effect of iron deficiency on expression of <i>PYE</i> and <i>FIT</i> in roots of WT, <i>spl9/spl15</i> , and <i>35S:miR156</i> plants. ....	51

**Figure 16.** Expression patterns of group I bHLH transcription factors after 48h and 96h under iron deficiency. .... 53

**Figure 17.** Expression patterns of iron uptake genes under iron deficiency condition.... 55

**Figure 18.** Localization of SPL9-GFP (upper panels) and SPL15-GFP (lower panels).. 56

**Figure 19.** Detection of SPL9 and SPL15 binding to *FIT* promoter by ChIP-qPCR. (A)57

**Figure 20.** Detection of SPL9 and SPL15 binding to *PYE* promoter by ChIP-qPCR. (A) ..... 58

**Figure 21.** A proposed model for the regulatory pathway involving miR156/SPL, pH, and iron availability. .... 71

## List of Appendices

- Appendix A.** Recipe for ½ MS medium.....**Error! Bookmark not defined.**
- Appendix B.** Primers used in this study .....**Error! Bookmark not defined.**
- Appendix C.** Recipe for Lysogeny broth (LB) medium**Error! Bookmark not defined.**
- Appendix D.** Recipe for buffers used in ChIP assay .....**Error! Bookmark not defined.**
- Appendix E.** List of differentially expressed genes derived from NG-RNA-SEQ**Error!**  
**Bookmark not defined.**
- Appendix F.** The location of putative SPL binding sites in FIT promoter and the  
primers used in ChIP-qPCR assay. ....**Error! Bookmark not defined.**
- Appendix G.** The location of putative SPL binding sites in PYE promoter and the  
primers used in ChIP-qPCR assay. ....**Error! Bookmark not defined.**

## List of Abbreviations

AHA	H <sup>+</sup> ATPase
ANOVA	Analysis of Variance
ATP	Adenosine triphosphate
bHLH	basic Helix-loop-helix protein
CBC	Nuclear Cap-Binding Complex
Cg1	Corngrass1
ChIP	Chromatin Immuno-Precipitation assay
Col-0	Arabidopsis ecotype Columbia-0
CSD	Cu/Zn Superoxide Dismutase
CTAB	Cetyltrimethyl Ammonium Bromide
DAPI	4',6-diamidino-2-phenylindole
DCL1	Dicer-like 1
ddH <sub>2</sub> O	Double distilled H <sub>2</sub> O
Fe	Iron
Fe·EDTA	Ethylenediaminetetraacetic acid iron sodium salt
Fe <sup>2+</sup>	Ferrous iron
Fe <sup>3+</sup>	Ferric iron
FIT	FER-LIKE IRON DEFICIENCY INDUCED TRANSCRIPTION FACTOR
FRO	Ferric Reductase Oxidase/ Ferric Chelate Reductase
FT	Flowering Locus T
<i>g</i>	G Force
GFP	Green Fluorescent Protein
GO	Gene Ontology

h	Hour
H <sup>+</sup>	Proton
HEN1	Hua Enhancer 1
HYL1	Hyponasty Leaves 1
IRT1	Iron-Regulator Transporter 1
kb	Kilobase
LB medium	Lysogeny broth medium
M	Molar
Mb	Mega-basepairs
MES	2-N-Morpholino Ethanesulfonic Acid hydrate
mg	Milligram
Min	Minute
MiR	microRNA
ml	Milliliter
MS medium	Murashige and Skoog medium
<i>nd</i>	Not Detected
ng	Nanogram
NG-RNA-SEQ	Next-generation RNA-Sequencing
nm	Nanometer
O <sub>2</sub>	Oxygen
°C	Degree Celsius
OD	Optical Density
P-adj	Adjusted P Value
PAGE	Parametric Analysis of Gene Set Enrichment
PCR	Polymerase Chain Reaction

pH	Potential Hydrogen
pre-miRNA	Precursor of miRNA
pri-miRNA	Primary-miRNA
PYE	POPEYE/ bHLH Transcription factor
qPCR	Quantitative PCR
RIN	RNA Integrity Number
RISC	RNA-Induced Silencing Complex
RNA POL II	RNA Polymerase II
rRNA	Ribosomal RNA
SE	Serrate
sec	Second
SPL	Squamosa Promoter Binding-like protein
TE buffer	Tris-EDTA buffer
tRNA	Transfer RNA
w/v	Weight/Volume
WT	Wild-type plant
μl	Microliter
μM	Micromole
<i>35S:miR156</i>	Overexpression of miR156 transgenic Arabidopsis plants

## Chapter I. Introduction

Due to their sessile nature, plants have evolved sophisticated mechanisms to cope with adverse conditions, including nutrient deficiency. To maintain normal growth and development, plants acquire metallic and non-metallic nutrients, such as zinc, copper, and iron, from the soil. Iron (Fe) was first discovered as an essential plant nutrient as early as 1843 by E. Gris (Reviewed by Fernández and Ebert in 2005). He showed that Fe was critical for plants to recover from the absence of green pigments in foliage by external application of a Fe solution to the rhizosphere or leaves (Fernández and Ebert 2005). Fe is also an essential nutrient for animals (including humans), which acquire a significant portion of their dietary Fe from plant sources either directly or indirectly (Cakmak 2002; Welch and Graham 2004). Given the importance of Fe to living organisms, a significant amount of effort has been invested in understanding the molecular mechanisms that govern iron homeostasis in plants to develop higher quality crops (Colangelo and Guerinot 2004; Fehr 1982; Lin *et al.* 1997; Sun 1986). Research on different species has provided a good understanding of the physiological and molecular mechanisms that control Fe absorption, transportation, and storage (Briat and Lobréaux 1997; Curie *et al.* 2001; Hell and Stephan 2003; Stocking 1975). All of this valuable information gave me a theoretical basis for conducting this project. In this dissertation, *Arabidopsis* was employed to examine the effect of overexpression of miR156 on plant growth under iron deficiency, as well as plant iron acquisition at the physiological and molecular levels.

## 1.1 The importance of iron for living organisms

Although Fe has been identified as the fourth most accumulated element on Earth, almost 30% of the land is still considered to be Fe-deficient (Grotz and Guerinot 2006). Fe has different oxidation states, from -2 to +6, with most of Fe existing as ferrous ( $\text{Fe}^{2+}$ ) and ferric ( $\text{Fe}^{3+}$ ) irons. Due to its ability to be easily involved in redox reaction and form chelate complexes, Fe is a vital element for living organisms (Desforges and Oski 1993; Iannotti *et al.* 2006; Korcak 1987; Mori *et al.* 1991).

In humans, hemoglobin and myoglobin require Fe as an essential component for  $\text{O}_2$  transportation (Saarinen and Siimes 1979), in which Fe serves as a loading dock to bind with  $\text{O}_2$ . Iron deficiency in the human body causes anemia, which can result in severe symptoms, such as heart failure (Gil and Ferreira 2014; Gunawardena and Dunlap 2012). The anemia caused by iron deficiency affects approximately one billion people worldwide (Vos *et al.* 2013). Furthermore, about 6% of the body's iron is utilized in forming vital enzymes. For instance, cytochromes that are responsible for ATP generation via electron transport chain require Fe for their function (Kranz *et al.* 2009).

In plants, Fe is also a vital element for maintaining normal growth. Fe serves as co-factor in many photosynthesis-associated enzymes, such as hydrogenase and chloroplast-ferredoxin (Briat *et al.* 2007; Fukuyama 2004; Tagawa and Arnon 1962). Also, iron is a component of glutamyl-tRNA reductase, which participates in chlorophyll biosynthesis in plants (Kumar and Söll 2000). As such, restricted iron acquisition in plants leads to chlorosis with limited chlorophyll biosynthesis and can lead to plant death (Mengel 1994). On the other hand, both humans and livestock rely on plant foods as a source of iron, making the study of plants' iron acquisition significant.

## 1.2 Iron homeostasis in plants

Reduced availability of Fe impacts plant metabolism and restricts chlorophyll biosynthesis, leading to iron chlorosis (Brown 1961; Naeve 2006). However, excessive levels of Fe are not desirable for plants either (Thomine and Vert 2013). Excessive Fe could lead to the accumulation of reactive oxygen species (ROS) and can further damage the cell structure (Ravet and Pilon 2013). Hence, maintaining the right balance (homeostasis) of Fe in plants is crucial for normal growth and development.

Plants have evolved two distinct strategies (I and II) to acquire iron from the environment (Hell and Stephan 2003; Kobayashi and Nishizawa 2012). While the graminaceous plants (the family Poaceae) use strategy II, other plants, dicotyledonous and non-graminaceous monocotyledonous plants, employ strategy I to acquire Fe (Schmidt 2003; Thomine and Lanquar 2011). The difference between these two strategies is that plants employing the strategy II mechanism release phytosiderophore, which is a Fe chelator, into soil to chelate  $\text{Fe}^{3+}$  ions and form a soluble complex that can be further transported by plant roots. On the other hand, plants that utilize strategy I, such as *Arabidopsis thaliana*, can only uptake free  $\text{Fe}^{2+}$  from soil. Furthermore, the existence of most Fe as  $\text{Fe}^{3+}$  makes Fe absorption from the rhizosphere problematic, because  $\text{Fe}^{3+}$ , unlike  $\text{Fe}^{2+}$ , has an extremely low solubility at neutral and basic pH (Schwertmann 1991). Plants utilize strategy I for iron uptake from the rhizosphere through three steps (Figure 1): first, proton-pumps localized on plasma membrane release  $\text{H}^+$  into soil to acidify the surrounding rhizosphere causing lower pH. Lower pH increases the solubility of  $\text{Fe}^{3+}$ . Then ferric chelate reductase is released to further reduce  $\text{Fe}^{3+}$  to  $\text{Fe}^{2+}$ . The final step in iron absorption is performed by a plasma membrane transporter, IRT1, which moves  $\text{Fe}^{2+}$

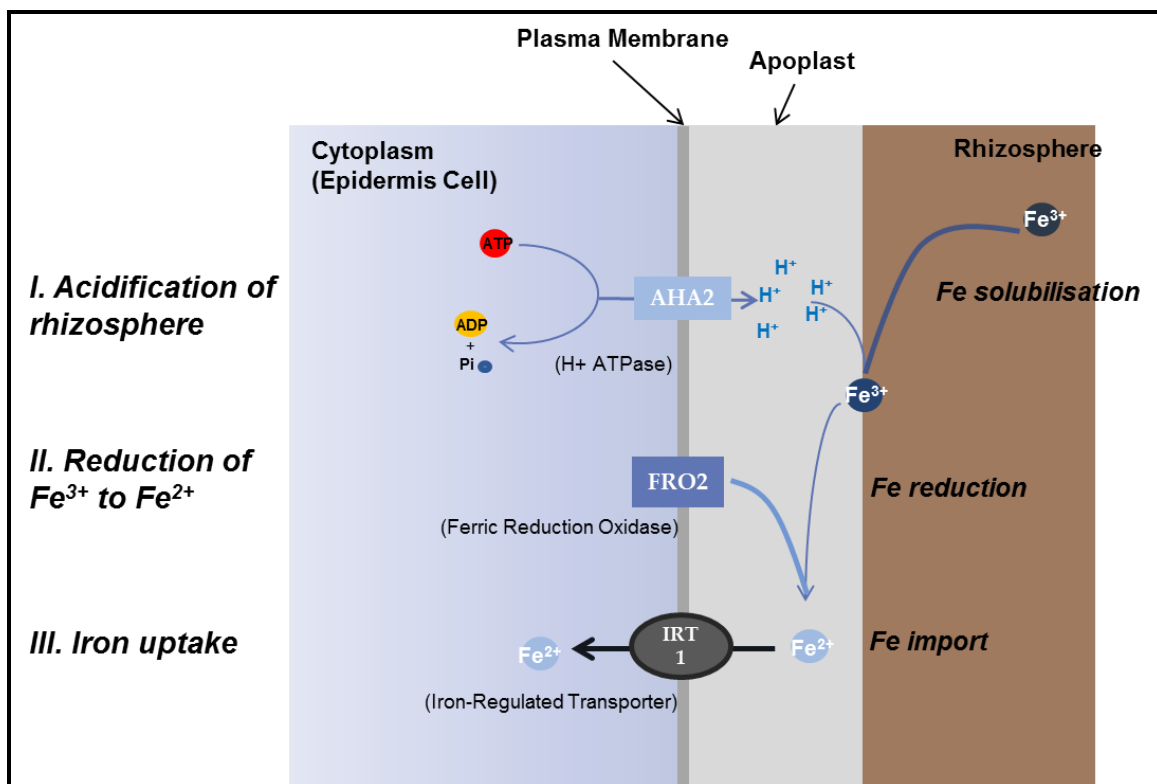


**Figure 1. Iron uptake mechanism in Arabidopsis.** Figure is modified from (Brumbarova *et al.* 2015). Arabidopsis employs Strategy I to uptake iron from soils. There are three major steps in this process: first, acidification of rhizosphere by AHA2 protein to make more Fe<sup>3+</sup> soluble; second, reduction of Fe<sup>3+</sup> to Fe<sup>2+</sup> by FRO2; at last, Fe<sup>2+</sup> transport to the cytoplasm by IRT1 (Detailed description in Section 1.2 for individual components shown here).

from the rhizosphere into the cell through positive transportation (Schmidt 2003).

In Arabidopsis, the H<sup>+</sup> ATPase (AHA) family acts as a proton pump to acidify the rhizosphere (Palmgren 2001; Santi and Schmidt 2009). The acidification induced by iron deficiency is mostly performed by AHA2 (Santi and Schmidt 2009). The Ferric Reductase Oxidase/ Ferric Chelate Reductase (FRO) family of enzymes serve in the reduction of Fe<sup>3+</sup> to Fe<sup>2+</sup> in Arabidopsis. Reduction of Fe<sup>3+</sup> by FRO was considered to be the rate limiting step in iron uptake (Connolly *et al.* 2003). There are eight putative *FRO* genes (*FRO1* to *FRO8*) in Arabidopsis. Among them, the transcript levels of *FRO2* and *FRO3* were significantly increased in roots under iron-deficiency compared to other *FRO* genes (Mukherjee *et al.* 2006). Of the several FRO proteins that have been reported to act as ferric chelate reductase, FRO2 utilizes the majority of the reduced iron during iron uptake. Overexpression of *FRO2* in Arabidopsis resulted in improved growth under iron-deficiency conditions (Robinson *et al.* 1999). The last step in iron uptake is performed by Iron Regulated Transporter 1 (IRT1), which transports Fe<sup>2+</sup> into the cytoplasm (Vert *et al.* 2002). Loss-of-function *irt1* mutant shows chlorosis and lethality (Vert *et al.* 2002). Interestingly, IRT1 not only transports Fe into plants, but also transports other nutrient elements, such as zinc, copper, cobalt, and cadmium (Halimaa *et al.* 2014). Thus plants growing under iron deficiency tend to have more of the other metallic elements.

### **1. 3 Molecular regulation of iron homeostasis in Arabidopsis**

Available evidence points to both transcriptional (Bauer *et al.* 2007, Long *et al.* 2010, Sivitz *et al.* 2012, Wang *et al.* 2007) and post-transcriptional regulation (Barberon *et al.*

2011; Kerkeb *et al.* 2008) for maintaining Fe homeostasis in plants. Current findings support the view that the iron homeostasis regulation pathway is centrally managed by FER-LIKE IRON DEFICIENCY INDUCED TRANSCRIPTION FACTOR (FIT, previously known as FRU/bHLH29), which belongs to the Basic Helix-Loop-Helix (bHLH) transcription factor family (Bauer *et al.* 2007). FIT is essential for the induction of many Strategy I-related genes (Figure 2A), such as *AHA2*, *FRO2*, and *IRT1* (Colangelo and Guerinot 2004; Jakoby *et al.* 2004). Furthermore, multiple Ib group bHLH family proteins, bHLH38, bHLH39, bHLH100, and bHLH101, were shown to form heterodimers with FIT to regulate the transcription of *IRT1*, *AHA2*, and *FRO2* (Wang *et al.* 2013; Yuan *et al.* 2008). The loss-of-function *fit1* mutant exhibits severe chlorosis which is lethal, but this lethality can be attenuated by the addition of supplementary iron.

Besides the FIT network, another bHLH transcription factor POPEYE (PYE) has been shown to participate independently from FIT pathway in iron homeostasis in *Arabidopsis* (Long *et al.* 2010) (Figure 2B). A transcriptome study revealed multiple genes related to iron storage (ferritin coding genes) and oxidative stress were highly expressed in *pye-1* mutants under both iron-sufficient and -deficient conditions. Both *bHLH39* and *bHLH101* genes were up-regulated under both normal and iron-deficiency conditions in *pye-1* mutant compared to WT plants. On the other hand, the *IRT1* gene was down-regulated under iron- deficiency in the *pye-1* mutant. Surprisingly, the *pye1* mutant has a higher iron content than WT plants under both normal and iron deficient conditions (Long *et al.* 2010). These authors also indicated that the potential role of PYE in iron homeostasis is highly related to iron relocation after iron uptake from the rhizosphere.

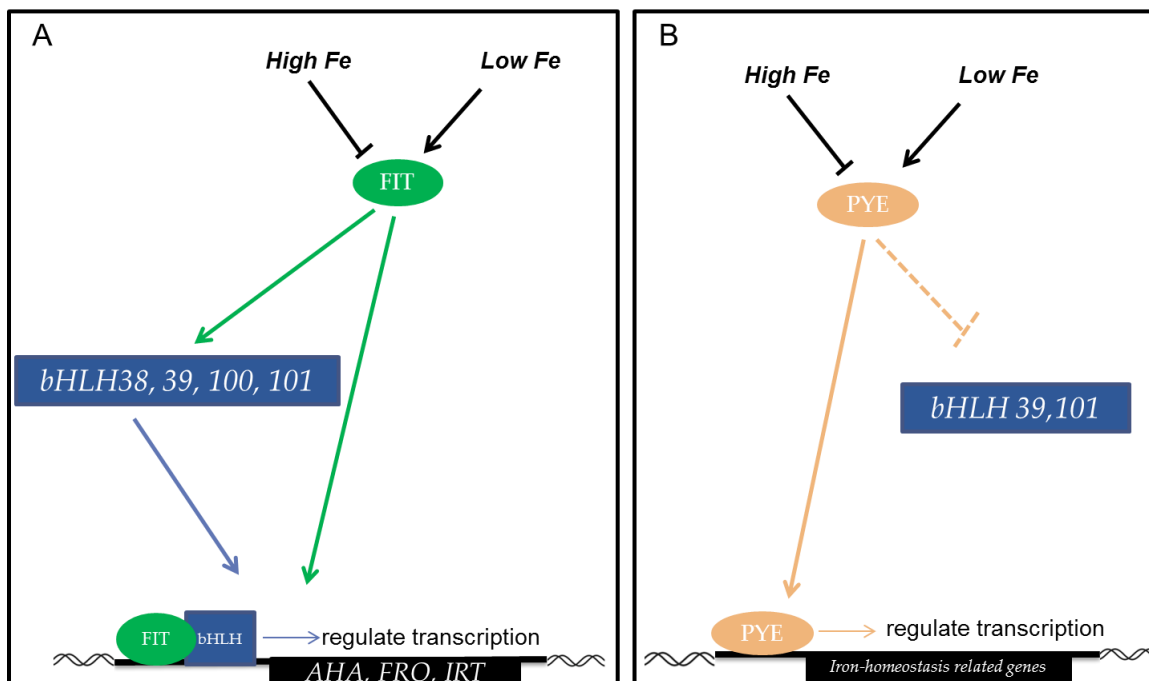


**Figure 2. A model depicting the molecular mechanism of the iron homeostasis regulatory pathway in *Arabidopsis thaliana*.** There are two reported regulatory pathways that control iron homeostasis-related genes, FIT- (A) and PYE-dependent (B) pathways. Both FIT and PYE can be triggered under low-iron conditions, and repressed under high-iron conditions. (A) FIT can activate the transcription of group Ib bHLH transcription factors and then form heterodimer with them to regulate down-stream iron acquisition genes, such as *AHA*, *FRO*, and *IRT*. (B) PYE regulates another set of iron homeostasis-related genes; such as genes that participate in iron re-localization in plants.

#### 1.4 Plant microRNAs

MicroRNAs (miRNA) are a class of newly discovered single-stranded non-coding small RNA molecules. They are usually 21 nt in length (Voinnet 2009). The biogenesis of miRNAs (Figure 3) has been well illustrated in plants, where it starts with the transcription of single-stranded RNA (primary-miRNA, pri-miRNA) that are transcribed by RNA polymerase II. The RNA molecule subsequently forms an imperfectly matched hairpin-structure precursor (precursor of miRNA, pre-miRNA). The precursors are further processed by Dicer-like 1 (DCL1) proteins in conjunction with Nuclear cap-binding complex (CBC), Serrate (SE), Hyponasty Leaves 1 (HYL1), and Hua Enhancer 1 (HEN1), into miRNA/miRNA\* duplex. This duplex is then transported into the cytoplasm. In the cytoplasm, miRNA is released and incorporated into a RNA-induced silencing complex (RISC), which negatively regulates target genes at the post-transcriptional level by base-pairing to complementary targets (Dugas and Bartel 2004; Kidner and Martienssen 2005). MiRNAs perform their functions at the transcriptional and post-transcriptional levels. At the post-transcriptional level, they can either induce cleavage of target mRNAs by complementarily binding to target sites, or inhibit protein translation by physically blocking translation. At the transcriptional level, they affect the expression of target genes through miRNA-mediated DNA methylation (Hu *et al.* 2014; Wu *et al.* 2010). Based on a recent miRbase release (<http://www.mirbase.org/>, Release 21, June 2014), 325 miRNA families were registered for *A. thaliana*, of which 187 were experimentally examined.

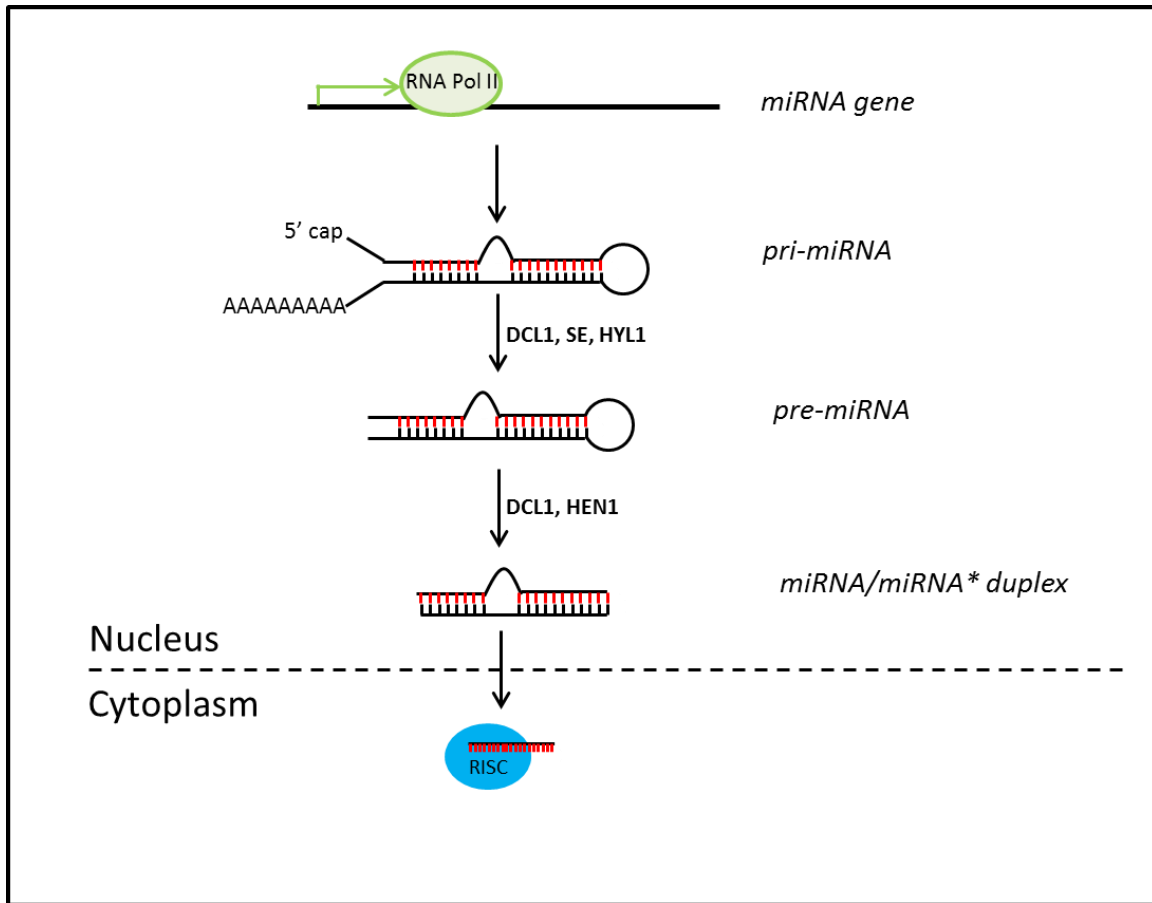


**Figure 3. An overview of miRNA biogenesis in plants.** Pathway was modified from (Zhu 2008). Key enzymes in the biogenesis process are labelled beside respective arrows. The biogenesis of miRNAs starts with the transcription of *pri-miRNA*. The *pri-miRNA* subsequently forms an imperfectly matched precursor *pre-miRNA*. The precursors are further processed by DCL1 in conjunction with CBC, SE, HYL1, and HEN1, into *miRNA/miRNA\** duplex. This duplex is then transported into the cytoplasm. In the cytoplasm, mature miRNA is released and incorporated into RISC, which negatively regulates target genes at the post-transcriptional level by base-pairing to complementary targets.

Temporal and spatial accumulations of a few highly conserved miRNAs are crucial for maintaining proper plant development. For example, *miRNA165* and *miR166* are involved in the determination of leaf patterns (Liu *et al.* 2009), *miR156* and *miR157* govern the transition from vegetative to reproductive phase (Wu *et al.* 2009), and *miR172* participates in controlling floral development (Wollmann *et al.* 2010). Meanwhile, some miRNAs participate in plant nutrient acquisition. MiR398 was first reported to be related to stress tolerance in Arabidopsis. Cu/Zn superoxide dismutase (CSD) coding genes were identified as direct targets of miR398. Reduced levels of miR398 can increase plant tolerance to oxidative stress by directly up-regulating *CSD1* and *CSD2* genes (Sunkar *et al.* 2006). MiR395 and miR399 participate in sulphate and phosphorus homeostasis in Arabidopsis, respectively (Chiou 2007). Furthermore, a number of transcriptome studies indicate that the expression levels of many miRNAs are induced by nutrient deprivation (Pant *et al.* 2009; Sunkar *et al.* 2007).

### **1.5 Characterization of miR156/SPL regulatory network in plants**

MiR156 is one of the most studied miRNAs and is highly abundant in many plant species with a strong sequence conservation (Cho *et al.* 2012; Hultquist and Dorweiler 2008; Wang *et al.* 2009; Wu *et al.* 2009; Wu and Poethig 2006). In Arabidopsis, there are 10 miR156 precursors (*pre-mir156a* to *pre-mir156j*). The first eight precursors (*pre-miR156a* to *pre-miR156h*) were identified experimentally (Reinhart *et al.* 2002; Xie *et al.* 2005), whereas *pre-miR156i* and *pre-miR156j* were only predicted by computational analysis. Although the members of miR156 precursors do not share significant sequence

similarity, the mature miR156 sequences derived from each of these precursors are nearly identical (Schmidt and Bancroft 2011).

In Arabidopsis, miR156 functions by targeting genes encoding members of a plant-specific transcription factor, SQUAMOSA PROMOTER BINDING PROTEIN-LIKE (SPL) proteins. MiR156 represses *SPL* by complementary binding to *SPL* mRNAs leading to transcript degradation (Figure 4A). MiR156 was first reported as a regulator in plant developmental phase transition. In the juvenile stage, plants keep a high level of miR156 expression (Wu *et al.* 2009). MiR156 can further repress the expression of *miR172* through targeting *SPL9* and *SPL10*, which can activate transcription of *pri-miR172* (Wu *et al.* 2009). Once the plant matures, the transcript level of miR156 gradually decreases and that of miR172 increases (May *et al.* 2013). Overexpression of miR156 in Arabidopsis causes a prolonged juvenile phase manifested by a slight delay in flowering and a drastic increase in number of rosette leaves (Wang *et al.* 2009; Wu and Poethig 2006). Another trait related to plant phase transition, the distribution of trichomes, is also regulated through the miR156/SPL network (Figure 4B). *In vitro* analysis showed that SPL9 protein can directly bind to the promoters of TRICHOMELESS1 and TRIPTYCHON, which are negative regulators of trichome formation, to activate their transcription (Yu *et al.* 2010).

In addition to its role in regulating plant development, miR156 has also been shown to influence secondary metabolism in Arabidopsis (Gou *et al.* 2011; Wei *et al.* 2012; Yu *et al.* 2014). The miR156-regulated SPL9 down-regulates anthocyanin biosynthesis by binding to bHLH proteins to physically block the formation of the MYB-

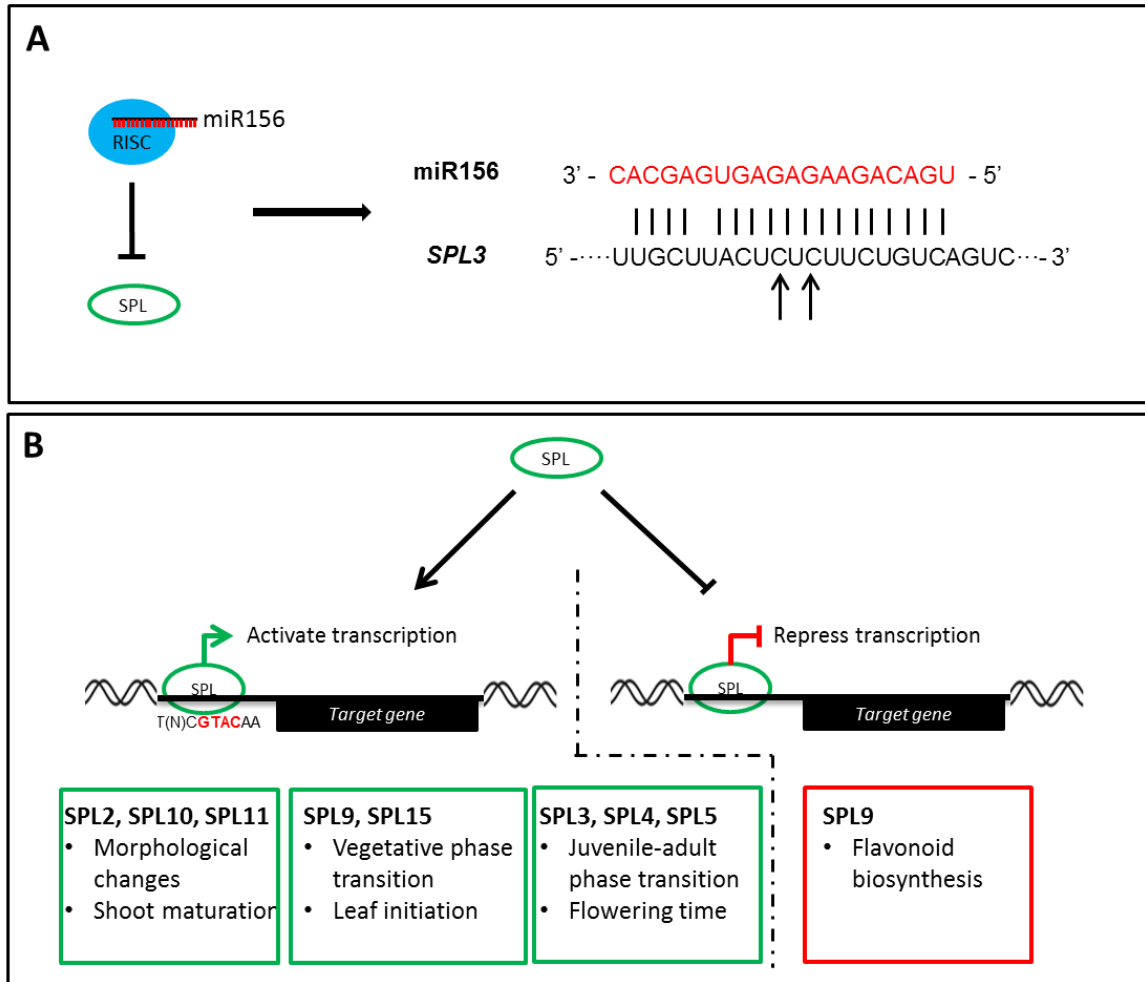


**Figure 4 The miR156-SPL regulatory network in *Arabidopsis thaliana*.** (A) An example of how miR156 represses *SPL* genes is shown. MiR156 can bind complementarily to its target mRNAs and result in cleavage of mRNA molecules. The arrows under *SPL3* show the cleavage sites of miR156. (B) The SPLs can bind to genomic fragments containing a consensus T(N)CGTACAA sequence (with the core sequence being GTAC) located in target gene's promoter region to activate its transcription. SPLs can also negatively regulate gene expression by physically blocking other transcription factor from binding to target gene's promoter.

bHLH-WD40 complex that is required for activating transcription of anthocyanin biosynthetic genes (Gou et al. 2011). Furthermore, overexpression of miR156 enhances the carotenoid content in *Arabidopsis* and *Brassica napus* seeds (Wei et al. 2010, Wei et al. 2012).

The function of miR156 has also been investigated in other plant species, such as *Zea mays* (Chuck et al. 2007), *Medicago sativa* (Aung et al. 2014), *Panicum virgatum* (Fu et al. 2012), and *Lotus japonicus* (Wang et al. 2014). The maize *Corngrass1* (*Cg1*) mutant was first identified as a mutant with a more extended juvenile stage than WT. Further study indicated the phenotype of *Cg1* was caused by overexpression of two tandem *miR156* genes (Chuck et al. 2007). Overexpression of miR156 in multiple plant species, such as *P. virgatum*, *M. sativa* and *L. japonicus*, caused drastically changed phenotypes, such as reduced plant height, enhanced branching, smaller organ size, and slightly delayed flowering time. Furthermore, a correlation between the severity of phenotype and the expression level of miR156 was demonstrated. Higher transcript levels of *miR156* yield more severe phenotypes compared to transgenic plants that exhibit moderate or lower transcript levels of miR156 in *P. virgatum* (Fu et al. 2012) and in *M. sativa* (Aung et al. 2014). Additionally, the role of miR156 in regulating symbiosis between legume and rhizobium was examined. In *G. max*, miR156 and miR172 showed reciprocal roles in symbiosis, with miR156 negatively regulating nodulation (Yan et al. 2013). In *L. japonicus*, ectopic expression of *miR156* represses nodulation and affects the transcription pattern of multiple nodulation-related genes, such as *Early Nodulin*, which is critical in the early stages of symbiosis (Wang et al. 2014).

## 1.6 SQUAMOSA PROMOTER BINDING-like proteins

In total, the Arabidopsis genome contains 16 *SQUAMOSA PROMOTER BINDING-like* (*SPL*) members. At least 10 of these (*SPL2*, 3, 4, 5, 6, 9, 10, 11, 13, and 15) are regulated by miR156. These miR156-targeted *SPL* genes can be divided into four groups based on phylogenetic tree analysis: *SPL3/SPL4/SPL5*, *SPL2/SPL10/SPL11*, *SPL9/SPL15*, and *SPL6/SPL13* (Guo *et al.* 2008). *SPL* proteins play various roles in the plant life cycle (Figure 4). For instance, *SPL3*, *SPL4*, and *SPL5* play a redundant role in controlling plant phase transition from juvenile to adult (Wu and Poethig 2006). Moreover, *SPL3* partially participates in control of flowering through transcriptional regulation of *FLOWERING LOCUS T (FT)* under various ambient temperatures in Arabidopsis (Hwan Lee *et al.* 2012; Kim *et al.* 2012). *SPL13* regulates the phase transition from cotyledons to the appearance of true leaves (Martin *et al.* 2010). *SPL9* and *SPL15* control shoot structure, as *spl9/spl15* double T-DNA knock-out mutant exhibited shortened plastochron during vegetative phase (Schwarz *et al.* 2008).

Interestingly, a feed-back regulatory mechanism has also been discovered between *SPL* and miR156. The transcript level of *miR156a* precursor was elevated in transgenic plants harboring miR156-insensitive *SPL9* and *SPL10* (the binding sites within *SPL9* and *SPL10* were modified to prevent miR156 from recognizing them) driven by their native promoters (Wu *et al.* 2009). Furthermore, a feed-back regulatory pathway was also observed between miR156 and *SPL15*. The transcript level of *miR156b* was significantly reduced when *SK156*, a *miR156* gain-of-function mutant, was complemented with expression of a miR156-insensitive *SPL15* gene. Also, the binding

capability of SPL15 to the promoter of *miR156b* was demonstrated *in vitro* (Wei *et al.* 2012).

Additionally, non-miR156 targeted *SPL* genes also play versatile roles in plant growth. A non-miR156 target *SPL* gene, *SPL7*, was shown to be essential for copper homeostasis in Arabidopsis through regulation of miR398, in which *SPL7* binds directly to the miR398 promoter *in vitro* and activates its expression. The *spl7* mutant showed strong retardation when grown under copper deficiency condition (Yamasaki *et al.* 2009). *SPL8*, another gene not targeted by miR156, together with three miR156-targeted *SPLs* (including *SPL2*, *SPL9*, and *SPL15*) are involved in sporogenous cell formation and cell proliferation in Arabidopsis, all of which influence plant fertility (Xing *et al.* 2013).

### **1.7 Proposed research**

Increased abundance of *miR156* in Arabidopsis alters various aspects of plant growth and development, including varied shoot architecture, delayed flowering, and altered carotenoid and flavonoid biosynthesis (Wang *et al.* 2014; Wei *et al.* 2012; Wu *et al.* 2009). Several recent studies have highlighted a potential role for miR156 in plant nutrient homeostasis and in plant response to environmental cues. When Arabidopsis plants were grown under potassium, nitrogen, and phosphorus deficiency conditions, miR156 was up-regulated in Arabidopsis roots (Hsieh *et al.* 2009). Other miRNAs involved in regulating plant growth and development are also regulated by various metal stresses (Mendoza-Soto *et al.* 2012).

Plants adapt to increased biomass yield by increasing the acquisition of essential nutrient elements (Chatzistathis and Therios 2013). As plants (including *Arabidopsis*) that overexpress miR156 showed significantly enhanced vegetative shoot yield, I hypothesized that these plants must have an improved ability to uptake mineral nutrients, including iron (Fe). However, there are no reports in the literature associating the miR156/*SPL* network with iron homeostasis.

In this dissertation, the effects of miR156 on iron homeostasis will be examined at the physiological and molecular levels. The thesis is divided into two parts. In the first part, I investigated global changes in gene expression caused by overexpression of miR156 in *Arabidopsis*. Total RNA from both roots and rosette leaves at the bolting stage were subjected to next-generation RNA-sequencing (NG-RNA-SEQ). Among the differentially expressed genes, a significant number of genes involved in iron uptake and storage were noticed. In the second part, physiological and molecular experiments were employed to investigate the potential role that miR156 and its target *SPL9* and *SPL15* genes play in plant adaptation to iron deficiency. Effects of miR156 on iron homeostasis-related genes, including *AHA2*, *FRO2*, *FRO3*, *IRT1*, *FIT*, *PYE*, *bHLH38*, *39*, *100*, and *101*, were tested in response to Fe-deficiency. I then used Chromatin Immunoprecipitation (ChIP)-qPCR to investigate if *SPL9* and *SPL15* directly bind to promoters of genes encoding major transcription factors involved in iron homeostasis to regulate their expression.

## Chapter II. Materials and Methods

### 2.1 Plant materials and growth conditions

*Arabidopsis thaliana* ecotype Columbia-0 was used in this work as wild-type (WT) plant. Transgenic *Arabidopsis* seeds that overexpress miR156 (*35S:miR156*) were kindly provided by Dr. Wang Jiawei (Wang *et al.* 2009). *SPL9* and *SPL15* double T-DNA knockout mutant (*spl9/spl15*) was acquired from the Arabidopsis Biological Resource Center (<https://abrc.osu.edu/>).

Plant seeds were first surface-sterilized by immersing in a solution containing 70% ethanol and 5% Triton X-100 (Sigma, USA) for 10 min with gentle agitation. The seeds were then rinsed briefly with 95% ethanol, followed by rinsing with double distilled H<sub>2</sub>O (ddH<sub>2</sub>O) for at least 5 times. Stratification was performed to break seed dormancy by incubating surface-sterilized seeds in dark at 4 °C for at least 48 h. After stratification, seeds were re-suspended in 0.1% agar solution then placed on growth medium [half-strength Murashige and Skoog (½MS) medium (Recipe shown in Appendix A) supplemented with 1% sucrose and 0.5% 2-(N-Morpholino) ethanesulfonic acid hydrate (MES), pH 5.7]. The plates containing seeds were placed in a growth room set at 21 °C under 16h-light/8h-dark photoperiods with 100~110 μmol·m<sup>-2</sup>·sec<sup>-1</sup> light intensity.

For NG-RNA-SEQ, seedlings were first germinated on plates until 7-day-old, then transplanted into commercial soil (Premier Tech Horticulture, Rivière-du-Loup, Quebec, Canada) and kept growing in a growth room. Rosette leaves and roots were collected from plants at the bolting stage (when primary shoots reach 5 mm in height).

Fresh tissues were rapidly cleaned and gently dried with paper towel. The cleaned tissue samples were immediately frozen in liquid nitrogen and stored in ultra-freezer (-80 °C) for further analysis.

To examine plants growth under iron-deficiency, seeds were grown on two types of medium: high-iron medium ( $\frac{1}{2}$ MS medium containing 50 $\mu$ M Fe·EDTA, 1% sucrose, and 0.5% MES, pH 5.7) or low-iron medium (Fe·EDTA was omitted from high-iron medium). For qPCR assay on iron homeostasis-related genes, seedlings were first grown on high-iron medium until 5-day-old. The seedlings were then transferred onto no-iron medium [low-iron medium supplemented with 300  $\mu$ M Ferrozine (Sigma, USA)].

## **2.2 Isolation and quality control of total RNA from Arabidopsis**

The total RNA was isolated with RNeasy Plant Mini Kit (QIAGEN, USA). After isolation, RNA samples were treated with Turbo DNase I (Ambion, USA) at 37 °C for 30 min to remove genomic DNA contaminants. The Turbo DNase I was then removed by using DNase Inactivation Reagent (Ambion, USA) following the manufacture's instruction. The integrity of total RNA was first tested by examining on 1% agarose gel and observing the 18S and 28S ribosomal RNA (rRNA) bands. The RNA samples, exhibiting band intensity ratio of 2:1 of 28S *versus* 18s rRNAs, were used for further experiments. For qRT-PCR, the total RNA was subjected to reverse transcription to produce cDNA (described in section 2.4). For NG-RNA-SEQ, the RNA samples were first diluted with nuclease-free ultra-pure water (Lifetechnologies, USA). The diluted samples were further tested by using Bioanalyzer (Agilent, USA) to examine the RNA

Integrity Number (RIN) as Illumina NG-RNA-SEQ requires RNA samples possess RIN greater than 8.

### **2.3 Illumina next-generation RNA-sequencing**

The NG-RNA-SEQ was performed through a service contract by PlantBiosis (Lethbridge, AB) using Genome Analyzer II (Illumina, USA). Single-end sequencing matrix was carried out. The sequencing libraries were multiplexed and amplified for 36 cycles. Six samples were loaded into each lane. The samples were distributed randomly across lanes. After sequencing, the raw data were analyzed by two steps: preparing raw data and mapping raw data to reference genome. For preparing raw data, basecalling and de-multiplexing was performed using Illumina CASAVA 1.8.1 with default parameters. The de-multiplexed reads were checked with FastQC program. Then raw reads were trimmed with Cutadapt. After trimming, data was examined by FastQC again to ensure the quality. The contaminating sequences (such as chloroplastom, mitochondrion, ribosomal RNAs, etc.) were removed by using BOWTIE aligner. Finally, DESeq pipeline was used to map clean data to Arabidopsis genome (TAIR10, <http://www.arabidopsis.org/>). Statistical comparison was performed by using DESeq R/Bioconductor package. Features with false discovery rate < 0.2 (20% false positive rate) were considered differentially expressed between conditions.

## 2.4 cDNA synthesis and qRT-PCR

A total of 0.2  $\mu$ g of total RNA was subjected to reverse-transcription reaction by using qScript cDNA synthesis Kit (Quanta Biosciences, USA) according to the manufacturer's instructions. QRT-PCR was carried out in a 96-well plate on a C1000 Thermal Cycler and CFX96 Real-Time System (Bio-Rad, Canada), with PerfeCTa SYBR Green FastMix (Quanta Biosciences). All primers for qRT-PCR are listed in Appendix B. For validation of NG-RNA-SEQ results,  *$\beta$ -actin* (AT3G18780) and *PP2AA3* (AT1G13320) were used as reference genes to calculate transcript levels. For iron deficiency test, *SAND* gene (AT2G28390) was used to normalize the data according to Han's test, that transcript level of *SAND* is stable in the presence of 300  $\mu$ M Ferrozine (Han *et al.* 2013). Transcript levels were calculated based on the  $\Delta\Delta$ CT method by using GeneStudy (Bio-Rad, USA). At least two technical replicates were performed for each primer and template set. The results were shown as mean  $\pm$  standard error that derived from three biological replicates.

## 2.5 Extract genomic DNA from Arabidopsis

The genomic DNA was extracted from young rosette leaves by a simplified Cetyltrimethyl ammonium bromide (CTAB) method. The rosette leaves were first homogenized by grinding in mortar and pestle with liquid nitrogen. Approximately 0.1 g of ground samples was transferred into 1.5 ml microcentrifuge tubes. 1 ml of CTAB solution [2% CTAB (w/v), 1.4 M NaCl, 20 mM Ethylenediaminetetraacetic acid, and 100 mM Tris-Cl (pH 8.0)] was added into the tube and gently mixed. Five-hundred  $\mu$ l chloroform was added into the solution and gently mixed by inverting the tube for 5 times.

The mixture was centrifuged at 4,000 *g* for 10 min. The supernatant was then transferred into a new tube and the leftover was discarded. Half volume of isopropanol was added into the supernatant and gently mixed by inverting the tubes for 5 times. The mixture was then centrifuged at 14,000 *g* for 15 min. The supernatant was discarded and the white pellet (nucleotides) at the bottom of tube was dissolved in 50  $\mu$ l of ddH<sub>2</sub>O and treated with Ribonuclease A (Sigma, USA) at 37 C for 30 min. The DNA samples were then stored at -20 °C for further application.

## **2.6 Generation of *pSPL:SPL-GFP* fusion constructs by Gateway cloning**

The simplified procedure for gateway cloning is shown in Figure 5. The genomic DNA fragments (*pSPL9:SPL9* and *pSPL15:SPL15*) containing about 2 kb native promoter and gene body without translation stop codon were first cloned by using Arabidopsis Col-0 genomic DNA as a template. The PCR primers (Appendix B) were designed by using Primer3 software ([http://biotools.umassmed.edu/bioapps/primer3\\_www.cgi](http://biotools.umassmed.edu/bioapps/primer3_www.cgi)). The PCR program was: denaturing at 98°C for 30 sec, then 35 cycles at 98°C for 30 sec, 55°C for 30 sec, 72°C for 4 min followed by final extension at 72°C for 10 min. *Phusion* High-Fidelity DNA Polymerase (New England Biolabs, Canada) was used for PCR amplification. The size of PCR amplicon was further examined on 1% agarose gel by comparing it with a DNA ladder (HyperLadder II, Medicorp Inc., Canada). The PCR products showing the expected size were then gel-purified by using QIAquick Gel Extraction kit (QIAGEN, Canada) following the manufacturer's instructions.

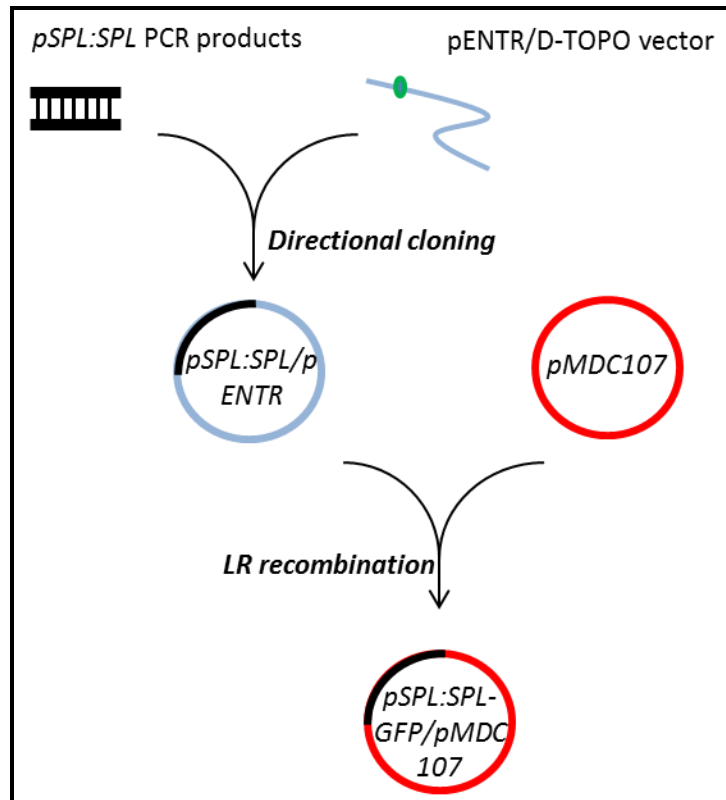


**Figure 5. A simplified Gateway cloning procedure for generating *pSPL:SPL-GFP* fusion constructs.** The blunt-end PCR products were first cloned into linearized pENTR/D-TOPO vector by directional cloning. This donor vector (blue circle) containing *pSPL:SPL* fragment (black portion) were further subjected into LR recombination with destination vector (pMDC107, red circle) to generate the final construct containing a fusion *SPL-GFP* gene driven by native *SPL* promoter.

The purified PCR products were ligated into pENTR/TOPO-D directional cloning vector (Lifetechnologies, Canada) by mixing 0.5  $\mu$ L purified PCR product, 1 $\mu$ L Salt solution (provided with the vector), and 1 $\mu$ L TOPO vector. The mixture was incubated at room temperature for 2 h. This *pSPL:SPL/pENTR* vector was then transformed into *Escherichia coli* TOP10 competent cells (method for preparing competent cells described in section 2.7). The colonies that survived through antibiotic screen were subjected to colony PCR to confirm the inserted fragments. The plasmids were then subjected to sequencing to confirm the genomic sequence was identical with the template derived from ABRC. Once the cloned nucleotide sequence was confirmed, LR recombination was carried out to generate the final construct harboring *pSPL:SPL* and *GFP* fusion gene. The LR recombination was performed by using LR Clonase II Enzyme Mix (Life Technologies). First, 7 $\mu$ L of the *pSPL:SPL/pENTR* vector (100ng/ $\mu$ L), 1 $\mu$ L of destination vector (pMDC107, 100ng/  $\mu$ L), and 2  $\mu$ L of LR Clonase II Enzyme was mixed. The mixture was incubated at room temperature for at least 4 h. This final construct, which contains *pSPL:SPL-GFP* fusion gene, was then transformed into *E. coli* TOP10 competent cells. Further colony PCR was carried out to check the presence of final construct in *E. coli*.

## **2.7 Preparing competent cells**

Starting culture was prepared from our lab stock and cultured overnight. The starting culture was then added into 200 ml of liquid LB medium (recipe shown in Appendix C). When OD600 reached 0.4, bacteria were collected by centrifuge at 3,000 g for 15 min at 4 °C. The pellet was washed with 100 mL of ice-cold 0.1 M MgCl<sub>2</sub> solution. The cells

were harvested by centrifugation at 3,000 *g* for 15 min at 4 °C. The supernatant was discarded and the pellet was re-suspended in 100 mL of ice-cold 0.1 M CaCl<sub>2</sub> solution. The suspension was centrifuged again as in the previous step. The supernatant decanted and the pellet was re-suspended in 2 mL of ice-cold 100 mM CaCl<sub>2</sub> and 20% glycerol solution. The re-suspended bacterial solutions were fast frozen in liquid nitrogen and stored in a -80 °C freezer for future use.

## **2.8 Transformation of competent bacterial cells**

Chemical transformation was used to introduce plasmids to *E. coli*. Briefly, the frozen competent cells were thawed on ice for 10 min. The plasmids was added to competent cells and gently mixed. The mixture containing competent cells and plasmid was incubated on ice for another 30 min. After incubation, the mixture was transferred into a water bath set as 42 °C for 45 s, then quickly put back on ice for another 1 min. Two-hundred µL of liquid LB medium was added into bacterial solution and incubated at 37 °C for 1 h. Finally, the bacterial solution was spread evenly on LB solid medium containing the appropriate antibiotics.

A similar procedure was followed for transformation of *Agrobacterium tumefaciens*. After incubating the mixture of plasmids and competent cells, the solution was incubated at 37 °C for 45 s, then quickly transferred into liquid nitrogen for 1 min. A portion of 200 µL liquid LB medium was added to the bacterial solution and incubated at 28 °C. The solution was then thawed and spread onto LB solid medium containing the appropriate antibiotics.

## **2.9 Arabidopsis transformation**

The Arabidopsis transformation was carried out using *Agrobacterium*-mediated floral-dip method as previously described in (Zhang *et al.* 2006).

## **2.10 Determination of iron content in rosette leaves**

The iron assay kit ab83366 (Abcam, USA) was used to determine the iron content of rosette leaves. Rosette leaves were harvested and washed with 0.1 calcium nitrate solution, then rinsed in ddH<sub>2</sub>O 3 times. Clean leaves were dried in an oven at 65 °C for 2 d. Dried sample was ground into fine powder with a mortar and a pestle. Approximate 0.01 g of dried sample was used to measure the iron contents. According to the iron assay kit, iron content was measured by comparing with a standard curve.

## **2.11 Root acidification assay**

After stratification, plant seeds were placed on high-iron medium or low-iron medium (described in section 2.1) and allowed to grow vertically. Five-day-old seedlings were rinsed in assay solution (low-iron medium without MES and sucrose, supplemented with 0.005% bromocresol purple), then transferred to 96-well containing 300 µl assay solution for 12 h. The absorption at 536 nm of assay solution was measured to indicate the proton extrusion.

### **2.12 Ferric (Fe<sup>3+</sup>) iron reduction assay**

The Ferric reduction assay was conducted to examine the roots' ability to reduce Fe<sup>3+</sup> to Fe<sup>2+</sup>. A set of seedlings were generated as described in section 2.11 for use in ferric reduction assay. The 5-day-old seedlings were first rinsed with 0.1 M calcium nitrate solution to remove excessive iron. The rinsed seedlings were then incubated in reduction assay solution (0.1M Fe·EDTA and 0.3M Ferrozine) for 1 h. The Fe<sup>2+</sup>·Ferrozine complex was quantified by measuring a molar extinction coefficient of 28.6 mM<sup>-1</sup> ·cm<sup>-1</sup> at 562 nm.

### **2.13 Chromatin Immuno-Precipitation (ChIP)-qPCR assay**

The ChIP-qPCR assay was employed to evaluate the binding capability of SPL9 and SPL15 proteins on selected candidate genes. The ChIP assay was performed according to a previously described protocol (Gendrel *et al.* 2005) with some modifications. Recipes for buffers used in this assay are listed in Appendix D.

Briefly, 500 mg of three-week-old transgenic seedlings harboring *pSPL:SPL-GFP* was first washed in ddH<sub>2</sub>O and gently blot dried. The samples were then cross-linked with 1% formaldehyde solution under vacuum for 15 min. The cross-linking was terminated by adding 0.125 M Glycine into the mixture and incubating under vacuum for another 5 min. Tissues were rinsed twice with 1X PBS and ground to fine powder by using liquid nitrogen. The powders were added to 10 ml of Extraction Buffer 1 in 50 mL conical centrifuge tubes and mixed well. The mixture was then filtered into a fresh tube on ice through two layers of Miracloth (Millipore, CANADA). The filtrate was centrifuged at 5,000 g at 4 °C for 15 min to collect chromatin. The supernatant was

discarded and the pellet was re-suspended in 300  $\mu$ l of extraction buffer 2. After centrifugation at 13,000  $g$  for 10 min, the pellet was re-suspended in 100  $\mu$ l of extraction buffer 3, layered on 400  $\mu$ l of extraction buffer 3 and centrifuged at 16,000  $g$  for 1 h at 4  $^{\circ}$ C. The pellet was re-suspended in 100  $\mu$ l of nuclei lysis buffer by gentle pipetting. The re-suspended chromatin solution was sheared by sonication twice for 17s each at power 3 (Sonic Dismembrator, Fisher Scientific). The fragmented chromatin solution was then centrifuged at 13,000  $g$  for 5 min. The supernatant was transferred to fresh tube and diluted to 1 ml in Dilution Buffer. 10  $\mu$ l of this chromatin solution was retrieved and stored at -20  $^{\circ}$ C serves as input DNA. The chromatin solution was divided equally to 3 micro-centrifuge tubes and 40  $\mu$ l of Protein agarose beads (Millipore) and GFP antibody Ab290 (Millipore) was added to each tube and incubated for 12 h at 4  $^{\circ}$ C.

The following day (after 12 h incubation), 50  $\mu$ l of protein A- agarose beads was added to each tube and incubated at 4  $^{\circ}$ C for 1 h. The beads were recovered by centrifuge at 3,800  $g$  at 4  $^{\circ}$ C for 30 s. The immune-complexes were then washed in a sequential order with following buffers: low-salt, high-salt, LiCl, and Tris-EDTA (TE) buffers. For each wash, the immune-complexes were washed at 4  $^{\circ}$ C for 10 min. After each wash, the beads were collected by centrifuge at 3,800  $g$  at 4  $^{\circ}$ C for 30 s. After the last wash, the agarose beads were collected by centrifuge at 3,800  $g$  at 4  $^{\circ}$ C for 30 s and eluted in 200  $\mu$ l of fresh Elution Buffer. Cross-linking of the immune-complexes was reversed by incubating at 65  $^{\circ}$ C for 4 h with 200 mM NaCl.

On the third day, 2  $\mu$ l of proteinase K (10 ng/  $\mu$ l), 20  $\mu$ l of 40 mM Tris-HCl (pH 6.5) and 10  $\mu$ l of 100 mM EDTA were added to each sample and incubated at 45  $^{\circ}$ C for 1 h. The DNA was purified with equal volume of phenol/chloroform and precipitated with

anhydrous ethanol, 0.3 M NaOAc (PH 5.2) and 15 µg of glycogen carrier (Roche, USA). The DNA pellet was washed with 70% ethanol and re-suspended in 200 µl of ddH<sub>2</sub>O. The DNA solution was stored at -20°C and ready for down-stream application.

The DNA derived from the ChIP-assay was used to quantify specific regions of the promoter that have putative SPL binding site(s) (binding sites were defined by the presence of SPL binding core sequence, GTAC) using qPCR with promoter-specific primers flanking the putative binding site(s) (Appendix A). The locations of putative SPL binding sites and primers used in ChIP-qPCR are listed in Appendix F and G. The relative amount of enriched ChIP-DNA was normalized against % input DNA using the  $\Delta\Delta C_t$  method (ChIP-analysis, Life Technologies, <http://www.lifetechnologies.com/>).

#### **2.14 Gene Ontology (GO) Parametric Analysis of Gene Set Enrichment (PAGE) analysis**

GO analysis was performed by using the agriGO online analysis tool (<http://bioinfo.cau.edu.cn/agriGO/>) (Du *et al.* 2010). The differentially expressed gene accession numbers with corresponding expression fold-changes were submitted to Parametric Analysis of Gene set Enrichment (PAGE) online software and analyzed with default parameters (Kim and Volsky 2005). The Z-score derived from PAGE analysis indicates whether the specific GO term occurs more or less frequently than expected. The extreme positive Z-score indicates the GO term occurs more frequently than expected, whereas a negative number indicates that the term occurs less than expected. The cut-off

for Z-score is usually set at 2.0. Any number greater than 2.0 or less than -2.0 is considered significant.

### **2.15 Confocal microscopy**

I investigated the production of SPL9-GFP and SPL15-GFP fusion proteins using confocal microscopy. The transgenic Arabidopsis plants harboring *pSPL9:SPL9-GFP* and *pSPL15:SPL15-GFP* respectively were grown on ½ MS medium for one month. The rosette leaves were first stained with 4',6-diamidino-2-phenylindole (DAPI) to show the location of nuclei. Then the stained leaves were examined on a DM IRE2 inverted microscope equipped with an HCX PL APO 1.20 63× water-immersion objective. Images were collected in a 512×512 format on a TCS SP2 confocal system (Leica Microsystems, German) using a scanning speed of 40Hz. GFP was visualized by exciting the samples with the 514 nm argon laser line and collecting fluorescence with an emission window set at 520-580 nm.

### **2.16 Statistical analyses**

For validation of NG-RNA-SEQ results by qRT-PCR, students' T-test was used to examine the significant differences between WT and *35S:miR156* plants. Statistically significant differences among the three Arabidopsis genotypes were determined with one-way Analysis of Variance (ANOVA), followed by post-hoc Duncan's test at P value  $\leq 0.05$ .

## Chapter III. Results

### 3.1 Overexpression of miR156 resulted in extensive changes in the global gene expression pattern

To investigate the transcriptome differences between WT plants and those overexpressing miR156 (hereafter denoted by *35S:miR156* plants), high-throughput Illumina NG-RNA-SEQ was performed using total RNA extracted from rosette leaves and roots when WT plants were at the bolting stage. The isolated RNA was subjected to a series of quality control assays to ensure RNA integrity before being subjected to NG-RNA-SEQ.

#### 3.1.1 RNA sample preparation and quality control for Illumina sequencing

For each type of tissue, total RNA was isolated from four independently pooled samples. 4 µg of total RNA was diluted to a final volume of 100 µl. The quality of each RNA sample was first tested on 1% agarose gel. Bioanalyzer was used to further examine the RIN from each RNA sample (Figure 6). The analysis showed that RINs for samples were greater than 8.0, which indicated these samples were suitable for NG-RNA-SEQ.

#### 3.1.2 General results of NG-RNA-SEQ

A total of 2,971 Mb nucleotides corresponding to 102.44 million raw reads were generated from NG-RNA-SEQ. A total of 6,644 and 1,944 genes could be detected in rosette leaf and root samples, respectively. Among them, 142 genes were differentially expressed (with at least two-fold change in expression) in root samples (50 were up-regulated and 92 were down-regulated in *35S:miR156* roots compared with WT roots)

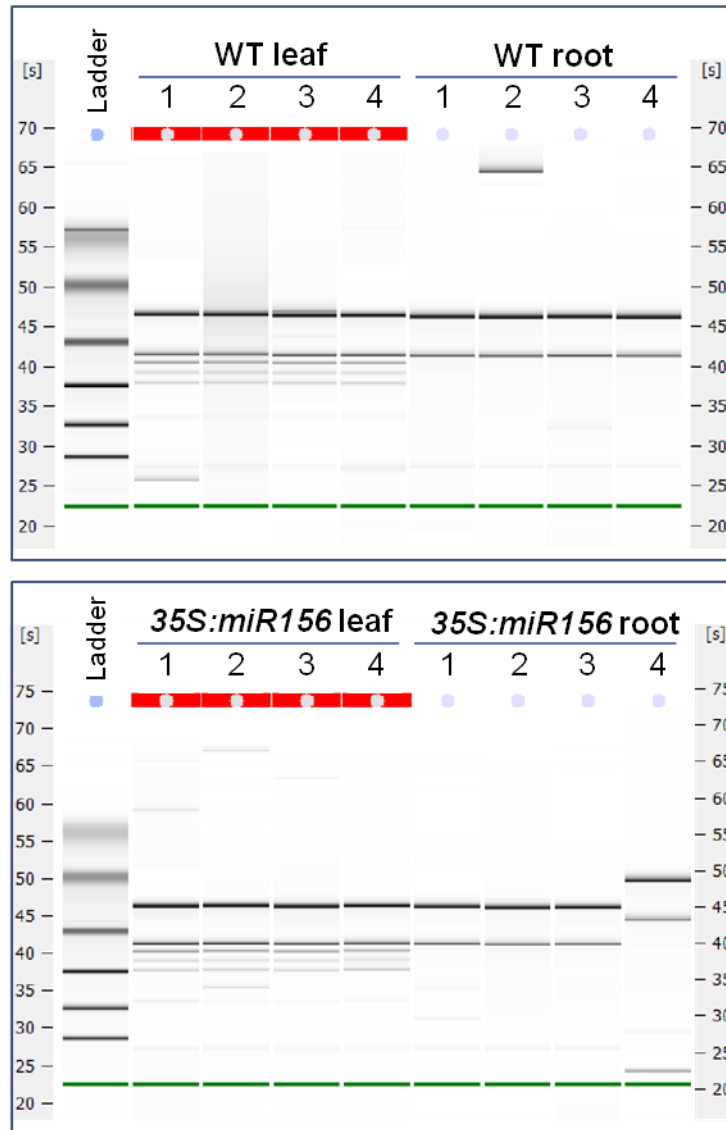


**Figure 6. Examination of RNA quality using Bioanalyzer.** Samples corresponding to different types of tissues and genotypes are underlined and labelled. Four independent biological replicates were used. The very left and right lanes on the upper and lower panels are ladders.

and 1,139 genes were differentially expressed in leaf samples (920 were up-regulated and 219 were down-regulated in *35S:miR156* leaves compared with WT leaves) (Appendix E). Eight genes showed contradictory results between roots and rosette leaves, whereas 23 genes showed the same trend in both sets of tissues (Figure 7). Among these 31 genes, 25 have putative functions based on a TAIR search, and six genes are of unknown functions (Table 1).

### **3.1.3 Validation of NG-RNA-SEQ results by qRT-PCR**

To validate the NG-RNA-SEQ results, a series of qRT-PCR assays were carried out using identical RNA samples. A total of 40 candidate differentially-expressed genes; i.e. 10 candidate genes from each category were randomly selected. Based on the qRT-PCR results, 37 out of 40 candidate genes (92.5%) showed similar expression trends to those found in the NG-RNA-SEQ experiment (Figure 8).

### **3.1.4 Transcriptomics of *35S:miR156* plants**

To determine how overexpression of miR156 affects certain classes of genes, Gene Ontology (GO) analysis was performed. In the leaf and root samples, 6142 out of 6644 (92.44%) and 1764 out of 1945 (90.69%) genes, respectively, could be functionally annotated. Of the 1250 genes that showed significantly varied expression between WT and *35S:miR156* plants, 1225 (98%) could be functionally annotated (Figure 9A) using tools available online at <http://www.ncbi.nlm.nih.gov/>. Based on the Parametric Analysis of Gene Set Enrichment (PAGE) analysis (<http://bioinfo.cau.edu.cn/agriGO/>) of the roots, DNA binding (GO: 0003677, Z-score: 3.7), nucleic acid binding (GO: 0003676, Z-score:

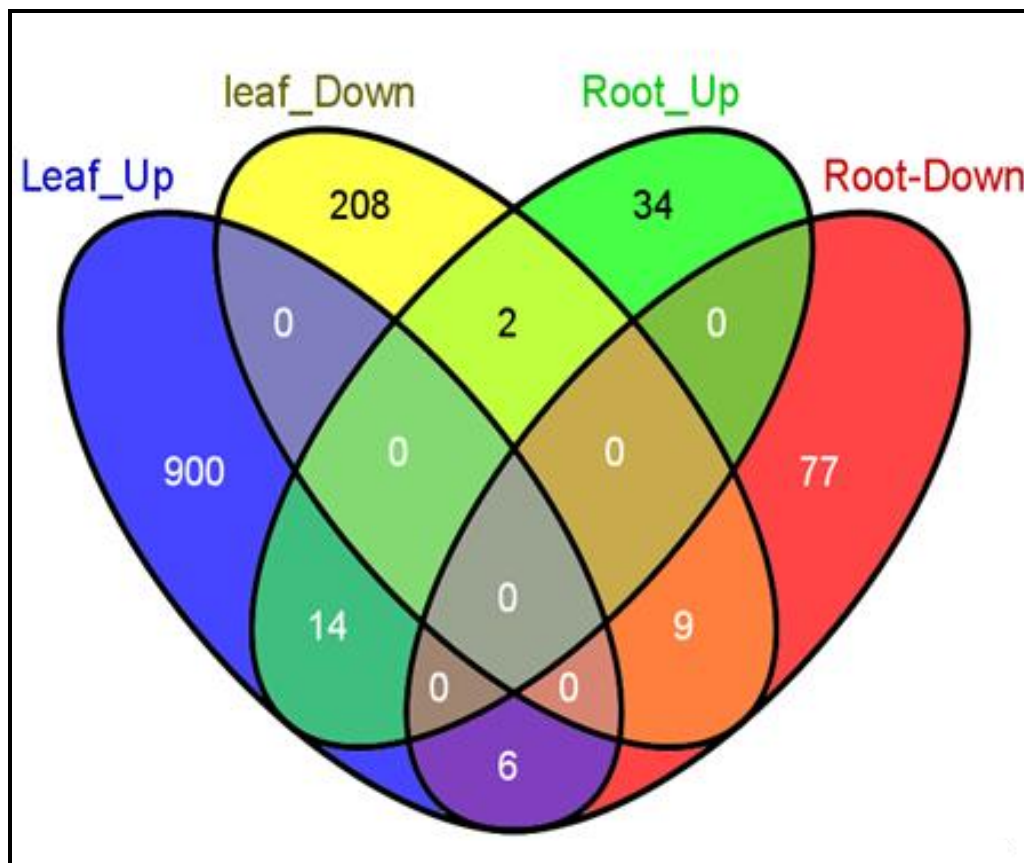


**Figure 7. Venn diagram of differentially expressed genes derived from NG-RNA-SEQ.** Down and up in the figure indicate down-regulated and up-regulated genes in *35S:miR156* plants compared to WT plants.

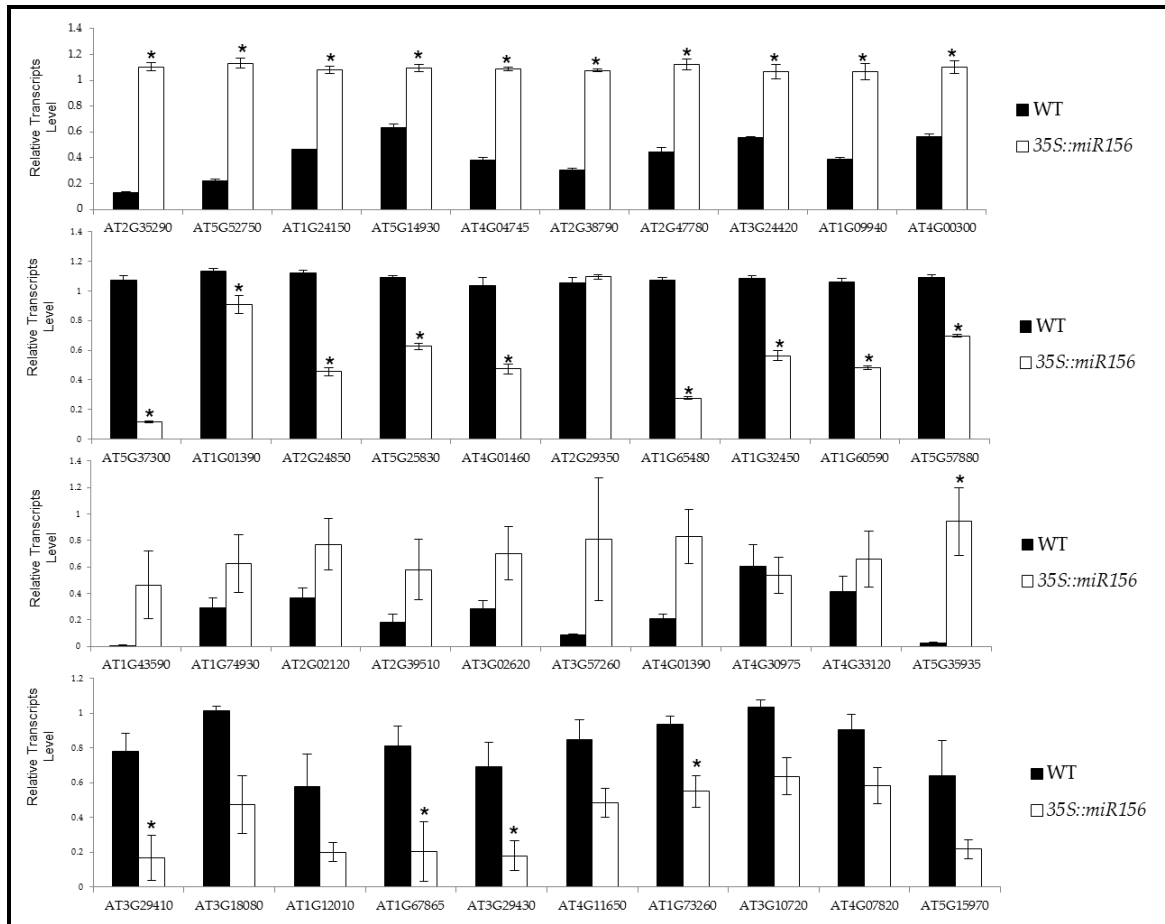


**Figure 8.** qRT-PCR using 40 randomly selected differentially expressed genes. Ten candidate genes were randomly selected from each category. The expression patterns of 37 out of these 40 candidate genes showed consistency with the NG-RNA-SEQ data. QRT-PCRs were performed on the same samples used for NG-RNA-SEQ. Both  $\beta$ -actin and *PP2AA3* were used as internal reference genes to calculate transcript levels by  $\Delta\Delta$ CT methods. Results are shown as means  $\pm$  standard error derived from four biological replicates. Asterisks indicate statistical significance at  $P < 0.05$ .

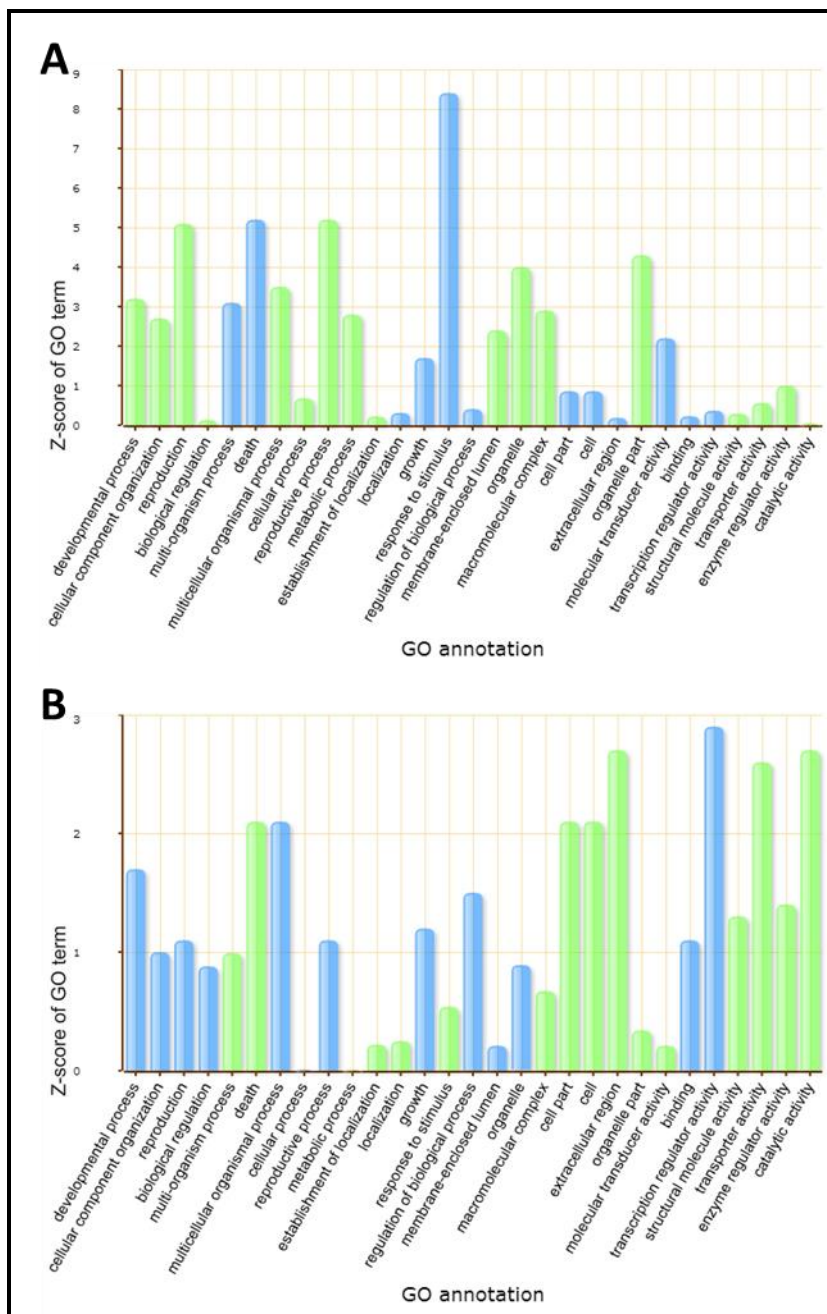


**Figure 9. Parametric Analysis of Gene Set Enrichment (PAGE) analysis of differentially expressed genes in rosette leaf (A) and root (B).** Blue and green colors indicate positive and negative Z-scores, respectively.

**Table 1. Genes with more than 2-fold change in expression were detected in both roots and rosette leaves.**

Genes	Expression trend (35S:miR156 vs WT)	Description
AT3G57260	↓Leaf ↑Root	beta 1,3-glucanase
AT2G24850	↓Leaf ↑Root	Encodes a tyrosine aminotransferase that is responsive to treatment with jasmonic acid.
AT3G10720	↑ Leaf ↓Root	Plant invertase/pectin methylesterase inhibitor superfamily
AT4G35770	↑ Leaf ↓Root	Senescence-associated gene that is strongly induced by phosphate starvation. Transcripts are differentially regulated at the level of mRNA stability at different times of day. mRNAs are targets of the mRNA degradation pathway mediated by the downstream (DST) instability determinant.
AT3G49780	↑ Leaf ↓Root	Phytosulfokine 3 precursor, coding for a unique plant peptide growth factor. Plants overexpressing this gene (under a 35S promoter), develop normal cotyledons and hypocotyls but their growth, in particular that of their roots, was faster than that of wildtype.
AT5G64120	↑ Leaf ↓Root	Encodes a cell wall bound peroxidase that is induced by hypo-osmolarity and is involved in the lignification of cell walls.
AT1G30730	↑ Leaf ↓Root	FAD-binding Berberine family protein
AT3G26500	↑ Leaf ↓Root	Encodes PIRL2, a member of the Plant Intracellular Ras-group-related

		LRRs (Leucine rich repeat proteins). PIRs are a distinct, plant-specific class of intracellular LRRs that likely mediate protein interactions, possibly in the context of signal transduction.
AT3G18080	↓ Leaf ↓Root	B-S glucosidase 44 (BGLU44)
AT5G54585	↓ Leaf ↓Root	unknown protein
AT1G67865	↓ Leaf ↓Root	unknown protein
AT2G41240	↓ Leaf ↓Root	bHLH100. Encodes a member of the basic helix-loop-helix transcription factor family protein.
AT2G13810	↓ Leaf ↓Root	AGD2-like defense response protein 1 (ALD1)
AT2G43590	↓ Leaf ↓Root	Chitinase family protein
AT1G77270	↓ Leaf ↓Root	unknown protein
AT2G25680	↓ Leaf ↓Root	Encodes a high-affinity molybdate transporter. Mutant has reduced concentrations of molybdate in roots and shoots, and reduced shoot and root length when growing on Mo-limited medium
AT5G04150	↓ Leaf ↓Root	bHLH101. Encodes a member of the basic helix-loop-helix transcription factor family protein.
AT1G72520	↑ Leaf ↑Root	PLAT/LH2 domain-containing lipoxygenase family protein
AT4G34410	↑ Leaf ↑Root	encodes a member of the ERF (ethylene response factor) subfamily B-3 of ERF/AP2 transcription factor family. The protein contains one AP2 domain.
AT5G35935	↑ Leaf ↑Root	copia-like retrotransposon family
AT4G30975	↑ Leaf ↑Root	Unknown gene

AT5G52050	↑ Leaf ↑Root	MATE efflux family protein
AT2G05380	↑ Leaf ↑Root	glycine-rich protein 3 short isoform (GRP3S)
AT1G12610	↑ Leaf ↑Root	Encodes a member of the DREB subfamily A-1 of ERF/AP2 transcription factor family (DDF1).
AT4G24380	↑ Leaf ↑Root	unknown protein
AT2G44840	↑ Leaf ↑Root	encodes a member of the ERF (ethylene response factor) subfamily B-3 of ERF/AP2 transcription factor family.
AT1G74930	↑ Leaf ↑Root	encodes a member of the DREB subfamily A-5 of ERF/AP2 transcription factor family.
AT1G43590	↑ Leaf ↑Root	unknown protein
AT3G02840	↑ Leaf ↑Root	ARM repeat superfamily protein
AT5G42380	↑ Leaf ↑Root	calmodulin like 37
AT4G01360	↑ Leaf ↑Root	Encodes a protein related to BYPASS1 (BPS1). Regulates production of mobile compound: bps signal.

3.5), transcription regulator activity (GO: 0030528, Z-score: 2.9), and transcription factor activity (GO: 0003700, Z-score: 2.6) were over-represented in *35S:miR156* plants. Also, transporter activity (GO: 0005215, Z-score: -2.6) and catalytic activity (GO: 0003824, Z-score: -2.7) were under-represented in *35S:miR156* roots. On the contrary, the GO analysis of the leaf transcriptome showed a different picture than the one derived from roots (Figure 9B). 35 GO terms were identified to be significantly affected, including 23 in biological process, 10 in cellular component, and 2 in molecular function. The ones with the highest score were: response to stimulus (GO:0050896, Z-score 8.4) and response to stress (GO:0006950, Z-score: 8.3).

### **3.1.5 Differential repression of *SPL* genes by miR156 in leaves and roots**

Based on previous reports in the literature, *SPL* genes were expected to be repressed in *35S:miR156* plants. My NG-RNA-SEQ results were consistent with this expectation. As shown in Tables 2 and 3, a number of *SPL* genes were down-regulated in *35S:miR156* plants compared to WT. Seven *SPL* genes, *SPL4*, 5, 6, 9, 10, 11, and 15, were down-regulated in leaves of *35S:miR156* plants compared to WT (Table 2), whereas only *SPL6*, 10, 11, and 15 were down-regulated in *35S:miR156* roots (Table 3). Based on the expression values derived from NG-RNA-SEQ results, miR156 appears to preferentially target *SPL5*, *SPL9*, and *SPL15*, as they are the only *SPL* genes showing more than 2-fold reduction in expression in *35S:miR156*. The effect of miR156 on other *SPL* genes was less pronounced.

**Table 2. Expression pattern of *SPL* genes in rosette leaves**

<b>Genes</b>	<b>Expression in WT</b>	<b>Expression in <i>35S:miR156</i> plants</b>	<b>Log<sub>2</sub>(Fold-Change)</b>	<b>P-adj</b>
<i>SPL4</i>	90.40	71.83	-0.33	0.137
<i>SPL5</i>	24.53	8.16	-1.59	9.27E-4
<i>SPL6</i>	67.69	45.05	-0.59	3.98E-3
<i>SPL9</i>	60.60	16.07	-1.92	6.43E-12
<i>SPL10</i>	82.39	57.01	-0.53	4.64E-3
<i>SPL11</i>	71.52	37.72	-0.92	1.64E-06
<i>SPL15</i>	30.69	15.93	-0.95	4.44E-3

**Table 3. Expression pattern of *SPL* genes in roots.**

<b>Genes</b>	<b>Expression in WT</b>	<b>Expression in 35S:miR156 plants</b>	<b>Log<sub>2</sub>(Fold-Change)</b>	<b>P-adj</b>
<i>SPL6</i>	123.04	92.08	-0.42	0.023
<i>SPL10</i>	121.65	60.77	-1.00	1.65E-11
<i>SPL11</i>	45.74	29.04	-0.66	0.08
<i>SPL15</i>	42.19	17.54	-1.27	8.15E-6

### 3.2 Iron homeostasis related genes are affected by overexpression of miR156

The transcription patterns of multiple iron homeostasis-related genes were affected by overexpression of miR156 (Figure 10). These genes can be divided into three groups, I (genes coding Ferritins, which can store iron in plants), II (iron uptake-related genes), and III (genes coding for transcription factors that participate in iron homeostasis). In group I, *FER4* was up-regulated in both roots and rosette leaves of *35S:miR156* plants. *FER1* and *FER3* were up-regulated in *35S:miR156* leaves, but were undetectable in roots. Genes in group II that participate in iron uptake and genes in group III coding for transcription factors were down-regulated in *35S:miR156* plants. Although the transcription levels of all group II genes were reduced, only *AHA7* and *FRO4* showed more than two-fold change in expression. Similarly, for the expression levels of transcription factors that participate in iron homeostasis, *bHLH38*, *bHLH39*, *bHLH100*, and *bHLH101* showed more than 2-fold changes in expression in at least one sample type (Figure 10).

### 3.3 MiR156 participates in iron homeostasis in Arabidopsis

Based on the NG-RNA-SEQ results, I hypothesized that elevated transcript levels of ferritin coding genes may correspond to a higher level of iron content in *35S:miR156* plants. I also hypothesized that the reduced transcript levels of key genes encoding enzymes and transcription factors that are involved in iron uptake may be caused by elevated iron content. To investigate these two hypotheses, a series of tests were performed on *35S:miR156* and WT plants to examine the impact of overexpression of miR156 on iron homeostasis, such as measurement of iron content,

	Gene	Accession	Root		Leaf		
			WT	35S:miR156	WT	35S:miR156	
I Ferritin coding genes	FER1	<a href="#">AT5G01600</a>	nd	nd	127.47	328.35	
	FER3	<a href="#">AT3G56090</a>	nd	nd	195.99	277.97	
	FER4	<a href="#">AT2G40300</a>	38.65	51.58	117.5	197.13	
II Iron-uptake	AHA1	<a href="#">AT2G18960</a>	nd	nd	2952.81	2729.26	H <sup>+</sup> ATPase
	AHA2	<a href="#">AT4G30190</a>	4005.79	3151.09	1588.77	1376.13	
	AHA3	<a href="#">AT5G57350</a>	nd	nd	2721.32	2366.46	FERRIC REDUCTION OXIDASE
	AHA7	<a href="#">AT3G60330</a>	44.99	21.18	nd	nd	
	FRO2	<a href="#">AT1G01580</a>	579.48	316.62	nd	nd	
	FRO3	<a href="#">AT1G23020</a>	262.72	181.33	526.99	358.42	IRON-REGULATED TRANSPORTER
	FRO4	<a href="#">AT5G23980</a>	nd	nd	17.88	6.31	
IRT1	<a href="#">AT4G19690</a>	736.01	404.46	nd	nd		
III Transcription Factor	bHLH038	<a href="#">AT3G56970</a>	182.22	124.68	49.47	7.06	
	bHLH039	<a href="#">AT3G56980</a>	205.51	123.73	21.65	2.98	
	bHLH100	<a href="#">AT2G41240</a>	64.34	24.25	43.38	8.45	
	bHLH101	<a href="#">AT5G04150</a>	56.64	26.94	17.17	3.54	



Low High

**Figure 10. Multiple iron homeostasis-related genes were affected by overexpression of miR156.** Genes related to iron homeostasis were retrieved from NG-RNA-SEQ results. These genes were further divided into three groups: Group I, Ferritin coding genes; Group II, Iron-uptake related enzymes coding genes; Group III, genes coding for transcription factors that participate in iron-homeostasis, including *AHA*, *FRO*, and *IRT* families. Numbers are normalized counts derived from NG-RNA-SEQ. Yellow color indicates a lower expression level compared to red. *nd*, not detected.

determination of growth under iron deficiency, evaluation of the rhizosphere acidification level and the ability to reduce ferric iron.

### **3.3.1 Iron content of rosette leaves is not affected by overexpression of miR156**

The iron content was measured in rosette leaves collected at the same developmental stage as those used for NG-RNA-SEQ. First, a standard curve for iron concentration ranging from 0 nM to 10 nM was generated (Figure 11A). The regression of the standard curve was 0.9998 indicating that it was accurate enough for calculating iron content. The results shown in Figure 11B indicate that the iron contents in WT, *spl9/spl15*, and *35S:miR156* were not statistically different.

### **3.3.2 Improved growth of *35S:miR156* plants under iron-deficiency condition**

To further examine the role of miR156 in plant response to iron stress, the growth of WT and *35S:miR156* was examined under different iron availability conditions (Figure 12A and 12B). To prove the effects of miR156 on plant growth under iron deficiency were exerted by down-regulating *SPL* genes, *spl9/spl15* double knock-out mutant plants were also tested (Figure 12A and 12B). All genotypes showed similar growth patterns under regular ½MS medium supplemented with 50 µM Fe·EDTA (+Fe) (Figure 12A). Under the low iron condition, the best growth was obtained with *35S:miR156* plants (Figure 12B), which showed elongated roots. The *spl9/spl15* double knockout mutants had similar root length as *35S:miR156* plants (Figure 12C and 12D), but with less lateral root branching (Figure 12E and 12F). WT plants, on the other hand, showed severely

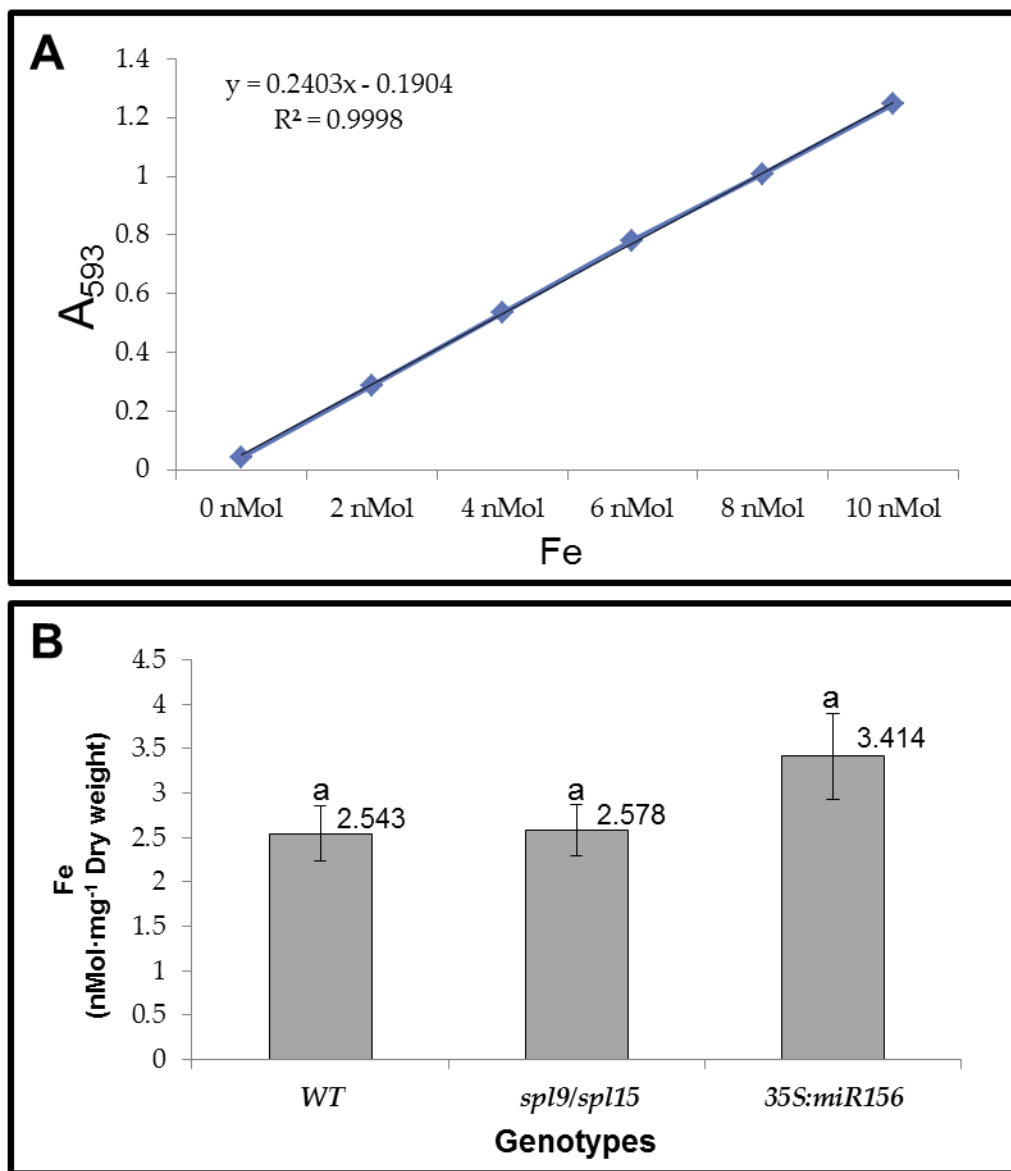


**Figure 11. Measurement of iron content in Arabidopsis rosette leaves.** **A**, Iron standard curve was made according to the manual (Section 2.10); **B**, iron concentrations in three Arabidopsis plant genotypes. The results are shown as mean  $\pm$  standard error of three biological replicates. Values shown with the same letter indicate no significant difference at  $P \leq 0.05$ .

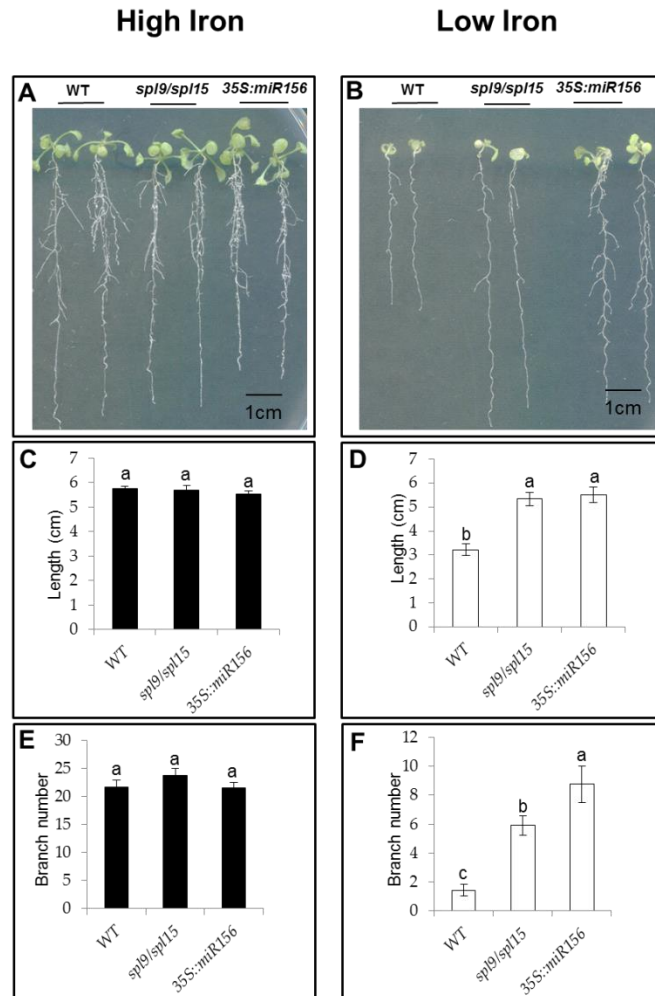


**Figure 12. Growth of WT, *spl9/spl15* and *35S:miR156* plants under iron deficiency.**

**A**, Plant growth on high iron medium ( $\frac{1}{2}$  MS medium containing  $50\mu\text{M}$  Fe·EDTA); and **B**, plant growth on low iron medium (Fe·EDTA was omitted from high iron medium) at 10 days post germination. The root length (**C** and **D**) and branch numbers (**E** and **F**) were shown as mean  $\pm$  standard error, which was calculated from three biological replicates. At least 10 seedlings were measured for each biological replicate. Values shown with the same letter under the same condition indicate no significant difference at  $P \leq 0.05$ .

retarded growth compared to *35S:miR156* and *spl9/spl15* mutants (Figure 12). Under low-iron condition, the number of lateral root of *35S:miR156* and *spl9/spl15* plants were approximate 6 and 4 times higher compared to WT plants, respectively (Figure 12F). Regarding the shoots, *35S:miR156* plants developed more true leaves compared to the other two genotypes (Figure 10B).

### **3.3.3 MiR156 has no effect on rhizosphere acidification**

To better understand why *35S:miR156* plants grew better than other plants under iron-deficiency, an acidification assay was performed to measure the plant's ability to acidify its rhizosphere. In nature, higher acidification levels (lower pH) of plant roots' rhizosphere lead to a higher solubility of  $\text{Fe}^{3+}$ , which can be transported into plants. In two independent experiments, *35S:miR156* plants showed no statistically significant difference in rhizosphere acidification levels compared to *spl9/spl15* and WT plants (Figure 13) under both high iron (+Fe) and low iron (-Fe) conditions.

### **3.3.4 MiR156 affects iron reduction partially through targeting *SPL9* and *SPL15***

An important aspect in iron homeostasis is the regulation of iron transport which requires the reduction of  $\text{Fe}^{3+}$  to  $\text{Fe}^{2+}$ . Plants utilize strategy I to uptake iron can only transport  $\text{Fe}^{2+}$  into roots but not  $\text{Fe}^{3+}$ , hence the reduction of  $\text{Fe}^{3+}$  to  $\text{Fe}^{2+}$  is critical step in plant iron uptake. To examine the effects of miR156 on iron reduction, a  $\text{Fe}^{3+}$  reductase assay was carried out using WT, *35S:miR156*, and *spl9/spl15* double T-DNA knockout mutant roots. Under normal growth condition, all three genotypes had the same level of

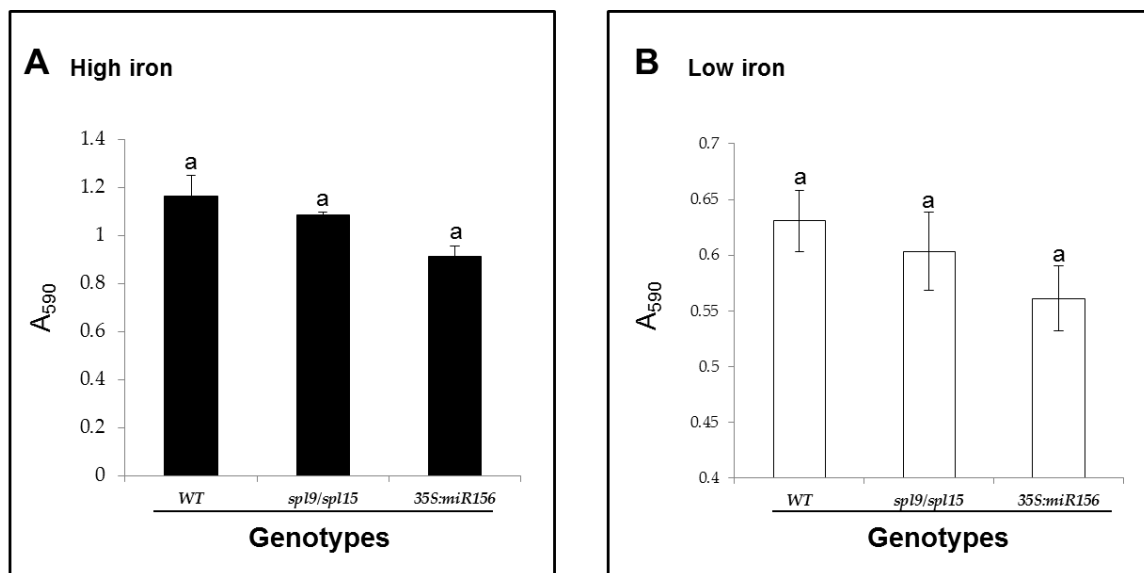


**Figure 13. Acidification of rhizosphere in WT, *sp19/sp115*, and *35S:miR156* plants under normal Fe condition (A) and iron-deficiency condition (B).** 5-day-old plants grown on high-iron ( $\frac{1}{2}$ MS medium containing  $50\mu\text{M}$  Fe·EDTA) and low-iron (Fe·EDTA was omitted from  $\frac{1}{2}$ MS medium) were used to perform acidification assays. The acidification levels were quantified by measuring absorbance at  $A_{590}$  of assay solution containing pH indicator. A higher absorbance indicates higher pH. Results are shown as mean  $\pm$  standard error ( $n \geq 4$ ). The same trends are observed from two independent biological replicates. Values shown with the same letter under the same condition indicate no significant difference at  $P \leq 0.05$ .

acidification ability (Figure 14). However, when plants were grown under iron deficiency (low iron), both *35S:miR156* and *spl9/spl15* showed higher iron reduction rates than WT. It should be noted also that the three sets of plants showed higher iron reduction rates under iron-deficiency condition than in the high iron medium.

### **3.4 MiR156 regulates iron homeostasis-related genes through SPL9 and SPL15**

To find out the effects caused by overexpression of miR156 on the regulatory machinery of iron homeostasis, the expression patterns of genes coding major transcription factors and enzymes that participate in iron homeostasis were tested under iron-deficiency condition. Five-day-old plants were transferred onto ½ MS medium with or without iron for either two days or four days, and total RNA was extracted from the roots and used for qRT-PCR to test for the transcript levels of genes of interest.

#### **3.4.1 *FIT* and *PYE* were transiently up-regulated in the roots of *spl9/spl15* and *35S:miR156* plants under iron deficiency compared with WT plants**

Ferrozine, a strong ferric iron chelator, was used to eliminate free iron from the medium, because it is a strong ferric iron chelator that can bind to free Fe<sup>2+</sup> ions. As *FIT* and *PYE* are two of the major transcription factors of iron homeostasis in Arabidopsis, their expression patterns were examined by qRT-PCR. *FIT* and *PYE* were induced under iron deficiency in all three plant genotypes, but *spl9/spl15* and *35S:miR156* plants exhibited relatively higher *PYE* expression levels than WT after 48 h under iron deficiency condition (Figure 15A). For *FIT* gene, *35S:miR156* plants had higher expression levels

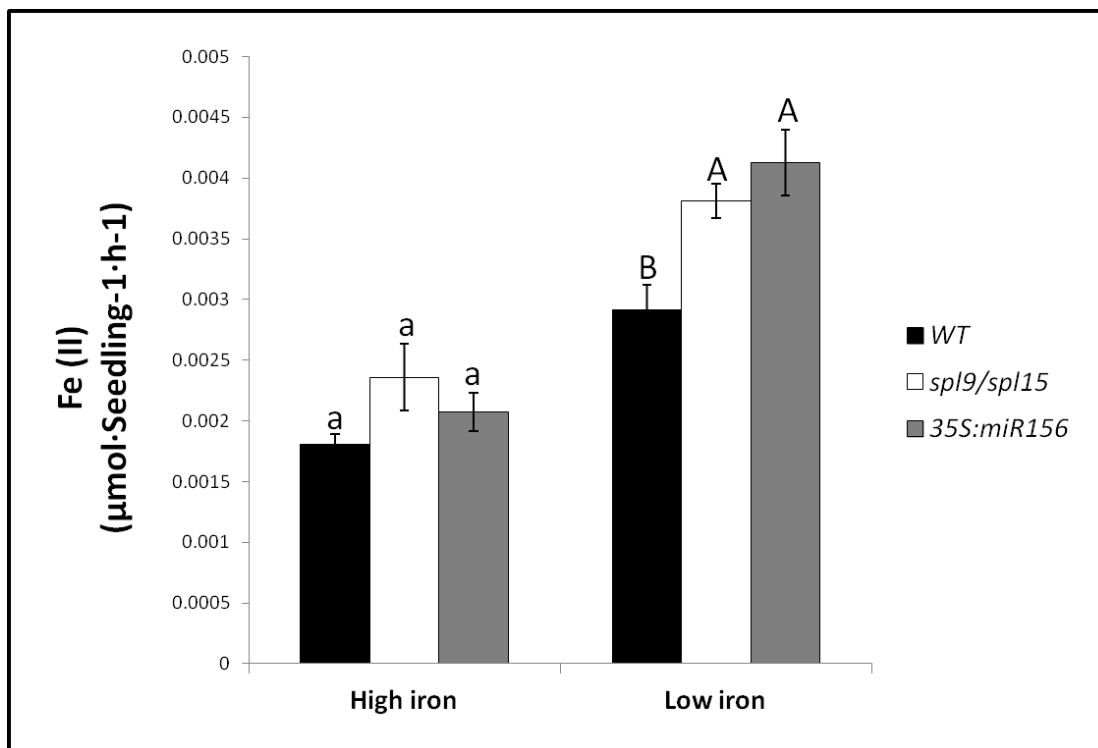


**Figure 14. Ferric reduction in WT, *spl9/spl15*, and *35S:miR156* roots.** 5-day-old plants grown on high-iron ( $\frac{1}{2}$ MS medium containing  $50\mu\text{M}$  Fe·EDTA) and low-iron (Fe·EDTA was omitted from  $\frac{1}{2}$ MS medium) were used to perform iron reduction assays. An iron chelator, Ferrozine, was used to quantify  $\text{Fe}^{2+}$  ions in assay solution. Ferrozine can bind with free  $\text{Fe}^{2+}$  ions to form a complex and shows purple color. The  $\text{Fe}^{2+}$ ·Ferozine complex was quantified by measuring a molar extinction coefficient of  $28.6\text{ mM}^{-1}\cdot\text{cm}^{-1}$  at 562 nm. Results are shown as mean  $\pm$  standard error derived from four biological replicates. Values shown with the same letter under the same condition indicate no significant difference at  $P \leq 0.05$ .

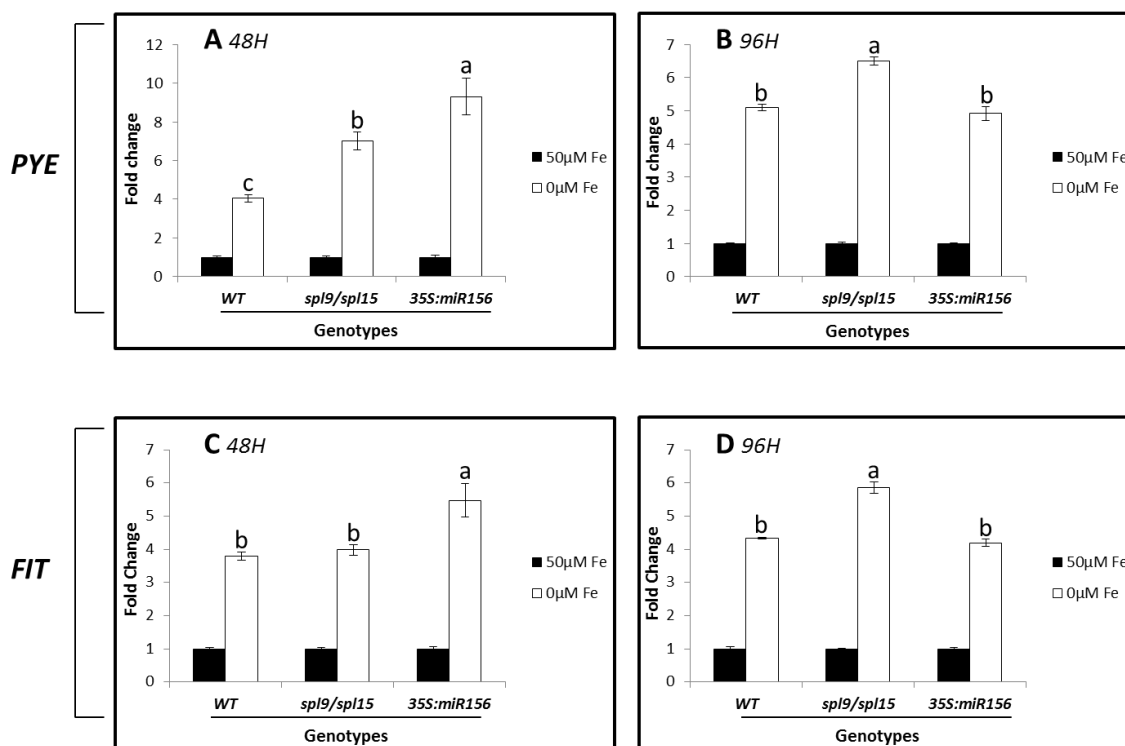


**Figure 15. Effect of iron deficiency on expression of *PYE* and *FIT* in roots of WT, *spl9/spl15*, and *35S:miR156* plants. A and B, Relative transcript levels of *PYE* after 48h and 96h under iron deficiency. C and D, relative transcript levels of *FIT* after 48h and 96 h under iron deficiency. The transcript level was first calculated by using  $\Delta\Delta\text{CT}$  method. *SAND* was used as internal reference gene for calculation. The mean of transcript levels derived from iron deficiency condition (no-iron medium, described in **Section 2.1**) is reported relative to the transcript levels derived from normal growth condition (high-iron medium, described in **Section 2.1**) control in the same genotype. The qRT-PCR results are shown as mean  $\pm$  standard error of three biological replicates. Values shown with the same letter under the same condition indicate no significant difference at  $P \leq 0.05$ .**

than WT and *spl9/spl15* after 48 h iron deficiency treatment (Figure 15C). In *spl9/spl15* double mutant, the increase in transcript levels of both *FIT* and *PYE* was delayed relative to *35S:miR156* plants (Fig. 15B and D).

### **3.4.2 MiR156 has different effects on the expression patterns of *bHLH38*, *bHLH39*, *bHLH100*, and *bHLH101* under short term iron deficiency**

Due to the critical roles of *bHLH38*, *bHLH39*, *bHLH100*, and *bHLH101* in plant iron homeostasis (Wang *et al.* 2013; Yuan *et al.* 2008), and the NG-RNA-SEQ results indicating that these genes were down-regulated in *35S:miR156* plants, their expression patterns under short term iron deficiency were tested in WT, *spl9/spl15*, and *35S:miR156* plants. In all three genotypes, *bHLH38*, *bHLH39*, *bHLH100*, and *bHLH101* were induced by iron deficiency after 48 h and 96 h relative to plants grown under control conditions (Figure 16). Different *bHLH* genes were affected differently by miR156. Under iron deficiency, the expression of *bHLH38* was induced by overexpression of miR156 after 48 h iron deficiency stress (Figure 16A). But after 96 h, the transcript level of *bHLH38* was relatively low in *35S:miR156* plants compared to WT and *spl9/spl15* plants. *BHLH39* and *bHLH101*, on the other hand, showed similar expression patterns under iron deficiency, as both of them were repressed by miR156 after 48 h and 96 h of iron deficiency stress (Figure 16B and D). The transcript level of *bHLH100* was not affected in *spl9/spl15* and *35S:miR156* plant roots after 48 h iron deficiency (Figure 16C).

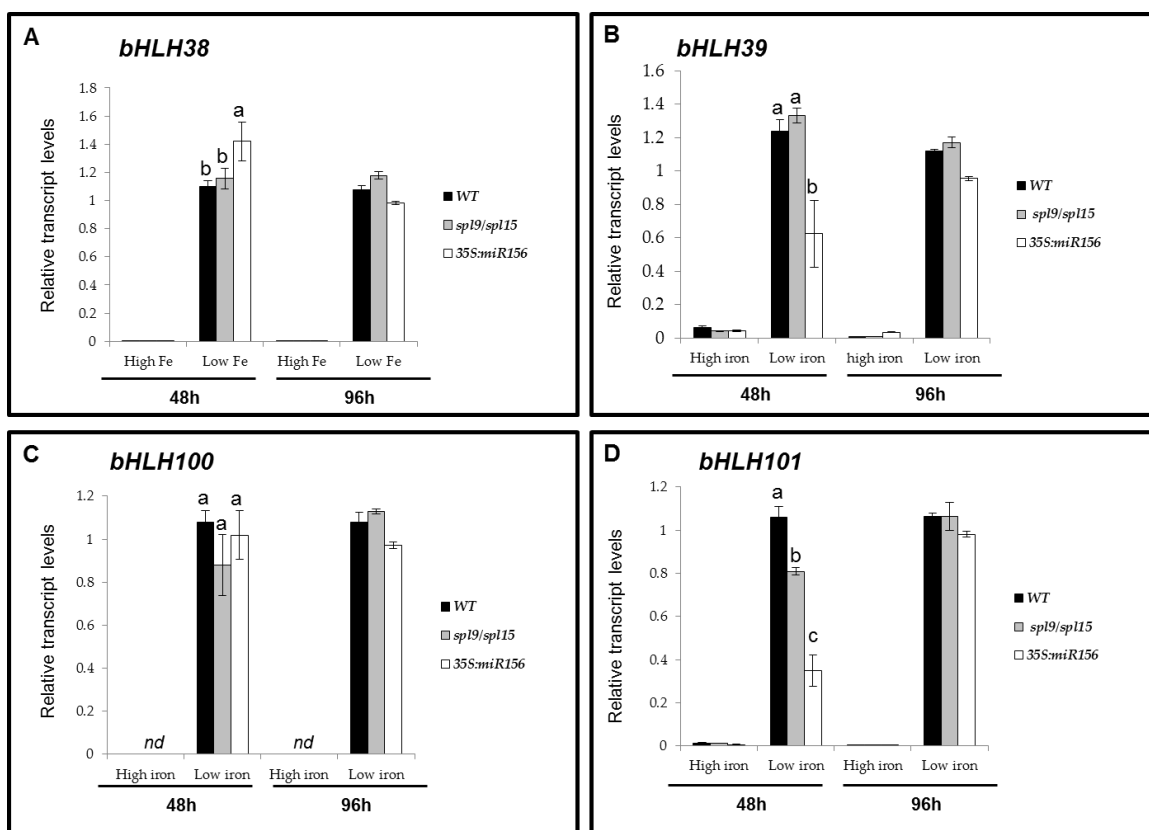


**Figure 16. Expression patterns of group I bHLH transcription factors after 48h and 96h under iron deficiency.** The transcript level was first calculated by using  $\Delta\Delta\text{CT}$  method. *SAND* was used as internal reference gene for calculation. The transcript levels of candidate genes derived from iron deficiency condition (no-iron medium, described in **section 2.1**) and the transcript levels derived from normal growth condition (high-iron medium) were tested. The qRT-PCR results are shown as mean  $\pm$  standard error of three biological replicates. Values shown with the same letter under the same condition indicate no significant difference at  $P \leq 0.05$ .

### 3.4.3 MiR156 transiently upregulates iron uptake genes

To assess the effect of miR156 on iron uptake under iron deficiency, we tested for expression of key genes involved in this transport, including *IRT1*, *AHA2*, *FRO2*, and *FRO3*. My analysis revealed that the transcription levels of *IRT1*, *FRO2*, and *FRO3* were enhanced in all three sets of plants under iron deficiency (Figure 17A, C, and D). *AHA2*, on the other hand, was only induced under iron deficiency in *35S:miR156* plants (Figure 17B)

### 3.5 SPL9 and SPL15 bind to the promoters of *FIT* and *PYE* genes

To test whether miR156 affects iron homeostasis directly through miR156/SPL regulatory network, ChIP-qPCR assay was used to determine the binding capability of SPL9 and SPL15 to the promoters of *FIT* and *PYE*. To examine whether SPL-GFP fusions were produced, the SPL9-GFP and SPL15-GFP fusion proteins were examined in transgenic *pSPL9:SPL9-GFP* and *pSPL15:SPL15-GFP* Arabidopsis plants using confocal microscopy. As the confocal microscopy showed, both SPL9-GFP and SPL15-GFP were co-localized with DAPI in the nucleus (Figure 18). This result indicated that the transgenic plants possess translated fusion proteins and are suitable for further examination. According to the ChIP-qPCR results, both SPL9 and SPL15 proteins could bind to the promoters of *FIT* (Figure 19) and *PYE* (Figure 20) genes. For *FIT* promoter (Figure 19A), both SPL9 and SPL15 showed similar binding strength to the putative SPL binding site I (Figure 19B). The binding capabilities of SPL9 and SPL15 to the putative

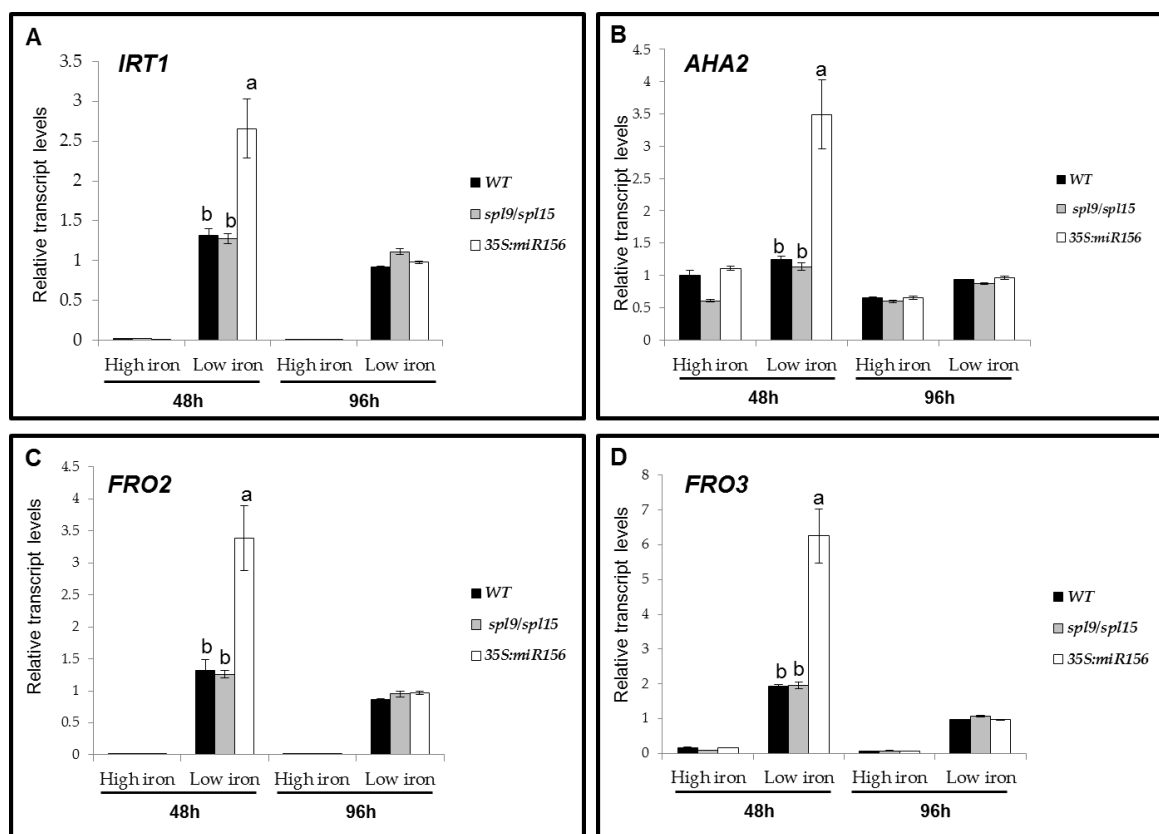


**Figure 17. Expression patterns of iron uptake genes under iron deficiency condition.**

The transcript level was first calculated by using  $\Delta\Delta CT$  method. *SAND* was used as internal reference gene for calculation. The transcript levels of candidate genes derived from iron deficiency condition (no-iron medium, described in **section 2.1**) and the transcript levels derived from normal growth condition (high-iron medium) were tested. The qRT-PCR results are shown as mean  $\pm$  standard error of three biological replicates. Values shown with the same letter under the same condition indicate no significant difference at  $P \leq 0.05$ .

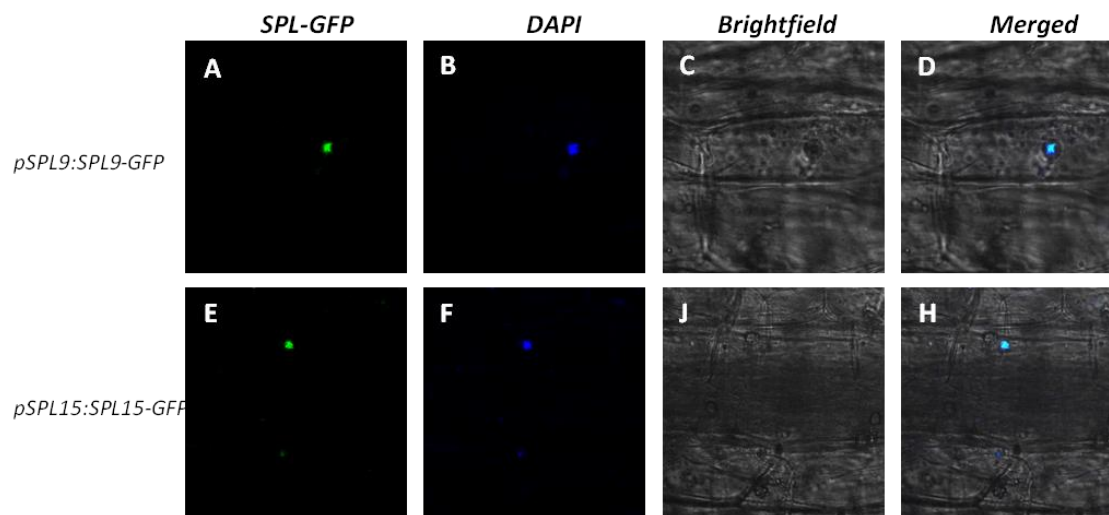


**Figure 18. Localization of SPL9-GFP (upper panels) and SPL15-GFP (lower panels).**

The SPL9-GFP and SPL15-GFP fusion proteins were first confirmed in transgenic plants harboring *pSPL9:SPL9-GFP* and *pSPL15:SPL15-GFP*. Because SPL proteins are transcription factors and localized in nucleus, the SPL-GFP fusion protein should be localized in nucleus. *In vivo* localization of the SPL-GFP fusion protein in leaves of positive transformants (**A** and **E**), the same area of leaf was stained with DAPI (**B** and **F**), which was used as a marker of nucleus. Brightfield images of the same leaf region (**C** and **J**) were captured. Merged pictures showing SPL-GFP and DAPI are co-localized in nucleus (**D** and **H**).

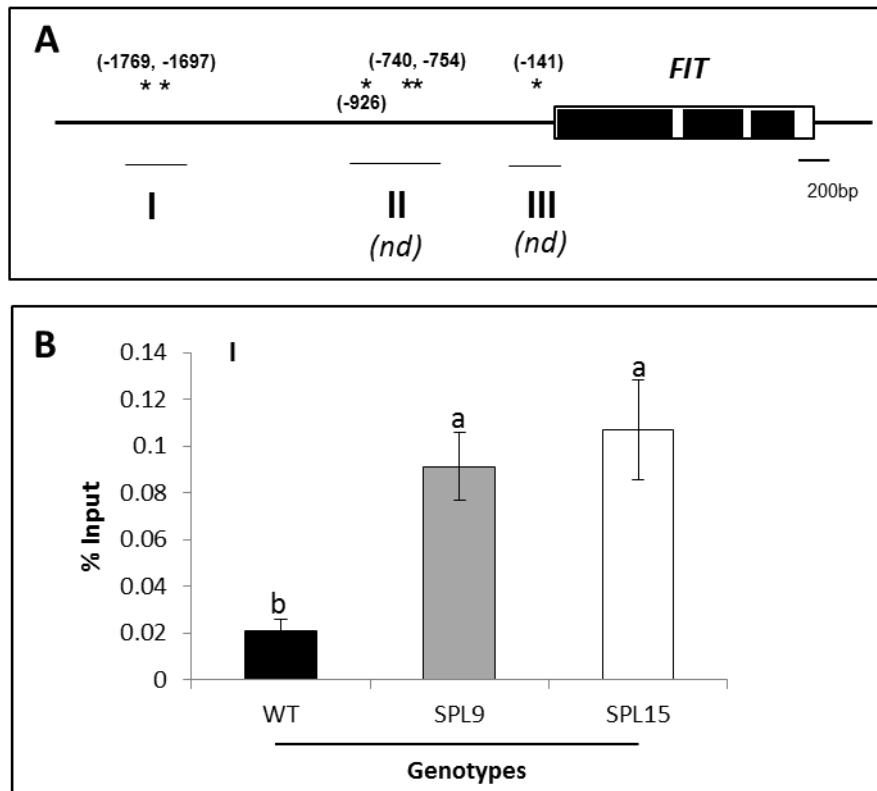


**Figure 19. Detection of SPL9 and SPL15 binding to *FIT* promoter by ChIP-qPCR.**

(A) Schematic representation of the promoter region of *FIT* showing putative SPL binding sites (indicated by asterisks). Numbers in brackets indicate the positions of binding sites relative to the translation start codon of *FIT*. Roman numerals indicate the sites were tested by qPCR. *nd*, not detected. (B) ChIP-qPCR analysis on putative SPL binding site I. Each ChIP-qPCR histogram indicates the mean  $\pm$  standard error of four biological replicates. Enrichment values were normalized to input. Genotype SPL9 and SPL15 indicate *pSPL9:SPL9-GFP* and *pSPL15:SPL15-GFP* transgenic plants.

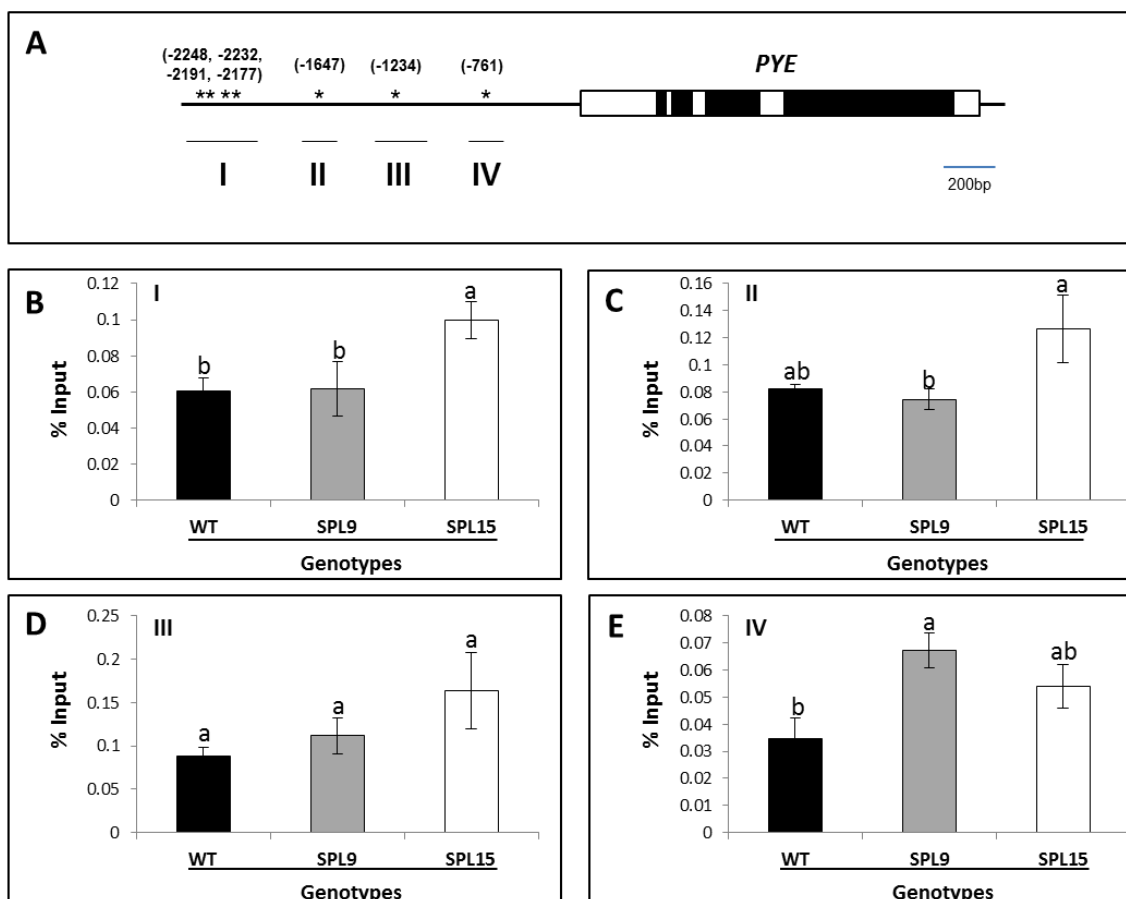


**Figure 20. Detection of SPL9 and SPL15 binding to *PYE* promoter by ChIP-qPCR.**

(A) Schematic representation of the promoter region of *PYE*. Asterisks indicate locations of putative SPL binding sites on *PYE* promoter. Numbers in brackets indicate the position of binding sites relative to the translation start codon of *PYE*. Roman numerals indicate the sites were tested by qPCR. (B-E) ChIP-qPCR analysis on putative SPL binding sites I, II, III, and IV, respectively. Each ChIP-qPCR histogram indicates the mean  $\pm$  standard error of four replicate results. Enrichment values were normalized to input. Genotypes SPL9 and SPL15 indicate *pSPL9:SPL9-GFP* and *pSPL15:SPL15-GFP* transgenic plants.

binding site II in *FIT* promoter were not conclusive for me to draw any conclusion, whereas binding site III could not be examined due to the very high background generated in the ChIP-qPCR assay. For *PYE* promoter (Figure 20A), SPL15 was found to bind to sites I, II, and IV (Figure 20B, C, D), but SPL9 could bind only to site IV (Figure 19E).

## Chapter IV. Discussion

### 4.1 Research overview

Since the discovery of the first miRNA (*lin-4*) back in the early 1990s (Lee *et al.* 1993), major advances have been made in investigating the function of miRNAs in animals and plants (Ambros 2004; Bartel 2004). MiR156 is one of the most studied miRNAs in plants. Functional characterization of miR156 revealed it has versatile roles in multiple aspects of plant growth and development. In this project, I attempted to identify novel functions for miR156 that have not been reported in the literature. To that end, Next-Generation RNA-Sequencing (NG-RNA-SEQ) was first employed to profile the differences in transcriptomes between miR156 overexpression line (*35S:miR156*) and wild-type (WT) plants at the bolting stage. The results of NG-RNA-SEQ revealed a cluster of iron homeostasis-related genes that were differentially expressed in *35S:miR156* relative to WT. This finding led me to hypothesize that the miR156/SPL regulatory network participates in regulating iron homeostasis in Arabidopsis.

### 4.2 Overexpression of miR156 impacts global gene expression

NG-RNA-SEQ results revealed that 1,139 and 142 genes were differentially expressed in rosette leaves and roots, respectively, in *35S:miR156* plants compared to WT. The number of differentially expressed genes in leaves is about eight times higher than that in roots. So far, no direct evidence indicates that overexpression of miR156 influences the root architecture in Arabidopsis. Meanwhile, our results indicated that when WT and *35S:miR156* plants are grown under normal condition for 10 days, their roots showed no

significant morphological difference. On the other hand, overexpression of miR156 in *Arabidopsis* leads to constant emerging of rosette leaves and delayed flowering (Wei *et al.* 2012). The differences in morphology between shoot and root might explain the higher number of differentially expressed genes in rosette leaves relative to roots of *35S:miR156*. The present NG-RNA-SEQ results mirror to some extent results of a similar analysis conducted in rice, where the expression of over 3000 genes was found to be affected by *miR156* overexpression (Xie *et al.* 2012), with most of the 3,000 genes being up-regulated in leaves. Although *Arabidopsis* and rice are not evolutionarily closely related, the functional conservation of miR156 among species may to some extent explain the similarity in the large number of genes that were differentially expressed.

Since the Gene Ontology (GO) can display only some broad or specific distribution of genes, the interesting question will be uncovering the correlation between GO distribution within a given reference genome and the global gene expression pattern. Based on this purpose, Parametric Analysis of Gene Set Enrichment (PAGE) which combines the expression value and GO analysis to provide a more accurate view of unexpected genes was carried out in this study.

Comparing the PAGE results between shoots and roots, it is obvious that the GO terms with significant Z-scores differentially occurred. Regarding the GO term response to stimuli in the rosette leaves, it is plausible that more stress existed in *35S:miR156* plants than in WT if as high as 8 times Z-score was shown. On the contrary, response to stimuli was not significantly observed in roots. In addition, the transcription regulator activity also displayed different change profiles in shoots, and unexpectedly also in the roots. All these results suggested that miR156 may play essential role in shoot and root

development and in stress response. However, interpreting this information is challenging due to the broad biological categories in the GO system and the coverage of NG-RNA-SEQ data.

### 4.3 Overexpression of miR156 affects multiple iron homeostasis genes

After obtaining NG-RNA-SEQ data, I manually examined the list of differentially expressed genes. Multiple iron homeostasis-related genes were affected by overexpression of miR156 (Figure 10). These differentially expressed genes were further divided into three groups: I, ferritin coding genes; II, genes coding transcription factors have role in iron homeostasis; III, iron uptake enzyme coding genes. Among the group I, only *FER4* was detectable in both roots and leaves. *FER1*, *FER3*, and *FER4* showed enhanced expression in leaves of *35S:miR156* compared to WT. I proposed that the elevated iron content in *35S:miR156* may explain the high expression of genes encoding iron storage proteins, including *FER1*, *FER3*, and *FER4*, in rosette leaves of *35S:miR156* plants. This may also explain why *35S:miR156* plants show decreased expression of genes that encode transcription factors and enzymes that participate in iron uptake, including *AHA2*, *FRO2*, and Ib group bHLH transcription factors.

Among the differentially expressed genes, two encoding bHLH family of transcription factors were down-regulated in rosette leaves and roots of *35S:miR156* plants compared to WT (Table 2). In Arabidopsis, the roles of these two genes are closely related to the regulation of iron homeostasis. Loss-of-function *bhlh100/bhlh101* double mutant produced hypersensitivity to iron deficiency. Interestingly, the *bhlh100/bhlh101*

mutant exhibits more rosette leaves at flowering compared to WT (Sivitz *et al.* 2012). One of the most pronounced phenotypes caused by overexpression of miR156 in Arabidopsis is the enhanced rosette leaf number. Due to the similarity in phenotype between *35S:miR156* and *bhlh100/bhlh101*, it is tempting to suggest a crosstalk between miR156/*SPL* gene regulatory network and *bHLH100/bHLH101* signalling pathway.

#### **4.4 MiR156 affects plant growth under iron deficiency but not iron contents**

There was no statistically significant difference in iron content between rosette leaves of WT and *35S:miR156* in my experimental set-up. Nevertheless, the difference in the expression patterns of iron homeostasis-related genes between the two plant lines warranted further investigation of their growth under iron deficiency.

Under normal growth conditions, there was no difference in shoot morphology between 10-day-old *spl9/spl15*, *35S:miR156* and WT plants, neither was there a significant difference in root architecture between the three sets of plants when grown under normal condition. On the other hand, when plants were grown in a low-iron medium, root elongation was severely repressed in WT compared to *spl9/spl15* and *35S:miR156* plants. Both *spl9/spl15* and *35S:miR156* plants maintained similar root length under both growth conditions, but *35S:miR156* had the most lateral root branches compared to *spl9/spl15* and WT. These results may indicate that overexpression of miR156 can enhance plant growth under iron deficiency conditions at least partially by targeting *SPL9* and *SPL15*.

It is worth noting that iron accumulation in mature rosette leaves was not affected by miR156, as WT, *spl9/spl15*, and *35S:miR156* plants had similar levels of iron in rosette leaves. However, NG-RNA-SEQ results clearly showed that the iron uptake-related genes were down-regulated in *35S:miR156* plants at the bolting stage. This may suggest the involvement of other signalling pathways in regulating iron accumulation to maintain iron levels at a certain range and avoid the negative impacts of excessive iron, which may cause increased reactive oxygen species (ROS) stress (Connolly and Guerinot 2002). Combined, these findings suggest that overexpression of miR156 in Arabidopsis acts to enhance plant growth but only under low-iron condition.

#### **4.5 Overexpression of miR156 affects ferric reduction but not rhizosphere acidification**

Schmidt et al. (2000) used the whole root as a unit to test root ferric reduction. This was done to avoid inaccurate results due to the non-linear relationship between reduction ability and root mass (Schmidt *et al.* 2000). In my study, there were significant differences in root length and lateral branch number (Figure 12C and E) between WT, *spl9/spl15*, and *35S:miR156* when grown under iron deficiency, and so I also used the whole root to study ferric reduction and rhizosphere acidification. These processes are two major steps in iron acquisition. Since *35S:miR156* plants showed better growth than WT under iron deficiency, it is possible that plants with enhanced miR156 expression have a better ability to mobilize iron from the rhizosphere.

Ferric reduction ability was increased in all three genotypes under iron deficiency. However, when grown under iron-deficiency, both *35S:miR156* and *spl9/spl15* roots showed higher levels of ferric reduction rate when compared with WT plants. This could partially explain why *35S:miR156* and *spl9/spl15* have better growth under iron deficiency. Ferric reduction is catalyzed by FRO family of proteins in Arabidopsis (Connolly *et al.* 2003, Mukherjee *et al.* 2006, Robinson *et al.* 1999). FRO2 contributes the most to the reduced ferric iron in the rhizosphere (Connolly *et al.* 2003). There is also bioinformatics evidence indicating that FRO3 is localized to the mitochondria and might contribute to mitochondrial iron homeostasis (Jain *et al.* 2014). FRO7 is critical for iron mobilization into the chloroplast. In *fro7* loss-of-function mutant, plant chloroplasts contain 33% less iron compared to WT plants (Jeong and Connolly 2009). My NG-RNA-SEQ results showed that *FRO2*, *FRO3*, and *FRO7* were down-regulated in *35S:miR156* roots grown under normal conditions, suggesting that the overexpression of miR156 not only affect iron uptake from the rhizosphere but also iron relocation within the plant.

#### **4.6 MiR156 up-regulates iron homeostasis genes under iron deficiency**

To gain an understanding of why *35S:miR156* plants maintain normal growth under iron deficiency, the expression patterns of major iron homeostasis-related genes were examined in roots of WT, *spl9/spl15*, and *35S:miR156* plants. The genes encoding two major transcription factors FIT and PYE, which are involved in iron homeostasis, were both up-regulated with different expression levels in WT, *spl9/spl15*, and *35S:miR156* plants under iron deficiency condition.

As a key regulator of iron homeostasis, FIT plays a critical role in activating the transcription of major iron homeostasis-related genes, such as *AHA2*, *IRT1*, and *FRO2* (Jakoby *et al.* 2004; Yuan *et al.* 2008). Under iron deficiency condition, *FIT* was up-regulated in all three genotypes after 48- and 96-h iron deprivation stress, more *FIT* expression was detected in roots of *35S:miR156* compared to WT and *spl9/spl15* after 48 h. It seems that *FIT* was up-regulated in *spl9/spl15* in a transient manner; i.e. up until 96 h of iron-deficiency stress. The enhanced level of FIT makes it possible that the transcription of down-stream genes that participate in iron homeostasis could be induced in *35S:miR156* plants. However, the fact that such a miR156 effect could only be partially mimicked in loss-of-function of *SPL9* and *SPL15* mutant shows that other SPL proteins may play a redundant role in regulating the transcription of *FIT* gene. Thus, the better growth of *35S:miR156* plants (relative to WT) under low-iron condition can be partially explained by a transient elevation in *FIT* transcript level.

PYE is critical for inducing about one third of the genes involved in Arabidopsis response to iron-deficiency (Long *et al.* 2010). Under iron-deficiency condition, loss of *PYE* function leads to severe plant growth retardation, including chlorosis and repressed root elongation. Interestingly, the *pye-1* mutant had elevated iron content, decreased tolerance to iron deprivation, decreased iron reductase activity, and a weaker iron deficiency response compared to WT (Long *et al.* 2010). These results indicate that *PYE* is critical in activating transcription of iron homeostasis-related genes as well as iron relocation within the plant. In my study, I found *PYE* to be up-regulated under iron-deficiency after 48- and 96-h treatment in both *spl9/spl15* and *35S:miR156* roots compared to WT plants. This result suggests that overexpression of miR156 not only

affects the transcription of iron homeostasis-related genes, but may also influence the iron relocation within plants.

*BHLH38*, *bHLH39*, *100*, *101* belong to the Ib subgroup of basic helix-loop-helix transcription factors. These genes have been shown to play critical roles in root response to iron deficiency (Sivitz *et al.* 2012; Yuan *et al.* 2008). In this research, I found this group of *bHLH* genes to be up-regulated under iron deficiency condition in WT, *spl9/spl15*, and *35S:miR156* plants. But the expression of *bHLH38*, *bHLH39*, *bHLH100*, and *bHLH101* showed different patterns in different sets of plants. After 48 h of growth under iron deficiency, only *bHLH38* was slightly up-regulated in *35S:miR156*, whereas the expression levels of *bHLH39* and *bHLH101* were transiently suppressed in this plant. Moreover, the expression of *bHLH100* was not affected by overexpression of miR156 or loss-function of SPL9 and SPL15, indicating that these group Ib bHLH transcription factors may participate in different levels of iron homeostasis regulation.

Furthermore, although FIT is required for activating transcription of *bHLH38*, *bHLH39*, *bHLH100*, and *bHLH101*, the expression of these Ib group *bHLH* genes was not affected by overexpression of *FIT* (Wang *et al.* 2007). This indicates that another regulatory pathway may be coordinating with the FIT-dependent pathway to regulate plant iron homeostasis through selective regulation of Ib group *bHLH* genes. Thus, the increased *FIT* level in *35S:miR156* plants did not yield enhanced expression of *bHLH39*, *100*, and *101*, suggesting that miR156 can only participate in FIT-dependent regulation of iron homeostasis.

Regarding the genes that participate in iron uptake, the transcript levels of *AHA2*, *FRO2*, *FRO3*, and *IRT1* were transiently up-regulated in *35S:miR156* plants. Although

AHA2 is critical for Arabidopsis rhizosphere acidification, higher transcript levels of *AHA2* did not increase the acidification ability of *35S:miR156* roots. This result indicates that miR156 can only participate in the transcriptional regulation of *AHA2* but not in the post-transcriptional regulation. Furthermore, the putative role of FRO3 in mitochondrial iron homeostasis indicates a potential role for miR156 in intracellular iron relocation. An important point here is that *spl9/spl15* double mutant could not mimic the effects caused by overexpression of miR156 on these genes, indicating a possible redundant role for other SPLs in regulating these genes, and that a higher order of knockout mutant may be required to fully mimic the effects caused by overexpression of miR156.

#### **4.7 Cross talk between phytohormone, miR156, and iron homeostasis**

MiR156 is induced in roots by phosphorus-, nitrogen-, and potassium-deficiency, with the highest induction occurring under nitrogen-deficiency (Hsieh *et al.* 2009). By combining the gene expression patterns of iron homeostasis-related genes and results of plant growth under iron deficiency, a putative role for miR156 in iron homeostasis can be proposed. Furthermore, as phytohormones, especially auxin and ethylene play important roles in the regulation of iron homeostasis (Chen *et al.* 2010; Garcia *et al.* 2011; Giehl *et al.* 2012; Lingam *et al.* 2011), a cross talk between miR156 and phytohormones should not be overlooked.

Relationships between miR156, auxin, and gibberellin signalling pathways have been proposed and partially examined (Xing *et al.* 2013; Yu *et al.* 2012). Recently, a grafting-based experiment showed that miR156 could serve as a mobile messenger between shoots and roots (Bhogale *et al.* 2014). Another study examined the ferric

reduction ability of a number of mutants with defects in auxin, cytokinin, ABA, and ethylene signalling pathways. The study found that none of the mutants totally lost the ability to reduce iron, indicating that phytohormones are not required for the induction of iron reduction activity (Schmidt *et al.* 2000). The authors further suggested that iron reduction activity caused by hormonal defects could be induced by altered root architecture, especially the increased root surface area in some of the mutants. Based on the close relationship between miR156 and phytohormones, it is probable that these hormones help *35S:miR156* plants achieve better growth under iron deficiency.

Previous studies of the expression patterns of *FIT* and *IRT1* indicated that iron uptake occurs mainly in the root hair zone (Jakoby *et al.* 2004; Seguela *et al.* 2008). Although the enhanced iron-reductase activity in *Arabidopsis* can be attributed to transient up-regulation of *PYE* gene, which then activates transcription of *FRO2* and *FRO3* genes, how other iron uptake related genes, such as *AHA2*, *IRT1* are activated is still unclear. Furthermore, the *spl9/spl15* double mutant can partially recover the phenotype of *35S:miR156* plants under low-iron condition, but only part of the iron homeostasis related genes tested in this study were affected at the transcriptional level by loss-of-function of *SPL9* and *SPL15*, including *FIT*, *PYE*, and *bHLH101*. This indicated that other *SPLs*, with *SPL9* and *SPL15*, play redundant roles in regulation of plant iron homeostasis.

It is also interesting to note that the core sequence of the *SPL* binding sequence (GTAC) is identical to the reported copper responsive element (GTAC). The binding capability of *SPL* to the copper responsive element has also been shown in *Chlamydomonas* (Kropat *et al.* 2005). Furthermore, a non-miR156 targeted *SPL* gene,

*SPL7*, is a key regulator in copper-homeostasis in Arabidopsis (Yamasaki *et al.* 2009). Copper is also involved in crucial processes including ethylene perception, and oxidative stress response (Pilon *et al.* 2006). In Arabidopsis, the induction of ferric reductase activity is caused by synergistic iron and copper deficiency, and indicates that the same set of genes may be responding to both Fe and Cu deficiency (Romera *et al.* 2003). All these results indicate that SPL proteins might participate in both iron and copper homeostasis, and miR156 can partially participate in this pathway.

There are a large number of transcriptomic studies on iron homeostasis in Arabidopsis, but none of them showed miR156 as being differentially expressed in response to iron-deficiency stress. In addition, none of the miR156-targeted *SPL* genes showed changes in expression in response to iron deprivation. However, *SPL* genes can be up-regulated by low pH (Iyer-Pascuzzi *et al.* 2011). Since the reduced pH in rhizosphere is a major step in iron uptake, it is tempting to assume that the iron uptake results in a lowered rhizosphere pH environment that could further trigger pH-induced *SPL* gene expression, which would negatively regulate the iron uptake genes at the transcriptional level (Figure 20). In summary, it appears that miR156/SPL is only “the tip of the iceberg” in a complicated gene regulatory network participating in iron homeostasis, and the role of miR156 in this pathway is not regulated by low iron condition.

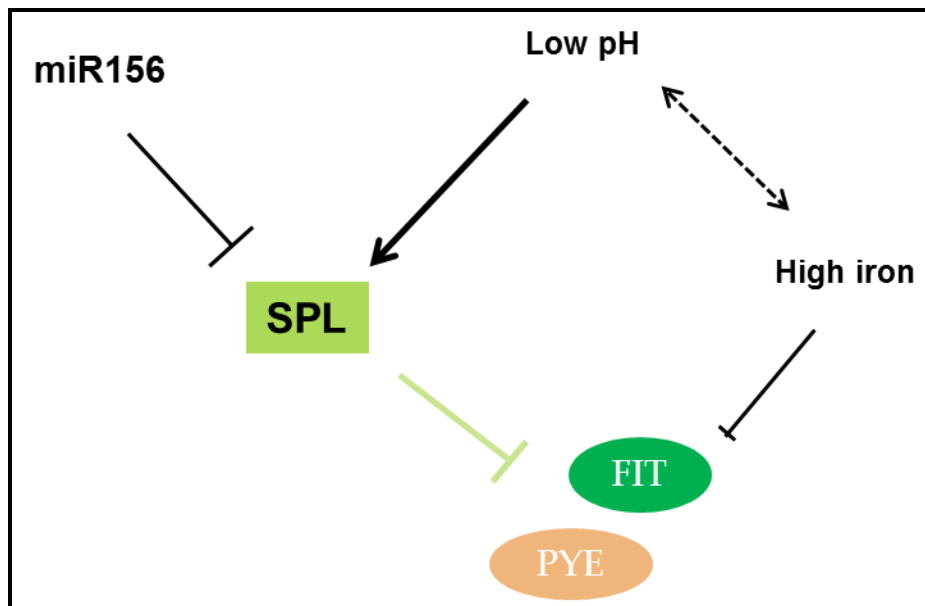


**Figure 21. A proposed model for the regulatory pathway involving miR156/SPL, pH, and iron availability.** Solid black or green lines with a perpendicular bar indicate repression of downstream genes expression. For the plants utilize strategy I to up-take iron from rhizosphere, the first step is to lower pH to release more free iron. On the other hand, higher iron accumulation within plants can repress the transcription of FIT and PYE. Furthermore, acidic environment can trigger transcription of SPL genes, which can be suppressed by miR156.

## Chapter V. Conclusions

Development of crop cultivars that can better tolerate limited minerals has always been a focus of the breeding industry (Ortiz-Monasterio *et al.* 2007; Welch and Graham 2004). My research clearly shows that overexpression of miR156 improves plant growth under low iron conditions due presumably to longer and more branched roots, which may allow the plant to reach deeper into the soil to acquire mineral nutrients under normal field conditions.

To our knowledge, based on the newly released transcriptomic data (Kong and Yang 2010; Schuler *et al.* 2011; Thimm *et al.* 2001; Waters *et al.* 2012), there are no reports in the literature pointing to the induction of the miR156/SPL regulatory network by iron deficiency. Furthermore, a synergistic role of miR156 and multiple phytohormones that can manipulate plant roots' architecture has been demonstrated (Eviatar-Ribak *et al.* 2013; Xing *et al.* 2013a). Given that iron uptake genes were only transiently up-regulated in *35S:miR156* plants under iron deficiency, combined with the tight relationship between miR156 and phytohormones, it is tempting to speculate that the phenotypes caused by overexpression of miR156 or loss-of-function of *SPL9* and *SPL15* under low-iron condition may be the side effects of phytohormone signalling pathways. It is important to note that a number of proteins in iron homeostasis also have roles in plant acquisition of other metallic nutrients, such as IRT1 which can transport zinc, iron, and manganese (Korshunova *et al.* 1999). It may be necessary to examine other elements in *35S:miR156* plants besides iron. It is also possible that SPL proteins may regulate down-stream genes through protein-protein interaction with other bHLH transcription factors (Gou *et al.* 2011a).

Although miR156 has been employed in crop molecular breeding for many years (Aung *et al.* 2014; Fu *et al.* 2012; Wang *et al.* 2014; Zhang *et al.* 2011), a more detailed understanding of its gene regulatory network is needed to fully assess the utility of this molecule in crop quality improvement. In this regard, my research may provide a slightly deeper understanding of the complicated regulatory network controlled by miR156.

## References

- Ambros, V.** (2004) The functions of animal microRNAs. *Nature*, **431**, 350-355.
- Aung, B., Gruber, M.Y., Amyot, L., Omari, K., Bertrand, A. and Hannoufa, A.**  
(2014) MicroRNA156 as a promising tool for alfalfa improvement. *Plant Biotechnology Journal*. (Epub ahead print, DOI: 10.1111/pbi.12308.)
- Barberon, M., Zelazny, E., Robert, S., Conejero, G., Curie, C., Friml, J. and Vert, G.** (2011) Monoubiquitin-dependent endocytosis of the iron-regulated transporter 1 (IRT1) transporter controls iron uptake in plants. *Proceedings of the National Academy of Sciences*, **108**, E450-458.
- Bartel, D.P.** (2004) MicroRNAs: genomics, biogenesis, mechanism, and function. *Cell*, **116**, 281-297.
- Bauer, P., Ling, H.-Q. and Guerinot, M.L.** (2007) FIT, the FER-like iron deficiency induced transcription factor in Arabidopsis. *Plant Physiology and Biochemistry*, **45**, 260-261.
- Bhogale, S., Mahajan, A.S., Natarajan, B., Rajabhoj, M., Thulasiram, H.V. and Banerjee, A.K.** (2014) MicroRNA156: a potential graft-transmissible microRNA that modulates plant architecture and tuberization in *Solanum tuberosum ssp. andigena*. *Plant Physiology*, **164**, 1011-1027.
- Briat, J.-F., Curie, C. and Gaymard, F.** (2007) Iron utilization and metabolism in plants. *Current Opinion in Plant Biology*, **10**, 276-282.
- Briat, J.-F. and Lobréaux, S.** (1997) Iron transport and storage in plants. *Trends in Plant Science*, **2**, 187-193.
- Brown, J.C.** (1961) Iron chlorosis in plants. *Advances in Agronomy*, **13**, 329-369.

- Brumbarova, T., Bauer, P. and Ivanov, R.** (2015) Molecular mechanisms governing Arabidopsis iron uptake. *Trends in Plant Science*, **20**, 124-133.
- Cakmak, I.** (2002) Plant nutrition research: Priorities to meet human needs for food in sustainable ways. In *Progress in Plant Nutrition: Plenary Lectures of the XIV International Plant Nutrition Colloquium*: Springer, pp. 3-24.
- Chatzistathis, T. and Therios, I.** (2013) How Soil Nutrient Availability Influences Plant Biomass and How Biomass Stimulation Alleviates Heavy Metal Toxicity in Soils: The Cases of Nutrient Use Efficient Genotypes and Phytoremediators, Respectively. In *Biomass Now - Cultivation and Utilization*: InTech, Chapter 18.
- Chen, W.W., Yang, J.L., Qin, C., Jin, C.W., Mo, J.H., Ye, T. and Zheng, S.J.** (2010) Nitric oxide acts downstream of auxin to trigger root ferric-chelate reductase activity in response to iron deficiency in Arabidopsis. *Plant Physiology*, **154**, 810-819.
- Chiou, T.J.** (2007) The role of microRNAs in sensing nutrient stress. *Plant, Cell & Environment*, **30**, 323-332.
- Cho, S.H., Coruh, C. and Axtell, M.J.** (2012) miR156 and miR390 regulate tasiRNA accumulation and developmental timing in *Physcomitrella patens*. *Plant Cell*, **24**, 4837-4849.
- Chuck, G., Cigan, A.M., Saeteurn, K. and Hake, S.** (2007b) The heterochronic maize mutant *Corngrass1* results from overexpression of a tandem microRNA. *Nature Genetics*, **39**, 544-549.
- Colangelo, E.P. and Guerinot, M.L.** (2004) The essential basic helix-loop-helix protein FIT1 is required for the iron deficiency response. *Plant Cell*, **16**, 3400-3412.

- Connolly, E.L. and Guerinot, M.L.** (2002) Iron stress in plants. *Genome Biology*, **3**, 1024.1-1024.4.
- Connolly, E.L., Campbell, N.H., Grotz, N., Prichard, C.L. and Guerinot, M.L.** (2003) Overexpression of the FRO2 ferric chelate reductase confers tolerance to growth on low iron and uncovers posttranscriptional control. *Plant Physiology*, **133**, 1102-1110.
- Curie, C., Panaviene, Z., Loulergue, C., Dellaporta, S.L., Briat, J.-F. and Walker, E.L.** (2001) Maize yellow stripe1 encodes a membrane protein directly involved in Fe (III) uptake. *Nature*, **409**, 346-349.
- Desforges, J.F. and Oski, F.A.** (1993) Iron deficiency in infancy and childhood. *New England Journal of Medicine*, **329**, 190-193.
- Du, Z., Zhou, X., Ling, Y., Zhang, Z. and Su, Z.** (2010) agriGO: a GO analysis toolkit for the agricultural community. *Nucleic Acids Research*, **38**, W64-70.
- Dugas, D.V. and Bartel, B.** (2004) MicroRNA regulation of gene expression in plants. *Current Opinion in Plant Biology*, **7**, 512-520.
- Eviatar-Ribak, T., Shalit-Kaneh, A., Chappell-Maor, L., Amsellem, Z., Eshed, Y. and Lifschitz, E.** (2013) A cytokinin-activating enzyme promotes tuber formation in tomato. *Current Biology*, **23**, 1057-1064.
- Fehr, W.R.** (1982) Control of iron-deficiency chlorosis in soybeans by plant breeding. *Journal of Plant Nutrition*, **5**, 611-621.
- Fernández, V. and Ebert, G.** (2005) Foliar iron fertilization: a critical review. *Journal of Plant Nutrition*, **28**, 2113-2124.

- Fu, C., Sunkar, R., Zhou, C., Shen, H., Zhang, J.Y., Matts, J., Wolf, J., Mann, D.G., Stewart, C.N., Jr., Tang, Y. and Wang, Z.Y.** (2012) Overexpression of miR156 in switchgrass (*Panicum virgatum* L.) results in various morphological alterations and leads to improved biomass production. *Plant Biotechnol Journal*, **10**, 443-452.
- Fukuyama, K.** (2004) Structure and function of plant-type ferredoxins. *Photosynthesis Research*, **81**, 289-301.
- Garcia, M.J., Suarez, V., Romera, F.J., Alcantara, E. and Perez-Vicente, R.** (2011) A new model involving ethylene, nitric oxide and Fe to explain the regulation of Fe-acquisition genes in Strategy I plants. *Plant Physiology and Biochemistry*, **49**, 537-544.
- Gendrel, A.V., Lippman, Z., Martienssen, R. and Colot, V.** (2005) Profiling histone modification patterns in plants using genomic tiling microarrays. *Nature Methods*, **2**, 213-218.
- Giehl, R.F., Lima, J.E. and von Wiren, N.** (2012) Localized iron supply triggers lateral root elongation in Arabidopsis by altering the AUX1-mediated auxin distribution. *Plant Cell*, **24**, 33-49.
- Gil, V.M. and Ferreira, J.S.** (2014) Anemia and iron deficiency in heart failure. *Revista Portuguesa de Cardiologia (English Edition)*, **33**, 39-44.
- Gou, J.Y., Felippes, F.F., Liu, C.J., Weigel, D. and Wang, J.W.** (2011b) Negative regulation of anthocyanin biosynthesis in Arabidopsis by a miR156-targeted SPL transcription factor. *Plant Cell*, **23**, 1512-1522.

- Grotz, N. and Guerinot, M.L.** (2006) Molecular aspects of Cu, Fe and Zn homeostasis in plants. *Biochimica et Biophysica Acta (BBA)-Molecular Cell Research*, **1763**, 595-608.
- Gunawardena, S. and Dunlap, M.E.** (2012) Anemia and iron deficiency in heart failure. *Current Heart Failure Reports*, **9**, 319-327.
- Guo, A.Y., Zhu, Q.H., Gu, X., Ge, S., Yang, J. and Luo, J.** (2008) Genome-wide identification and evolutionary analysis of the plant specific SBP-box transcription factor family. *Gene*, **418**, 1-8.
- Halimaa, P., Lin, Y.F., Ahonen, V.H., Blande, D., Clemens, S., Gyenesi, A., Haikio, E., Karenlampi, S.O., Laiho, A., Aarts, M.G., Pursiheimo, J.P., Schat, H., Schmidt, H., Tuomainen, M.H. and Tervahauta, A.I.** (2014) Gene expression differences between *Noccaea caerulea* ecotypes help to identify candidate genes for metal phytoremediation. *Environmental Science & Technology*, **48**, 3344-3353.
- Han, B., Yang, Z., Samma, M.K., Wang, R. and Shen, W.** (2013) Systematic validation of candidate reference genes for qRT-PCR normalization under iron deficiency in Arabidopsis. *Biometals*, **26**, 403-413.
- Hell, R. and Stephan, U.W.** (2003) Iron uptake, trafficking and homeostasis in plants. *Planta*, **216**, 541-551.
- Hsieh, L.C., Lin, S.I., Shih, A.C., Chen, J.W., Lin, W.Y., Tseng, C.Y., Li, W.H. and Chiou, T.J.** (2009) Uncovering small RNA-mediated responses to phosphate deficiency in Arabidopsis by deep sequencing. *Plant Physiology*, **151**, 2120-2132.

- Hu, W., Wang, T., Xu, J. and Li, H.** (2014) MicroRNA mediates DNA methylation of target genes. *Biochemical and Biophysical Research Communications*, **444**, 676-681.
- Hultquist, J.F. and Dorweiler, J.E.** (2008) Feminized tassels of maize mop1 and ts1 mutants exhibit altered levels of miR156 and specific SBP-box genes. *Planta*, **229**, 99-113.
- Hwan Lee, J., Joon Kim, J. and Ahn, J.H.** (2012) Role of SEPALLATA3 (SEP3) as a downstream gene of miR156-SPL3-FT circuitry in ambient temperature-responsive flowering. *Plant Signaling & Behavior*, **7**, 1151-1154.
- Iannotti, L.L., Tielsch, J.M., Black, M.M. and Black, R.E.** (2006) Iron supplementation in early childhood: health benefits and risks. *American Journal of Clinical Nutrition*, **84**, 1261-1276.
- Iyer-Pascuzzi, A.S., Jackson, T., Cui, H., Petricka, J.J., Busch, W., Tsukagoshi, H. and Benfey, P.N.** (2011) Cell identity regulators link development and stress responses in the Arabidopsis root. *Developmental Cell*, **21**, 770-782.
- Jain, A., Wilson, G.T. and Connolly, E.L.** (2014) The diverse roles of FRO family metalloredutases in iron and copper homeostasis. *Frontiers in Plant Science*, **5**, 100.
- Jakoby, M., Wang, H.Y., Reidt, W., Weisshaar, B. and Bauer, P.** (2004) FRU (BHLH029) is required for induction of iron mobilization genes in Arabidopsis thaliana. *FEBS Letters*, **577**, 528-534.
- Jeong, J. and Connolly, E.L.** (2009) Iron uptake mechanisms in plants: functions of the FRO family of ferric reductases. *Plant Science*, **176**, 709-714.

- Kerkeb, L., Mukherjee, I., Chatterjee, I., Lahner, B., Salt, D.E. and Connolly, E.L.** (2008) Iron-induced turnover of the Arabidopsis IRON-REGULATED TRANSPORTER1 metal transporter requires lysine residues. *Plant Physiology*, **146**, 1964-1973.
- Kidner, C.A. and Martienssen, R.A.** (2005) The developmental role of microRNA in plants. *Current Opinion in Plant Biology*, **8**, 38-44.
- Kim, J.J., Lee, J.H., Kim, W., Jung, H.S., Huijser, P. and Ahn, J.H.** (2012) The microRNA156-SQUAMOSA PROMOTER BINDING PROTEIN-LIKE3 module regulates ambient temperature-responsive flowering via FLOWERING LOCUS T in Arabidopsis. *Plant Physiology*, **159**, 461-478.
- Kim, S.Y. and Volsky, D.J.** (2005) PAGE: parametric analysis of gene set enrichment. *BMC Bioinformatics*, **6**, 144.
- Kobayashi, T. and Nishizawa, N.K.** (2012) Iron uptake, translocation, and regulation in higher plants. *Annual Review of Plant Biology*, **63**, 131-152.
- Kong, W.W. and Yang, Z.M.** (2010) Identification of iron-deficiency responsive microRNA genes and cis-elements in Arabidopsis. *Plant Physiology and Biochemistry*, **48**, 153-159.
- Korcak, R.F.** (1987) Iron deficiency chlorosis. *Horticultural Reviews*, **9**, 133-186.
- Korshunova, Y.O., Eide, D., Clark, W.G., Guerinot, M.L. and Pakrasi, H.B.** (1999) The IRT1 protein from *Arabidopsis thaliana* is a metal transporter with a broad substrate range. *Plant Molecular Biology*, **40**, 37-44.
- Kranz, R.G., Richard-Fogal, C., Taylor, J.-S. and Frawley, E.R.** (2009) Cytochrome c biogenesis: mechanisms for covalent modifications and trafficking of heme and

for heme-iron redox control. *Microbiology and Molecular Biology Reviews*, **73**, 510-528.

**Kropat, J., Tottey, S., Birkenbihl, R.P., Depege, N., Huijser, P. and Merchant, S.**

(2005) A regulator of nutritional copper signaling in *Chlamydomonas* is an SBP domain protein that recognizes the GTAC core of copper response element.

*Proceedings of the National Academy of Sciences*, **102**, 18730-18735.

**Kumar, A.M. and Söll, D.** (2000) Antisense HEMA1 RNA expression inhibits heme

and chlorophyll biosynthesis in *Arabidopsis*. *Plant Physiology*, **122**, 49-56.

**Lee, R.C., Feinbaum, R.L. and Ambros, V.** (1993) The *C. elegans* heterochronic gene

lin-4 encodes small RNAs with antisense complementarity to lin-14. *Cell*, **75**, 843-854.

**Lin, S., Cianzio, S. and Shoemaker, R.** (1997) Mapping genetic loci for iron deficiency

chlorosis in soybean. *Molecular Breeding*, **3**, 219-229.

**Lingam, S., Mohrbacher, J., Brumbarova, T., Potuschak, T., Fink-Straube, C.,**

**Blondet, E., Genschik, P. and Bauer, P.** (2011) Interaction between the bHLH transcription factor FIT and ETHYLENE INSENSITIVE3/ETHYLENE

INSENSITIVE3-LIKE1 reveals molecular linkage between the regulation of iron acquisition and ethylene signaling in *Arabidopsis*. *Plant Cell*, **23**, 1815-1829.

**Liu, P.P., Montgomery, T.A., Fahlgren, N., Kasschau, K.D., Nonogaki, H. and**

**Carrington, J.C.** (2007) Repression of AUXIN RESPONSE FACTOR10 by

microRNA160 is critical for seed germination and post-germination stages. *Plant Journal*, **52**, 133-146.

- Liu, Q., Yao, X., Pi, L., Wang, H., Cui, X. and Huang, H.** (2009) The ARGONAUTE10 gene modulates shoot apical meristem maintenance and establishment of leaf polarity by repressing miR165/166 in Arabidopsis. *Plant Journal*, **58**, 27-40.
- Long, T.A., Tsukagoshi, H., Busch, W., Lahner, B., Salt, D.E. and Benfey, P.N.** (2010) The bHLH transcription factor POPEYE regulates response to iron deficiency in Arabidopsis roots. *Plant Cell*, **22**, 2219-2236.
- Lu, M., Zhang, Q., Deng, M., Miao, J., Guo, Y., Gao, W. and Cui, Q.** (2008) An analysis of human microRNA and disease associations. *PloS One*, **3**, e3420.
- Marin, E., Jouannet, V., Herz, A., Lokerse, A.S., Weijers, D., Vaucheret, H., Nussaume, L., Crespi, M.D. and Maizel, A.** (2010) miR390, Arabidopsis TAS3 tasiRNAs, and their AUXIN RESPONSE FACTOR targets define an autoregulatory network quantitatively regulating lateral root growth. *Plant Cell*, **22**, 1104-1117.
- Martin, R.C., Asahina, M., Liu, P.-P., Kristof, J.R., Coppersmith, J.L., Pluskota, W.E., Bassel, G.W., Goloviznina, N.A., Nguyen, T.T. and Martínez-Andújar, C.** (2010) The regulation of post-germinative transition from the cotyledon-to vegetative-leaf stages by microRNA-targeted SQUAMOSA PROMOTER-BINDING PROTEIN LIKE13 in Arabidopsis. *Seed Science Research*, **20**, 89-96.
- May, P., Liao, W., Wu, Y., Shuai, B., McCombie, W.R., Zhang, M.Q. and Liu, Q.A.** (2013) The effects of carbon dioxide and temperature on microRNA expression in Arabidopsis development. *Nature Communications*, **4**, 2145.

- Mendoza-Soto, A.B., Sánchez, F. and Hernández, G.** (2012) MicroRNAs as regulators in plant metal toxicity response. *Frontiers in Plant Science*, **3**.
- Mengel, K.** (1994) Iron availability in plant tissues-iron chlorosis on calcareous soils. *Plant and Soil*, **165**, 275-283.
- Mori, S., Nishizawa, N., Hayashi, H., Chino, M., Yoshimura, E. and Ishihara, J.** (1991) Why are young rice plants highly susceptible to iron deficiency? *Plant and Soil*, **130**, 175-188.
- Mukherjee, I., Campbell, N.H., Ash, J.S. and Connolly, E.L.** (2006) Expression profiling of the Arabidopsis ferric chelate reductase (FRO) gene family reveals differential regulation by iron and copper. *Planta*, **223**, 1178-1190.
- Naeve, S.L.** (2006) Iron Deficiency Chlorosis in Soybean. *Agronomy Journal*, **98**, 1575-1581.
- Ortiz-Monasterio, J., Palacios-Rojas, N., Meng, E., Pixley, K., Trethowan, R. and Pena, R.** (2007) Enhancing the mineral and vitamin content of wheat and maize through plant breeding. *Journal of Cereal Science*, **46**, 293-307.
- Palmgren, M.G.** (2001) PLANT PLASMA MEMBRANE H<sup>+</sup>-ATPases: Powerhouses for Nutrient Uptake. *Annual Review of Plant Physiology and Plant Molecular Biology*, **52**, 817-845.
- Pant, B.D., Musialak-Lange, M., Nuc, P., May, P., Buhtz, A., Kehr, J., Walther, D. and Scheible, W.R.** (2009) Identification of nutrient-responsive Arabidopsis and rapeseed microRNAs by comprehensive real-time polymerase chain reaction profiling and small RNA sequencing. *Plant Physiol*, **150**, 1541-1555.

- Pilon, M., Abdel-Ghany, S.E., Cohu, C.M., Gogolin, K.A., Ye, H.** (2006) Copper cofactor delivery in plant cells. *Current Opinion in Plant Biology*, **3**, 256-263.
- Ravet, K. and Pilon, M.** (2013) Copper and iron homeostasis in plants: the challenges of oxidative stress. *Antioxidants & Redox Signaling*, **19**, 919-932.
- Reinhart, B.J., Weinstein, E.G., Rhoades, M.W., Bartel, B. and Bartel, D.P.** (2002) MicroRNAs in plants. *Genes & Development*, **16**, 1616-1626.
- Robinson, N.J., Procter, C.M., Connolly, E.L. and Guerinot, M.L.** (1999) A ferric-chelate reductase for iron uptake from soils. *Nature*, **397**, 694-697.
- Romera, F.J., Frejo, V.M. and Alcántara, E.** (2003) Simultaneous Fe-and Cu-deficiency synergically accelerates the induction of several Fe-deficiency stress responses in Strategy I plants. *Plant Physiology and Biochemistry*, **41**, 821-827.
- Saarinen, U.M. and Siimes, M.A.** (1979) Iron absorption from breast milk, cow's milk, and iron-supplemented formula & colon; an opportunistic use of changes in total body iron determined by hemoglobin, ferritin, and body weight in 132 infants. *Pediatric Research*, **13**, 143-147.
- Santi, S. and Schmidt, W.** (2009) Dissecting iron deficiency-induced proton extrusion in Arabidopsis roots. *New Phytologist*, **183**, 1072-1084.
- Schmidt, R. and Bancroft, I.** (2011) *Genetics and Genomics of the Brassicaceae*: in *Plant Genetics and Genomics: Crops and Models*: Springer.
- Schmidt, W.** (2003) Iron solutions: acquisition strategies and signaling pathways in plants. *Trends in Plant Science*, **8**, 188-193.
- Schmidt, W., Tittel, J. and Schikora, A.** (2000) Role of hormones in the induction of iron deficiency responses in Arabidopsis roots. *Plant Physiology*, **122**, 1109-1118.

- Schuler, M., Keller, A., Backes, C., Philippar, K., Lenhof, H.P. and Bauer, P.** (2011) Transcriptome analysis by GeneTrail revealed regulation of functional categories in response to alterations of iron homeostasis in *Arabidopsis thaliana*. *BMC Plant Biology*, **11**, 87.
- Schwarz, S., Grande, A.V., Bujdoso, N., Saedler, H. and Huijser, P.** (2008) The microRNA regulated SBP-box genes SPL9 and SPL15 control shoot maturation in Arabidopsis. *Plant Molecular Biology*, **67**, 183-195.
- Schwertmann, U.** (1991) Solubility and dissolution of iron oxides. In *Iron nutrition and interactions in plants*: Springer, pp. 3-27.
- Seguela, M., Briat, J.F., Vert, G. and Curie, C.** (2008) Cytokinins negatively regulate the root iron uptake machinery in Arabidopsis through a growth-dependent pathway. *Plant Journal*, **55**, 289-300.
- Sivitz, A.B., Hermand, V., Curie, C. and Vert, G.** (2012) Arabidopsis bHLH100 and bHLH101 control iron homeostasis via a FIT-independent pathway. *PloS One*, **7**, e44843.
- Stocking, C.R.** (1975) Iron deficiency and the structure and physiology of maize chloroplasts. *Plant Physiol*, **55**, 626-631.
- Sun, P.** (1986) Iron deficiency chlorosis resistant soybean variety: USA Patents.
- Sunkar, R., Chinnusamy, V., Zhu, J. and Zhu, J.-K.** (2007) Small RNAs as big players in plant abiotic stress responses and nutrient deprivation. *Trends in Plant Science*, **12**, 301-309.
- Sunkar, R., Kapoor, A. and Zhu, J.K.** (2006) Posttranscriptional induction of two Cu/Zn superoxide dismutase genes in Arabidopsis is mediated by downregulation

of miR398 and important for oxidative stress tolerance. *Plant Cell*, **18**, 2051-2065.

**Tagawa, K. and Arnon, D.I.** (1962) Ferredoxins as electron carriers in photosynthesis and in the biological production and consumption of hydrogen gas. *Nature*, **195**, 537-543.

**Thimm, O., Essigmann, B., Kloska, S., Altmann, T. and Buckhout, T.J.** (2001) Response of Arabidopsis to iron deficiency stress as revealed by microarray analysis. *Plant Physiology*, **127**, 1030-1043.

**Thomine, S. and Lanquar, V.** (2011) Iron transport and signaling in plants. In *Transporters and Pumps in Plant Signaling*: Springer, pp. 99-131.

**Thomine, S. and Vert, G.** (2013) Iron transport in plants: better be safe than sorry. *Current Opinion in Plant Biology*, **16**, 322-327.

**Vert, G., Grotz, N., Dédaldéchamp, F., Gaymard, F., Guerinot, M.L., Briat, J.-F. and Curie, C.** (2002) IRT1, an Arabidopsis transporter essential for iron uptake from the soil and for plant growth. *Plant Cell*, **14**, 1223-1233.

**Voinnet, O.** (2009) Origin, biogenesis, and activity of plant microRNAs. *Cell*, **136**, 669-687.

**Volinia, S., Calin, G.A., Liu, C.-G., Ambs, S., Cimmino, A., Petrocca, F., Visone, R., Iorio, M., Roldo, C. and Ferracin, M.** (2006) A microRNA expression signature of human solid tumors defines cancer gene targets. *Proceedings of the National Academy of Sciences*, **103**, 2257-2261.

**Vos, T., Flaxman, A.D., Naghavi, M., Lozano, R., Michaud, C., Ezzati, M., Shibuya, K., Salomon, J.A., Abdalla, S. and Aboyans, V.** (2013) Years lived with

disability (YLDs) for 1160 sequelae of 289 diseases and injuries 1990–2010: a systematic analysis for the Global Burden of Disease Study 2010. *The Lancet*, **380**, 2163-2196.

**Wang, H.Y., Klatte, M., Jakoby, M., Baumlein, H., Weisshaar, B. and Bauer, P.**

(2007) Iron deficiency-mediated stress regulation of four subgroup Ib BHLH genes in *Arabidopsis thaliana*. *Planta*, **226**, 897-908.

**Wang, J.W., Czech, B. and Weigel, D.** (2009) miR156-regulated SPL transcription

factors define an endogenous flowering pathway in *Arabidopsis thaliana*. *Cell*, **138**, 738-749.

**Wang, N., Cui, Y., Liu, Y., Fan, H., Du, J., Huang, Z., Yuan, Y., Wu, H. and Ling,**

**H.Q.** (2013) Requirement and functional redundancy of Ib subgroup bHLH proteins for iron deficiency responses and uptake in *Arabidopsis thaliana*. *Molecular Plant*, **6**, 503-513.

**Wang, Y., Wang, Z., Amyot, L., Tian, L., Xu, Z., Gruber, M.Y. and Hannoufa, A.**

(2014) Ectopic expression of miR156 represses nodulation and causes morphological and developmental changes in *Lotus japonicus*. *Molecular Genetics and Genomics*, **290**, 471-484.

**Waters, B.M., McInturf, S.A. and Stein, R.J.** (2012) Rosette iron deficiency transcript

and microRNA profiling reveals links between copper and iron homeostasis in *Arabidopsis thaliana*. *Journal of Experimental Botany*, **ers239**.

**Wei, S., Gruber, M.Y., Yu, B., Gao, M.J., Khachatourians, G.G., Hegedus, D.D.,**

**Parkin, I.A. and Hannoufa, A.** (2012) *Arabidopsis* mutant sk156 reveals

complex regulation of SPL15 in a miR156-controlled gene network. *BMC Plant Biology*, **12**, 169-185.

**Wei, S., Yu, B., Gruber, M.Y., Khachatourians, G.G., Hegedus, D.D. and Hannoufa,**

**A.** (2010) Enhanced seed carotenoid levels and branching in transgenic *Brassica napus* expressing the Arabidopsis miR156b gene. *Journal of Agricultural and Food Chemistry*, **58**, 9572-9578.

**Welch, R.M. and Graham, R.D.** (2004) Breeding for micronutrients in staple food crops

from a human nutrition perspective. *Journal of Experimental Botany*, **55**, 353-364.

**Wollmann, H., Mica, E., Todesco, M., Long, J.A. and Weigel, D.** (2010) On

reconciling the interactions between APETALA2, miR172 and AGAMOUS with the ABC model of flower development. *Development*, **137**, 3633-3642.

**Wu, G., Park, M.Y., Conway, S.R., Wang, J.W., Weigel, D. and Poethig, R.S.** (2009)

The sequential action of miR156 and miR172 regulates developmental timing in Arabidopsis. *Cell*, **138**, 750-759.

**Wu, G. and Poethig, R.S.** (2006) Temporal regulation of shoot development in

*Arabidopsis thaliana* by miR156 and its target SPL3. *Development*, **133**, 3539-3547.

**Wu, L., Zhou, H., Zhang, Q., Zhang, J., Ni, F., Liu, C. and Qi, Y.** (2010) DNA

methylation mediated by a microRNA pathway. *Molecular Cell*, **38**, 465-475.

**Xie, K., Shen, J., Hou, X., Yao, J., Li, X., Xiao, J. and Xiong, L.** (2012) Gradual

increase of miR156 regulates temporal expression changes of numerous genes during leaf development in rice. *Plant Physiology*, **158**, 1382-1394.

- Xie, Z., Allen, E., Fahlgren, N., Calamar, A., Givan, S.A. and Carrington, J.C.**  
(2005) Expression of Arabidopsis MIRNA genes. *Plant Physiology*, **138**, 2145-2154.
- Xing, S., Salinas, M., Garcia-Molina, A., Höhmann, S., Berndtgen, R. and Huijser, P.** (2013) SPL8 and miR156-targeted SPL genes redundantly regulate Arabidopsis gynoecium differential patterning. *Plant Journal*, **75**, 566-577.
- Yamasaki, H., Hayashi, M., Fukazawa, M., Kobayashi, Y. and Shikanai, T.** (2009) SQUAMOSA Promoter Binding Protein-Like7 Is a Central Regulator for Copper Homeostasis in Arabidopsis. *Plant Cell*, **21**, 347-361.
- Yan, Z., Hossain, M.S., Wang, J., Valdes-Lopez, O., Liang, Y., Libault, M., Qiu, L. and Stacey, G.** (2013) miR172 regulates soybean nodulation. *Molecular Plant-Microbe Interactions*, **26**, 1371-1377.
- Yu, N., Cai, W.J., Wang, S., Shan, C.M., Wang, L.J. and Chen, X.Y.** (2010) Temporal control of trichome distribution by microRNA156-targeted SPL genes in Arabidopsis thaliana. *Plant Cell*, **22**, 2322-2335.
- Yu, S., Galvao, V.C., Zhang, Y.C., Horrer, D., Zhang, T.Q., Hao, Y.H., Feng, Y.Q., Wang, S., Schmid, M. and Wang, J.W.** (2012) Gibberellin regulates the Arabidopsis floral transition through miR156-targeted SQUAMOSA promoter binding-like transcription factors. *Plant Cell*, **24**, 3320-3332.
- Yu, Z.X., Wang, L.J., Zhao, B., Shan, C.M., Zhang, Y.H., Chen, D.F. and Chen, X.Y.** (2014) Progressive Regulation of Sesquiterpene Biosynthesis in Arabidopsis and Patchouli (*Pogostemon cablin*) by the miR156-Targeted SPL Transcription Factors. *Molecular Plant*. **8**, 98-110.

- Yuan, Y., Wu, H., Wang, N., Li, J., Zhao, W., Du, J., Wang, D. and Ling, H.Q.** (2008) FIT interacts with AtbHLH38 and AtbHLH39 in regulating iron uptake gene expression for iron homeostasis in Arabidopsis. *Cell Research*, **18**, 385-397.
- Zampetaki, A., Kiechl, S., Drozdov, I., Willeit, P., Mayr, U., Prokopi, M., Mayr, A., Weger, S., Oberhollenzer, F. and Bonora, E.** (2010) Plasma microRNA profiling reveals loss of endothelial miR-126 and other microRNAs in type 2 diabetes. *Circulation Research*, **107**, 810-817.
- Zhang, B. and Wang, Q.** (2015) MicroRNA-based biotechnology for plant improvement. *Journal of Cellular Physiology*, **230**, 1-15.
- Zhang, X., Henriques, R., Lin, S.S., Niu, Q.W. and Chua, N.H.** (2006) Agrobacterium-mediated transformation of *Arabidopsis thaliana* using the floral dip method. *Nature Protocols*, **1**, 641-646.
- Zhang, X., Zou, Z., Zhang, J., Zhang, Y., Han, Q., Hu, T., Xu, X., Liu, H., Li, H. and Ye, Z.** (2011) Over-expression of sly-miR156a in tomato results in multiple vegetative and reproductive trait alterations and partial phenocopy of the sft mutant. *FEBS Letters*, **585**, 435-439.
- Zhu, J.K.** (2008) Reconstituting plant miRNA biogenesis. *Proceedings of the National Academy of Sciences of the United States of America*, **105**, 9851-9852.

## Appendices

**Appendix A. Recipe for ½ MS medium.** Stock solutions for 10X macronutrients, 1000X micronutrients, and 200X Fe·EDTA were prepared and stored in 4°C, respectively.

	<b>Chemicals</b>	<b>Final concentration (mg/l)</b>
<b>Macronutrients</b>	NH <sub>4</sub> NO <sub>3</sub>	825
	CaCl <sub>2</sub> · 2H <sub>2</sub> O	220
	MgSO <sub>4</sub> · 7H <sub>2</sub> O	185
	KH <sub>2</sub> PO <sub>4</sub>	85
	KNO <sub>3</sub>	950
<b>Micronutrients</b>	H <sub>3</sub> BO <sub>3</sub>	3.1
	CoCl <sub>2</sub> · 6H <sub>2</sub> O	0.0125
	CuSO <sub>4</sub> · 5H <sub>2</sub> O	0.0125
	MnSO <sub>4</sub> · 4H <sub>2</sub> O	11.15
	KI	0.415
	Na <sub>2</sub> MoO <sub>4</sub> · 2H <sub>2</sub> O	0.125
	ZnSO <sub>4</sub> · 7H <sub>2</sub> O	4.3
<b>Fe·EDTA</b>	FeSO <sub>4</sub> · 7H <sub>2</sub> O	13.9
	Na <sub>2</sub> EDTA · 2H <sub>2</sub> O	18.6

### Appendix B. Primers used in this study

Name	Sequence (5'-3')	Product size (bp)	Description
<b>WY130235</b>	CACCTCGGCAGTTTCCTATTGGTTAC	4,038	Gateway cloning of <i>pSPL9:SPL9</i> genomic fragment for GFP fusion construct
<b>WY130236</b>	GAGAGACCAGTTGGTATGGTGAGAAGA	4,038	Gateway cloning of <i>pSPL9:SPL9</i> genomic fragment for GFP fusion construct
<b>WY130243</b>	CACCTCTTGCTTTCGTGTTTATGATTG	3,525	Gateway cloning of <i>pSPL15:SPL15</i> genomic fragment for GFP fusion construct
<b>WY130244</b>	AAGAGACCAATTGAAATGTTGAGGAGAG	3,525	Gateway cloning of <i>pSPL15:SPL15</i> genomic fragment for GFP fusion construct
<b>WY140701Q</b>	GGTAGGGAAGGAGAAGAAGG	225	qRT-PCR AT2G35290 Forward primer
<b>WY140702Q</b>	GAACATCCAAATCCGAAAAC	225	qRT-PCR AT2G35290 Reverse primer
<b>WY140703Q</b>	GTTGATGTACCGTTATCGT	185	qRT-PCR AT5G52750 Forward primer
<b>WY140704Q</b>	GCAGGATTGTATTGGTAAGG	185	qRT-PCR AT5G52750 Reverse primer
<b>WY140705Q</b>	TAACCGAAGGACTAACCGTA	204	qRT-PCR AT1G24150 Forward primer
<b>WY140706Q</b>	TCTAGACGTAAGAGCCAAG	204	qRT-PCR AT1G24150 Reverse primer

			primer
<b>WY140707Q</b>	GTCCCTTATGCATCACATTT	227	qRT-PCR AT5G14930 Forward primer
<b>WY140708Q</b>	ATGAACACCGTTTAGCAACT	227	qRT-PCR AT5G14930 Reverse primer
<b>WY140709Q</b>	ATAGCAAGACCAGACAGCAT	161	qRT-PCR AT4G04745 Forward primer
<b>WY140710Q</b>	AGATTTGAGGAAACGAGTGA	161	qRT-PCR AT4G04745 Reverse primer
<b>WY140711Q</b>	GTTTGACGACCCTGAATCTA	167	qRT-PCR AT2G38790 Forward primer
<b>WY140712Q</b>	CTCTCATGTCCATCCTTGAT	167	qRT-PCR AT2G38790 Reverse primer
<b>WY140713Q</b>	CCTCTACGAGTTGGCTAAAG	173	qRT-PCR AT2G47780 Forward primer
<b>WY140714Q</b>	TCTCAACATCGAAGAACACA	173	qRT-PCR AT2G47780 Reverse primer
<b>WY140715Q</b>	CTTTGACTGGCTTTTCTCTG	224	qRT-PCR AT3G24420 Forward primer
<b>WY140716Q</b>	GAGAAGCAGCAATAAGGAGA	224	qRT-PCR AT3G24420 Reverse primer
<b>WY140717Q</b>	AGAAATCTGTCAGCATCGTT	173	qRT-PCR AT1G09940 Forward primer
<b>WY140718Q</b>	CACTGATATTCCTCCCAAAA	173	qRT-PCR AT1G09940 Reverse primer

<b>WY140719Q</b>	AGGTGAATGTGGGTTACAAG	202	qRT-PCR AT4G00300 Forward primer
<b>WY140720Q</b>	TTGTTGTCATCAGCAGTAG	202	qRT-PCR AT4G00300 Reverse primer
<b>WY140721Q</b>	GTGTAGATGGGGAAACTTCA	198	qRT-PCR AT5G37300 Forward primer
<b>WY140722Q</b>	TTTCCAAAAGCTTCTACTGC	198	qRT-PCR AT5G37300 Reverse primer
<b>WY140723Q</b>	AGACCCCTTTTCGTTTTTAC	171	qRT-PCR AT1G01390 Forward primer
<b>WY140724Q</b>	GGTACACCGTTTACAATGCT	171	qRT-PCR AT1G01390 Reverse primer
<b>WY140725Q</b>	CCATCCGCCAACATTCTACT	167	qRT-PCR AT2G24850 Forward primer
<b>WY140726Q</b>	ACCATTGCGACGGTATTCTC	167	qRT-PCR AT2G24850 Reverse primer
<b>WY140727Q</b>	GATTTTGCCGTTGATGACCT	90	qRT-PCR AT5G25830 Forward primer
<b>WY140728Q</b>	GAGCTGTCGGTTATGGTGGT	90	qRT-PCR AT5G25830 Reverse primer
<b>WY140729Q</b>	CGGAAAAGGATCCAAGAACA	203	qRT-PCR AT4G01460 Forward primer
<b>WY140730Q</b>	CCGTTGAAGAAACGAAGGAG	203	qRT-PCR AT4G01460 Reverse primer
<b>WY140731Q</b>	CTTACGTGAATGGCAAGCAA	140	qRT-PCR AT2G29350 Forward primer
<b>WY140732Q</b>	CCACATTGTTGACGAGGATG	140	qRT-PCR AT2G29350 Reverse primer
<b>WY140733Q</b>	CTTGCCAGGCAAACAGTGTA	127	qRT-PCR AT1G65480 Forward primer
<b>WY140734Q</b>	AGCCACTCTCCCTCTGACAA	127	qRT-PCR AT1G65480 Reverse primer
<b>WY140735Q</b>	CCTTGTTGGAACACCGAGAT	230	qRT-PCR AT1G32450 Forward primer
<b>WY140736Q</b>	TGATGTACGCTGCTTTGTCC	230	qRT-PCR AT1G32450 Reverse primer
<b>WY140737Q</b>	ACGGTTCACCTGTTGTGTCA	174	qRT-PCR AT1G60590 Forward primer

<b>WY140738Q</b>	CTTCAAACGCCTGAGTGTC	174	qRT-PCR AT1G60590 Reverse primer
<b>WY140739Q</b>	TGGGAGTATTCAGCGGTAGG	114	qRT-PCR AT5G57880 Forward primer
<b>WY140740Q</b>	TCCGCGCTAAGGATAAAATG	114	qRT-PCR AT5G57880 Reverse primer
<b>WY140741Q</b>	CAGTTCAGCGGCTCTTTACC	96	qRT-PCR AT5G35935 Forward primer
<b>WY140742Q</b>	AGGAACTAATGGTGGCGTTG	96	qRT-PCR AT5G35935 Reverse primer
<b>WY140743Q</b>	CCAGCACTTCTCTCGTCTC	142	qRT-PCR AT4G30975 Forward primer
<b>WY140744Q</b>	TGGAGAGCACACACACACA	142	qRT-PCR AT4G30975 Reverse primer
<b>WY140745Q</b>	CCGAAGATGACGCTATCCAT	151	qRT-PCR AT2G39510 Forward primer
<b>WY140746Q</b>	TAAAGGCAAAGGCAGGAAGA	151	qRT-PCR AT2G39510 Reverse primer
<b>WY140747Q</b>	CTCAGCCGTTCTTTTCTTGG	129	qRT-PCR AT2G02120 Forward primer
<b>WY140748Q</b>	TCGCAGTTTGTATCGCTCAC	129	qRT-PCR AT2G02120 Reverse primer
<b>WY140749Q</b>	AAGCAAGCGATGAAGGAAGA	156	qRT-PCR AT1G74930 Forward primer
<b>WY140750Q</b>	CTCGGGAGTGTCGTAAGAGC	156	qRT-PCR AT1G74930 Reverse primer
<b>WY140751Q</b>	ATGAGCTTCTTGCCGTCAGT	100	qRT-PCR AT4G01390 Forward primer
<b>WY140752Q</b>	TCACGAAACCCCTCACTACC	100	qRT-PCR AT4G01390 Reverse primer
<b>WY140753Q</b>	ATCCAATCTATTTCACTTCCACAA	142	qRT-PCR AT1G43590 Forward primer
<b>WY140754Q</b>	CCCAAATAAGAGCAGGATGTT	142	qRT-PCR AT1G43590 Reverse primer
<b>WY140755Q</b>	TTCTTCAGCGGAGGAACAAT	134	qRT-PCR AT4G33120 Forward primer
<b>WY140756Q</b>	TCCATTCCTTTCAGCCACTC	134	qRT-PCR AT4G33120 Reverse primer
<b>WY140757Q</b>	TCAAGGAAGGTTTCAGGGATG	90	qRT-PCR AT3G57260 Forward primer
<b>WY140758Q</b>	AGATTCACGAGCAAGGGAGA	90	qRT-PCR AT3G57260 Reverse primer

			primer
<b>WY140759Q</b>	CTCGACGATGACTGTGGCTA	140	qRT-PCR AT3G02620 Forward primer
<b>WY140760Q</b>	GAAACGTCTTGCTCGGGTTA	140	qRT-PCR AT3G02620 Reverse primer
<b>WY140767Q</b>	TCGAGCAAGAGATGAGCAGA	91	qRT-PCR AT3G29410 forward primer
<b>WY140768Q</b>	TCTTCAACCGCTGCTTCTTT	91	qRT-PCR AT3G29410 reverse primer
<b>WY140769Q</b>	ACATCCCACCACCAAACCTA	104	qRT-PCR AT3G18080 forward primer
<b>WY140770Q</b>	ACGAGTAAGCCCTTGGACCT	104	qRT-PCR AT3G18080 reverse primer
<b>WY140771Q</b>	TTTTGGGAAGAGGCTTGAGA	194	qRT-PCR AT1G12010 forward primer
<b>WY140772Q</b>	CTGCATCTGTGTGAGCCCTA	194	qRT-PCR AT1G12010 reverse primer
<b>WY140773Q</b>	TGACGAGTCCGGGAAACTAC	114	qRT-PCR AT1G67865 forward primer
<b>WY140774Q</b>	ACTGGGTGTGGTCAGGAGTC	114	qRT-PCR AT1G67865 reverse primer
<b>WY140775Q</b>	GGCTGTTGTTTCAGGTGGTT	168	qRT-PCR AT3G29430 forward primer
<b>WY140776Q</b>	CCGCTGCTTCTCTTCTCAGT	168	qRT-PCR AT3G29430 reverse primer
<b>WY140777Q</b>	TAGGCTCGGTGCTACTGGAT	100	qRT-PCR AT4G11650 forward primer
<b>WY140778Q</b>	CACCCTCACACACACACACA	100	qRT-PCR AT4G11650 reverse primer
<b>WY140779Q</b>	TTCCCGAATCACAGAACCTC	102	qRT-PCR AT1G73260 forward primer
<b>WY140780Q</b>	GCTTCCTCTCGTGGTCAAAC	102	qRT-PCR AT1G73260 reverse primer
<b>WY140781Q</b>	CTCGTGGAGGCTAAGAGTGG	104	qRT-PCR AT3G10720 forward primer
<b>WY140782Q</b>	TTAAGTGC GTGGCTCACAAG	104	qRT-PCR AT3G10720 reverse primer
<b>WY140783Q</b>	CTCTGAAAGCCCAAGACCAG	117	qRT-PCR AT4G07820 forward primer
<b>WY140784Q</b>	AGGCTTGAGCATAGGCAGTC	117	qRT-PCR AT4G07820 reverse primer

<b>WY140785Q</b>	CTGGCAAAGCTGAGGAGAAG	165	qRT-PCR AT5G15970 forward primer
<b>WY140786Q</b>	CGGATCGCTACTTGTTTCAGG	165	qRT-PCR AT5G15970 reverse primer
<b>WY140211Q</b>	ACCGACGCAAGAAGATCAAC	132	qRT-PCR bHLH38 AT3G56970 forward primer
<b>WY140212Q</b>	GCTGTTGCAGCTCTGGTATG	132	qRT-PCR bHLH38 AT3G56970 reverse primer
<b>WY140209Q</b>	CTGGCCAATCGAAGAAGCTA	130	qRT-PCR bHLH39 AT3G56980 forward primer
<b>WY140210Q</b>	TGACCTGAAATTTGCACCAA	130	qRT-PCR bHLH39 AT3G56980 reverse primer
<b>WY140201Q</b>	GTCTTCCTCCCACCAATCAA	138	qRT-PCR bHLH100 AT2G41240 forward primer
<b>WY140202Q</b>	CCGAAATTTGAAACGAGAGC	138	qRT-PCR bHLH100 AT2G41240 reverse primer
<b>WY140205Q</b>	CTTCGTGCTCTCTGCCTCT	175	qRT-PCR bHLH101 AT5G04150 forward primer
<b>WY140206Q</b>	TTTCAGCTGCTCTTGGTGA	175	qRT-PCR bHLH101 AT5G04150 reverse primer
<b>WY140217Q</b>	GCTTAAGCGTGAGCATTTGA	130	qRT-PCR PYE AT3G47640 forward primer
<b>WY140218Q</b>	TTGACCAAACACGTCCTTCA	130	qRT-PCR PYE AT3G47640 reverse primer
<b>WY140809Q</b>	ATGTTCCAATGATGGTCGT	149	qRT-PCR FRO2 (AT1G01580) forward primer
<b>WY140810Q</b>	ATTCCTAATGGCCCCTTAC	149	qRT-PCR FRO2 (AT1G01580) reverse primer

			reverse primer
<b>WY140811Q</b>	GTTTCGTTCTCCAACCAGA	149	qRT-PCR IRT1 (AT4G19690) forward primer
<b>WY140812Q</b>	TTATGCCACGGGTTCTCTTC	149	qRT-PCR IRT1 (AT4G19690) reverse primer
<b>WY140813Q</b>	GTCGGAGTCAAGCACCAAGT	149	qRT-PCR FRO3 (AT1G23020) forward primer
<b>WY140814Q</b>	AATGCGAGATACCGGTCCTA	149	qRT-PCR FRO3 (AT1G23020) reverse primer
<b>WY140815Q</b>	GCTGGAATCAGGGAAGTTCA	150	qRT-PCR AHA2 (AT4G30190) forward primer
<b>WY140816Q</b>	AAGATCATTGCTGGCTTTGG	150	qRT-PCR AHA2 (AT4G30190) reverse primer
<b>WY140823Q</b>	CATGCTCCTGATGCTCAAAA	147	qRT-PCR FIT (AT2G28160) forward primer
<b>WY140824Q</b>	TGGAGCAACACCTTCTCCTT	147	qRT-PCR FIT (AT2G28160) reverse primer
<b>WY150201</b>	TTTTGCTTCATAAGTTTGTGACTT	153	FIT (AT2G28160) ChIP qPCR I
<b>WY150202</b>	TTTGCCACATGATTATCTTTCAG	153	FIT (AT2G28160) ChIP qPCR I
<b>WY150205</b>	GCCGATTGCAAATTAATTCCT	151	FIT (AT2G28160) ChIP qPCR II
<b>WY150206</b>	AAATCGATCAGACCGTATTAATAA	151	FIT (AT2G28160) ChIP qPCR II
<b>WY150207</b>	CATGCATGACATTACAAGACG	173	FIT (AT2G28160) ChIP qPCR III
<b>WY150208</b>	TGTTGACAACGAAAGAGAGACAA	173	FIT (AT2G28160) ChIP qPCR III
<b>WY140356</b>	CGAATGGTAACCTCGGTTTT	171	ChIP-qPCR PYE AT3G47640 I

<b>WY140357</b>	TAATCCGCACCGCAAATAAT	171	ChIP-qPCR PYE AT3G47640 I
<b>WY140358</b>	GGTAACTAGTGATTCTGATGCACAC	142	ChIP-qPCR PYE AT3G47640 II
<b>WY140359</b>	GCCTTTGCCTCTTCCATACA	142	ChIP-qPCR PYE AT3G47640 II
<b>WY140360</b>	ATAGACCGCCCCAAAAC	149	ChIP-qPCR PYE AT3G47640 III
<b>WY140361</b>	TAGTTTTGCGGTTCGAATGA	149	ChIP-qPCR PYE AT3G47640 III
<b>WY140362</b>	CTTCACGTTGACCCACAT	132	ChIP-qPCR PYE AT3G47640 IV
<b>WY140363</b>	CAGATTAATCGGGTAAAAAGTTG	132	ChIP-qPCR PYE AT3G47640 IV

**Appendix C. Recipe for Lysogeny broth (LB) medium**

<b>Chemicals</b>	<b>Concentration (g/l)</b>
<b>Tryptone</b>	10
<b>Yeast extract</b>	5
<b>NaCl</b>	10

## Appendix D. Recipe for buffers used in ChIP assay

<b>Buffers</b>	<b>Composition</b>
<b>1X PBS</b>	NaCl 137 mM, KCl 2.7 mM, Na <sub>2</sub> HPO <sub>4</sub> 10 mM, KH <sub>2</sub> PO <sub>4</sub> 1.8 mM
<b>Extraction buffer 1</b>	Sucrose 0.4 M, Tris-Cl 10 mM (pH 8), MgCl <sub>2</sub> 10 mM. β-ME 5 mM, PMSF 0.1 mM, Protease inhibitor 2 tablets/100ml
<b>Extraction buffer 2</b>	Sucrose 0.25 M, Tris-Cl 10 mM (pH 8), MgCl <sub>2</sub> 10 mM. β-ME 5 mM, PMSF 0.1 mM, Triton X-100 1%, Protease inhibitor half tablet/10ml
<b>Extraction buffer 3</b>	Sucrose 1.7 M, Tris-Cl 10 mM (pH 8), MgCl <sub>2</sub> 2 mM. β-ME 5 mM, PMSF 0.1 mM, Triton X-100 0.15%, Protease inhibitor half tablet/10ml
<b>Nuclei lysis buffer</b>	Tris-Cl 50 mM (pH 8), EDTA 10 mM, SDS 1%, Protease inhibitor one tablet/10ml
<b>Dilution buffer</b>	Triton X-100 1.1%, EDTA 1.2 mM, Tris-Cl 16.7 mM (pH 8), NaCl 167 mM
<b>Low-salt buffer</b>	150 mM NaCl, 0.1% SDS, 1% Triton X-100, 2 mM EDTA, 20 mM Tris-HCl (pH 8)
<b>High-salt buffer</b>	500 mM NaCl, 0.1% SDS, 1% Triton X-100, 2 mM EDTA, 20 mM Tris-HCl (pH 8)
<b>LiCl buffer</b>	0.25 M LiCl, 1% NP-40 (or IGEPAL CA-360), 1% DOC, 1 mM EDTA, 10 mM Tris-HCl (pH 8)
<b>Elution buffer</b>	0.1% SDS, NaHCO <sub>3</sub> 8.4g

## Appendix E. List of differentially expressed genes derived from NG-RNA-SEQ

Tissue type	Gene expression trend  (35S:miR156 vs WT)	Accession numbers
Rosette leaves	Up-regulated	AT1G17420, AT1G19180, AT1G20450, AT1G35140, AT1G55450, AT1G57990, AT1G59870, AT1G61890, AT1G72520, AT1G78850, AT2G17840, AT2G24600, AT2G41100, AT4G08950, AT4G20830, AT4G31800, AT4G34150, AT5G20230, AT5G57560, AT5G67300, AT1G08930, AT3G01290, AT5G19240, AT4G25100, AT4G02380, AT4G23180, AT3G55980, AT4G30270, AT4G30280, AT3G45970, AT2G41430, AT2G27690, AT1G20510, AT3G57520, AT2G44500, AT5G24030, AT1G20440, AT5G66210, AT3G19680, AT1G09970, AT3G15356, AT2G40000, AT1G27770, AT3G54810, AT4G36850, AT4G13340, AT4G30210, AT2G22500, AT2G23810, AT1G56660, AT4G29780, AT1G03220, AT4G24570, AT4G20860, AT5G56980, AT1G80840, AT5G48380, AT1G61100, AT1G70700, AT1G21130, AT5G44070, AT5G37770, AT3G59350, AT1G69840, AT1G19380, AT2G06050, AT3G25780, AT4G08850, AT4G12720, AT2G17230, AT3G10720, AT2G27080, AT1G72450, AT5G14120, AT3G55430, AT2G44490, AT4G02330, AT3G57450, AT1G18740, AT4G17230, AT1G32640, AT1G09070, AT1G07135, AT1G22190, AT2G27500, AT3G47960, AT2G34930, AT3G52400, AT3G06500, AT1G76680, AT3G16530, AT5G42650, AT3G57530, AT3G45640, AT5G35735, AT4G19520, AT2G34600, AT1G74450, AT2G01450, AT1G73080, AT1G76650, AT2G19800, AT3G52800, AT1G21910, AT1G02660, AT5G19230, AT3G11820, AT4G14365, AT1G22530, AT1G28380, AT5G26030, AT5G01100, AT1G19770, AT5G64310, AT1G78830, AT4G27280, AT1G19020, AT3G25760, AT5G45340, AT2G47060, AT5G20250, AT1G79245, AT3G50950, AT4G34410, AT5G51550, AT5G49360, AT3G44260, AT5G35935, AT5G06320, AT5G47910, AT1G65490, AT1G33590, AT1G74950, AT2G41110, AT5G54380, AT4G26690, AT4G18010, AT5G41750, AT1G76160, AT2G06850, AT4G18205, AT5G13220, AT4G16563, AT5G62570, AT5G42050, AT3G21070, AT5G07440, AT1G01120, AT2G38470, AT4G37260, AT4G30975, AT1G63860, AT1G17620, AT3G28180, AT5G52882, AT2G47730, AT2G31810, AT4G30440, AT1G70090, AT3G48520, AT3G04640, AT3G08720, AT1G72430, AT4G21570, AT1G13210, AT3G62720, AT5G57220, AT4G23220, AT1G23030, AT4G17490, AT3G19010, AT3G51450, AT2G13790, AT5G06870, AT3G15450, AT1G11260, AT5G52050, AT3G09260, AT5G28630, AT4G21990, AT2G37940, AT3G56200, AT1G05675, AT1G15010, AT2G28630, AT2G31880, AT3G23030, AT1G32920, AT4G34390, AT2G41640, AT3G09830, AT5G05600, AT5G04870, AT1G24170, AT5G45750, AT5G25930, AT1G17380, AT3G05490, AT3G10300, AT1G29690, AT1G33610, AT5G62520, AT3G47340, AT2G01180, AT1G03870, AT1G56510, AT3G51920, AT5G58120, AT4G33920, AT1G65390, AT5G13190, AT3G13080, AT1G51760, AT4G38470, AT1G53430, AT5G67480, AT2G06530, AT4G33050, AT1G50040, AT5G54710, AT3G56880, AT1G57680, AT5G49520, AT4G11280, AT1G75750, AT1G31130, AT5G22690, AT4G00300, AT3G15210, AT4G30290, AT3G44860, AT5G63160, AT1G50740, AT4G17500, AT3G28200, AT2G35930, AT3G48360, AT3G16420, AT3G16470, AT1G66160, AT1G14740, AT5G54170, AT4G22690, AT1G27730, AT5G45280, AT5G47220, AT1G02400, AT4G29950, AT5G41740, AT5G64260, AT3G58120, AT5G61210,

	<p> AT1G66180, AT2G23120, AT3G28340, AT3G49530, AT3G47570, AT4G03400,  AT1G61340, AT2G34510, AT2G23320, AT3G22060, AT3G19030, AT3G24550,  AT2G15880, AT1G44350, AT2G18690, AT3G16400, AT5G25440, AT4G02540,  AT2G32150, AT1G78070, AT1G56140, AT5G53750, AT3G07780, AT5G24590,  AT5G46510, AT4G18950, AT2G41420, AT1G30135, AT2G47440, AT1G65310,  AT4G15800, AT5G27520, AT1G54010, AT2G29340, AT2G39650, AT1G28370,  AT4G14370, AT5G01600, AT5G42800, AT3G54020, AT2G03240, AT1G04240,  AT4G35770, AT1G22280, AT4G36670, AT5G11650, AT4G17615, AT4G22880,  AT2G30990, AT4G25810, AT1G16370, AT1G78280, AT5G08760, AT3G57930,  AT2G15390, AT2G30930, AT3G23730, AT1G17860, AT4G27410, AT2G31800,  AT4G23190, AT1G36370, AT3G59080, AT1G63750, AT1G18890, AT2G30250,  AT5G02290, AT5G19120, AT1G27100, AT2G42760, AT1G35350, AT3G10020,  AT2G43290, AT3G15950, AT4G32480, AT4G27652, AT1G71697, AT3G02880,  AT4G34180, AT5G52750, AT5G56170, AT2G23130, AT5G54720, AT4G04570,  AT1G09950, AT1G12580, AT3G44630, AT2G17480, AT5G22250, AT5G05140,  AT3G06070, AT1G58270, AT1G30040, AT1G07000, AT1G50460, AT5G65470,  AT4G24230, AT3G14870, AT2G46510, AT5G18400, AT2G17290, AT3G11420,  AT4G27654, AT4G09570, AT5G52310, AT2G05380, AT1G09940, AT3G19970,  AT5G04480, AT1G72416, AT3G50930, AT1G05135, AT5G52320, AT4G30470,  AT3G50060, AT1G12610, AT4G36010, AT4G11320, AT3G13520, AT4G24380,  AT5G40780, AT1G61667, AT4G12040, AT1G06620, AT5G23050, AT5G64870,  AT1G31540, AT2G35710, AT1G20823, AT3G22275, AT3G05320, AT5G44568,  AT5G48540, AT4G38550, AT1G76700, AT1G21100, AT2G30020, AT4G24160,  AT2G41010, AT1G52400, AT1G25400, AT2G28400, AT4G22710, AT5G40340,  AT1G18210, AT1G66500, AT5G05440, AT4G36500, AT2G30040, AT3G26910,  AT3G61640, AT2G21500, AT1G16130, AT1G66760, AT4G08500, AT4G17460,  AT1G11960, AT4G14130, AT5G64750, AT1G75230, AT2G21120, AT4G35320,  AT5G15870, AT1G69760, AT1G72900, AT4G00970, AT3G13790, AT2G39210,  AT3G29000, AT1G74430, AT3G16860, AT5G13200, AT4G01950, AT5G23510,  AT1G60140, AT5G44130, AT1G14330, AT3G49780, AT1G18300, AT1G62440,  AT4G32800, AT1G22882, AT5G45110, AT1G18570, AT1G42990, AT3G16460,  AT4G21390, AT2G25460, AT1G59910, AT5G48450, AT4G28085, AT2G27310,  AT5G65300, AT2G39400, AT5G54860, AT5G51190, AT1G63830, AT2G39360,  AT1G76600, AT2G25735, AT2G26190, AT3G50260, AT4G31000, AT3G01830,  AT2G39420, AT3G50650, AT1G14540, AT2G29300, AT5G22500, AT1G33760,  AT4G30350, AT1G51660, AT2G32140, AT1G72790, AT4G30910, AT3G05165,  AT2G22880, AT1G51800, AT1G61260, AT2G22770, AT3G20600, AT4G25830,  AT1G03230, AT1G65845, AT1G22890, AT5G66675, AT5G58090, AT1G64760,  AT3G28180, AT1G66090, AT4G20780, AT1G73805, AT1G67060, AT3G25610,  AT5G41080, AT2G44840, AT5G01040, AT2G23680, AT3G23170, AT1G52040,  AT1G03370, AT5G03360, AT1G10550, AT1G08920, AT3G02140, AT1G24150,  AT3G48650, AT5G19110, AT2G32800, AT3G62150, AT2G24330, AT1G05575,  AT2G27260, AT5G63770, AT3G54200, AT2G33570, AT4G22780, AT4G27350,  AT4G13575, AT4G28490, AT2G15090, AT2G39310, AT5G22630, AT5G64120,  AT5G09440, AT5G59730, AT4G11330, AT2G32210, AT2G46400, AT1G30730,  AT3G26980, AT1G27020, AT5G61380, AT4G15760, AT5G17350, AT5G11970,  AT5G11740, AT2G17120, AT1G50750, AT3G60260, AT1G33600, AT2G39180,  AT1G69900, AT3G49350, AT4G18340, AT5G43620, AT4G35985, AT1G79700,  AT1G69890, AT4G10390, AT5G12940, AT4G30060, AT4G11000, AT5G36925,  AT4G08170, AT1G56540, AT5G03545, AT1G73540, AT5G65920, AT3G45040,  AT2G46270, AT1G74930, AT3G27960, AT5G17220, AT4G36900, AT2G35290,  AT3G02070, AT1G14480, AT3G27210, AT1G11670, AT3G49160, AT2G23290,  AT1G64380, AT1G11185, AT1G74330, AT3G55840, AT5G25250, AT4G01870,  AT1G30640, AT1G51270, AT5G39580, AT5G25050, AT3G10640, AT1G22810,  AT3G61190, AT5G10695, AT5G38700, AT4G33420, AT5G48530, AT3G03020,  AT3G05580, AT2G33580, AT4G26400, AT2G17660, AT4G19230, AT4G15260,  AT3G44735, AT1G51820, AT2G46780, AT4G01750, AT4G02200, AT1G02390, </p>
--	--

	<p> AT1G29330, AT1G47380, AT4G36950, AT5G40540, AT1G43590, AT3G07195,  AT1G21110, AT2G27660, AT5G62470, AT3G02840, AT5G42380, AT5G13170,  AT1G61360, AT2G28120, AT4G27657, AT5G58620, AT1G14370, AT4G30510,  AT5G25240, AT5G66640, AT1G21120, AT5G26770, AT2G36220, AT1G09932,  AT4G23810, AT1G73830, AT1G72280, AT3G56410, AT2G38240, AT1G22510,  AT4G18280, AT5G41100, AT1G16110, AT3G25600, AT4G29740, AT1G30720,  AT3G04110, AT5G49280, AT4G01360, AT2G33830, AT1G07870, AT2G39200,  AT5G16360, AT1G14870, AT3G05200, AT1G18390, AT5G66070, AT3G15060,  AT1G15670, AT5G66480, AT1G78860, AT1G43886, AT5G27420, AT1G61610,  AT3G59310, AT5G52760, AT1G52200, AT5G14930, AT3G24420, AT4G28190,  AT5G66650, AT1G02380, AT2G23690, AT4G13180, AT4G17030, AT1G05340,  AT1G43910, AT4G24275, AT5G24110, AT4G11521, AT3G46930, AT2G23100,  AT2G38530, AT1G68690, AT5G10750, AT3G44320, AT1G70740, AT3G46090,  AT4G37610, AT3G03030, AT2G43320, AT1G26730, AT5G66620, AT4G01250,  AT2G41330, AT1G18400, AT3G14590, AT2G13800, AT5G59550, AT1G17147,  AT3G17690, AT5G22940, AT5G67450, AT5G52020, AT2G20142, AT5G59820,  AT5G17850, AT5G65390, AT5G63450, AT3G55500, AT2G32200, AT3G08860,  AT5G64660, AT3G15630, AT5G23130, AT4G20820, AT2G31730, AT4G37370,  AT4G39890, AT3G45730, AT5G35777, AT1G78000, AT5G16200, AT5G17490,  AT3G44400, AT1G32170, AT1G72140, AT3G16030, AT4G13395, AT2G29720,  AT5G44050, AT4G15233, AT2G30360, AT5G38210, AT1G61560, AT3G45960,  AT5G18150, AT5G57550, AT4G29700, AT1G14520, AT3G10930, AT3G59880,  AT5G26920, AT1G66920, AT3G62260, AT2G17705, AT3G16330, AT4G38400,  AT4G30850, AT1G77450, AT1G28010, AT1G80610, AT3G13437, AT1G02360,  AT5G07100, AT2G38790, AT5G39020, AT5G46910, AT5G62865, AT4G08040,  AT1G65790, AT3G23250, AT1G11000, AT1G28660, AT3G50800, AT4G37240,  AT3G29170, AT1G65486, AT4G35480, AT1G76790, AT1G18200, AT1G74440,  AT4G13110, AT3G46385, AT3G49620, AT1G52890, AT3G50470, AT3G26680,  AT1G03457, AT2G45680, AT1G67470, AT2G22860, AT1G17060, AT1G63180,  AT5G03720, AT4G25390, AT3G22910, AT3G59750, AT2G34355, AT5G39785,  AT1G11210, AT1G51090, AT3G55950, AT5G54060, AT4G01010, AT1G33770,  AT1G24140, AT4G05010, AT1G09575, AT3G18560, AT1G31290, AT3G57640,  AT3G19580, AT5G48850, AT1G52830, AT1G60190, AT5G13700, AT1G24145,  AT4G33985, AT4G19380, AT3G49580, AT5G07990, AT5G63970, AT1G01560,  AT5G12340, AT1G20350, AT4G04810, AT4G30090, AT4G25835, AT5G66790,  AT3G54000, AT1G69430, AT1G36622, AT2G29440, AT3G51970, AT1G58420,  AT3G52450, AT1G69570, AT5G37540, AT1G66400, AT5G54490, AT5G65280,  AT4G37770, AT5G60270, AT4G15230, AT3G01430, AT2G47780, AT3G46110,  AT5G48657, AT4G04745, AT4G23870, AT2G28500, AT2G01300, AT5G08240,  AT3G52520, AT1G69260, AT3G49110, AT5G07070, AT1G80120, AT1G77290,  AT2G28140, AT2G16060, AT1G68330, AT4G11290, AT2G20880, AT4G23680,  AT4G39830, AT4G29050, AT5G61600, AT1G01110, AT1G72920, AT1G71400,  AT5G66630, AT3G15620, AT4G33960, AT3G16690, AT5G63905, AT1G18710,  AT2G31020, AT5G26220, AT3G16510, AT1G65890, AT1G07150, AT3G54150,  AT3G09520, AT3G21330, AT1G28480, AT3G02410, AT4G01540, AT4G23215,  AT3G04010, AT5G06720, AT4G38552, AT1G70800, AT2G40095, AT3G26500,  AT5G36000, AT2G16870, AT1G51620, AT5G01730, AT5G19340, AT4G21865,  AT3G15650, AT5G09800, AT1G11740, AT4G29270, AT4G23230, AT1G21550,  AT3G48390, AT4G23550, AT5G02200, AT1G79680, AT5G06865, AT1G49530,  AT5G59720, AT1G61460, AT5G07620, AT1G17830, AT2G15480, AT4G18250,  AT2G32190, AT4G18195, AT1G57560, AT5G13210, AT4G22490, AT1G35230,  AT3G25597, AT2G15760, AT5G46500, AT3G20660, AT2G03540, AT5G19020,  AT1G05020, AT1G78410, AT3G11402, AT3G43430, AT5G03700, AT2G33350,  AT4G38530, AT5G65925, AT1G32690, AT4G23610, AT5G52250, AT1G66930,  AT3G07000, AT2G34080 </p>
--	---

	<b>Down-regulated</b>	AT4G19170, AT1G69530, AT2G25900, AT5G53450, AT1G02205, AT4G36040, AT5G49740, AT4G24780, AT3G18080, AT4G26850, AT3G09440, AT1G25440, AT2G14610, AT3G18290, AT3G57260, AT1G71030, AT2G40610, AT1G13650, AT5G05250, AT3G59940, AT1G23390, AT5G10930, AT4G13840, AT5G63180, AT3G03470, AT4G33790, AT1G14880, AT2G30766, AT1G64390, AT3G26290, AT2G45660, AT1G68570, AT5G01820, AT5G13740, AT1G32450, AT2G24850, AT2G06950, AT2G15020, AT3G22231, AT5G54585, AT2G30770, AT1G67865, AT3G55646, AT4G12290, AT2G32010, AT1G10640, AT2G46710, AT3G63210, AT2G28720, AT4G21650, AT4G19430, AT1G47400, AT1G60590, AT3G56970, AT2G14247, AT3G55710, AT2G43570, AT4G05070, AT1G13609, AT5G37300, AT2G45560, AT1G74940, AT4G01460, AT1G14890, AT5G59130, AT2G29350, AT2G14560, AT3G51860, AT3G47640, AT5G13320, AT3G18773, AT1G01190, AT1G48120, AT5G67280, AT3G26830, AT5G15800, AT2G18560, AT3G46130, AT1G33170, AT2G04160, AT4G32280, AT5G03230, AT2G41240, AT1G80440, AT1G47395, AT4G21215, AT5G43870, AT2G36970, AT2G13810, AT2G47880, AT1G65480, AT2G21320, AT2G42200, AT4G16260, AT3G30122, AT2G38180, AT5G39860, AT4G10500, AT2G45220, AT4G29190, AT5G60910, AT5G59350, AT3G52740, AT1G66140, AT5G38140, AT5G01790, AT4G16447, AT3G56980, AT2G04240, AT1G33960, AT2G32390, AT1G49230, AT3G49650, AT2G29090, AT5G16570, AT2G43590, AT1G77270, AT4G11360, AT5G59670, AT1G18330, AT1G18810, AT1G56120, AT3G14760, AT3G16670, AT3G61880, AT5G54190, AT4G03510, AT5G44430, AT1G51170, AT4G09500, AT2G18660, AT4G23020, AT3G03440, AT2G25680, AT3G08505, AT5G55450, AT4G32290, AT1G04180, AT2G05440, AT1G20470, AT5G04150, AT3G26200, AT2G39920, AT4G13800, AT3G61970, AT3G22600, AT4G30710, AT1G69490, AT3G06868, AT2G40390, AT3G22235, AT5G28910, AT1G70420, AT3G05690, AT3G46880, AT5G63580, AT5G44780, AT1G24260, AT5G51850, AT4G01490, AT2G39705, AT5G53200, AT3G22810, AT2G42530, AT1G09080, AT5G43860, AT2G38995, AT3G62070, AT2G21640, AT5G46830, AT1G52770, AT4G12480, AT2G37100, AT3G15270, AT3G12220, AT3G63380, AT4G25000, AT4G10380, AT5G67550, AT5G64510, AT1G01390, AT4G37580, AT1G51460, AT1G53490, AT1G51890, AT3G02550, AT3G51340, AT5G25830, AT4G26680, AT4G13260, AT1G68620, AT5G28030, AT2G34180, AT3G14280, AT5G57880, AT2G43700, AT5G12360, AT1G23060, AT1G19510, AT1G62870, AT4G39010, AT1G72540, AT2G15830, AT5G24330, AT4G12490, AT3G26320, AT5G47610, AT1G16830, AT5G50800, AT5G01880, AT1G12570, AT4G38320, AT4G22760, AT5G61350, AT3G24360, AT1G22900, AT5G23980, AT4G25420, AT1G21240
<b>Roots</b>	<b>Up-regulated</b>	AT5G35935, AT4G30975, AT2G39510, AT2G02120, AT1G74930, AT4G01390, AT1G43590, AT4G33120, AT3G57260, AT3G02620, AT5G42600, AT1G16410, AT4G33550, AT4G34410, AT4G14548, AT1G66800, AT2G38540, AT1G72520, AT5G52050, AT2G21650, AT2G25150, AT1G19210, AT2G24850, AT2G26370, AT4G24380, AT2G44840, AT3G13784, AT2G05380, AT1G11460, AT1G12610, AT4G37850, AT1G45020, AT2G35585, AT5G58680, AT4G01360, AT2G14290, AT4G36570, AT5G62330, AT3G02840, AT4G22505, AT1G35186, AT2G28860, AT5G42380, AT3G55515, AT2G30540, AT3G27940, AT3G24255, AT3G44870, AT1G76952, AT2G37210
	<b>Down-regulated</b>	AT3G29410, AT3G18080, AT1G12010, AT1G67865, AT3G29430, AT4G11650, AT1G73260, AT3G10720, AT4G07820, AT5G15970, AT5G48430, AT4G08770, AT3G23290, AT5G43270, AT1G13710, AT1G52820, AT3G05650, AT5G14330, AT2G43590, AT1G64400, AT2G27402, AT4G04410, AT1G27370, AT1G50050, AT2G43050, AT3G30260, AT2G41240, AT4G24350, AT5G40590, AT1G30730, AT2G44220, AT3G47710, AT3G03670, AT1G48930, AT5G04960, AT5G64120, AT2G13810, AT2G21330, AT3G49780, AT2G36870, AT1G77270, AT3G57920, AT5G52720, AT4G33070, AT5G23660, AT2G43620, AT3G60160, AT1G68040, AT1G33840, AT3G12900, AT1G67860, AT4G35770, AT1G19250, AT2G25680, AT3G51660, AT2G32270, AT3G48770, AT2G15780, AT5G44973, AT3G60330,

		AT1G74880, AT5G67400, AT1G64160, AT4G08620, AT1G53635, AT5G04150, AT4G33666, AT3G62760, AT1G53480, AT4G19680, AT3G26500, AT3G47380, AT5G54585, AT5G15960, AT4G13390, AT2G42250, AT1G52800, AT5G66700, AT5G06690, AT5G56370, AT5G06640, AT5G06630, AT4G15700, AT2G42350, AT1G61750, AT5G36260, AT1G05680, AT2G26820, AT3G07070, AT1G73120, AT3G61390, AT3G15370
--	--	--

**Appendix F. The location of putative SPL binding sites in FIT promoter and the primers used in ChIP-qPCR assay.** Putative SPL binding sites are boxed. Primers used in ChIP-qPCR are underlined. The translation start codon is shaded in blue. Red and yellow characters indicate 5' UTR and exon, respectively.

aagaagatggatggaccactgttactgattgggtggtcattgttactgattgggtggtcattgtaggttggtttattagtgaatccatgccat  
 ttcggtttcaaaattgaaccgatagttacggttatctgaaaatctgacacaactttattgatgttcatgagtcagacttatccgctgtgtgttc  
 taaagatgtgctgataagtcacataaaaattgaattgttccatgtctgtatagagaagaaaaggagtttcatatttccccattttgtggggtga  
 acaaaataaaagtatctgctagtgcacataaaggttagaggaaaaagaaaagaaaaagaaaaagtttgcataaatatttgcctcat  
aagtttgtgacttattcagagttatgttctaaagatgtgata**gtac**agcaaaattgatttgtccaaatgcaattagtgaagaaaaagaaaag  
 agttgcataatttggga**gtact**gaaagataatcatgtgcaaaaaaaaaaacgaaataggaagaatttcagtaaaaattatgctagctcaca  
 gtatcaaatatattgaaccaaagtatgccatattcatgaattgttttacaacaattttattgttttaactctagaggctatatgtgaaaaaaatt  
 tacagcaaaaataagattatatacagaacattacagaccgaaatttacagccagatctaaccaaacatctactaaattgacataatgcattat  
 caaatatttattggaaattggtgatgttttgaaagttgaggatataccaaaaatccaatgttgctcaaaagttcagtttctataaaattcaaca  
 cctagatggaatctataattggtgacttttttttttttttttacagtatatactgaaaaaatccaactgaaatattataaagagttgatttt  
 gtccaaaccggccaagactttaattttactgtcttcttctctatccttgttgggtgagacaagaacgaaaaccgtgcattgaaccggctt  
 ctccataatttattgcttcttaaatgattgaaaaatggaaatgcatttatcaaaaataaaagaaaataattgaaatgctattatattccaga  
 gttggtttgtatttgaatattgctggttaagttatattgaaattaatttggccgttttctacaaaacatatttatcatattgga**gtac**ttttaa  
 aactaataaaaaatgttgagaaaaacttttftaaattctagcttggacaactaaaccagttgacatctacagttgtaataa gccgattgcaa  
attaattcctaacattttaataaacaagaatataatgtgatctaaattcaaaaataaaca**gtac**actaacatt**gtac**gtctaataatcgtagtaa  
 ctttacttatgaacaccttttaatacggctctgacgatttttatttatataaccaaaactcatatataatcataaactaaattatataagtaacaggat  
 atattatgagcttaataatagctatagcctatataaggtcttaataacaaaactcataataatgtattcataaactaaattatagtaaatatttt  
 ggtatatttataactftaaaaaacttaaatatttgggtattttgaaaatggataaaaatgatattttggaaagtagtataatttataaaaactctc  
 ccaataaagacatgacaaaaatgtgttatttctatataatttttttttttgatcaacataactctgttctaatctgattccctccaccaca  
 aaaaaaattcaaatgataaaatataaagaagaacaatgtggaatataattgtcatgcaacacgacaaattaatcattcagtaacataattat  
 acatataatatacaggtcatgcatgacattacaagacgtaactgaataaactaatcaaccaactatcaaga**gtac**atttctttaaattgttttaa  
 ttgatttcttaacttattatgtaaftaatacagtttattcactactctattatataaaactcattt**gtctctcttcggtgcaaca**actttcttcattga  
 caaaaacacaaa**ATG**GAAGGAAGAGTCAACGCTCTGTCAAACATAAACGATCTCGAACTT  
 CACAATTTCTTGGTCGATCCAAACTTCGATCAGTTCATAAACCTCATAAGAGGAGAT  
 CATCAAACCATGACGAAAACCCAGTTCTTGATTTCGATCTTGGTCCATTACAAAACA  
 G

**Appendix G. The location of putative SPL binding sites in PYE promoter and the primers used in ChIP-qPCR assay.** Putative SPL binding sites are boxed. Primers used in ChIP-qPCR are underlined. The translation start codon is shaded in blue. Red, purple, and yellow characters indicate 5' UTR, intron, and exon, respectively.

ttgggccaacgagattagtttctaacagatgttttccggaccggaccggaataaccacgatccgcttaattatttggtcctgtctagctcta  
 aatcccgggcaaacgaaccggcaaaccaacgacctagcgggtcgggtattttgttctgaaatctgaacctccgatttgtctctttttttt  
 cttttataatgcaacaattgatgaaaaatattatgtcgcgaatgtaacctcggttttaatatgtgagaaaagggtataacattgcagtac  
 agtcaattacgtacgtgcgagaaaaatatttgcgggacaaatattggtttgtacaaaaaagcgtacagaataatgtttgattgatgaaaa  
 aattatttgcgggtcgggattataaattatataatataatataatataatataatataatataatataatataatataatataatataat  
 taatacataaataaatcaaaatatacatttttaaagttaacatacatattattaaattcgttgaatagttcacaataaaatgaaaaaaatca  
 aatttttactagtaaattgattatagaacttataaagcttatagtgataataatgtcaaaatttctataagtattatgatttcttctgttaattac  
 attttctagatttaattaataaaaagaataaaactataatttgcataatataatataatataatataatataatataatataatataatataat  
 agcaaatgttatgtctacgtatatttttctttatgactaggtaactagtgattctgatgcacacatatactctcttttttgtacatataatg  
 gggagctaatggaaaaaaatataaattgcttaagtaaggagtaataaacgagggatgtgtatggaaggagcaaaaggctgagaaact  
 ttggttgggacgtaggacataacaatttgccttaagtaaggagtaataaacgagtttttgggaatgcggttttgagcaaaacactaggtaaa  
 tgatftttctctttgaaaagcattccagtgattgttttagacaaaattgcaaaactttttctttttttctgaaaacgcaatttgttaaagattg  
 attgtaactgtattgatttttaataaaaaacaagaaaacgcctttgtatgtttctaatcacagtgatgaatggtgacatagaccgccccca  
aaaccgtacgtaactgtaacagtataaaaaatctctatatatacatatatactatgatttttgtattatttgaaccgtccatacttttccgtatca  
 caaataacagtcattcgaaccgcaaaactatataatagatttccggttttgaattcaaaatgaaggagaagaggaataggcagattaataaa  
 ttcggtatttcttttaatttctctatctcaattttctcaccactgaattgactatgccataaaaaatgtgtataactaatcatataaccgtcaataat  
 agagtttgggaaacacacgacagacagtcacgtctcgcggcgttccatgcctttattatccttcacgttgacccacatgccct  
 gtttttttttgggttctacggtatattttgtgaaaatggtactttctactcagataaaattcttaacagatagtacaaacttttaccgattaatc  
 gtgaaaaatacaatgtatttacactcaacaacatttccattatagaactttaccgattaaaccacttccactcgattaatattatttttatt  
 aattaaagatacgtacgtgcatgagagatgagctttagtggcacgcaacgtaagagaagaagacaaaagtaaaaaagagaaaggca  
 catgctgaactcacgtgtccacttaaacgcaccacttctctgctctccacgcgctccacacgcctcctcaacttggaccttctctcc  
 aaaaaacaattcactctcatttctcagattctctattatttcttactcgttccgaatcctaactgctacagttccgacgagattctaccg  
gagaagaaggtagtcttttctgaatctggtgtgagaacttagccgtaattttgagaattattctcactattgattgacaagaatagg  
 gtaataaagacagaatctaaaacactgcttcagttttgaggaatcaaaaacacacgaaagtgttttttttctgctcctatgtttctggtgcg  
 ttgtgtatttgacattaggagtgattgattataaagatgaatgattgtagattcattaagatcactgttcttttgattaatcatctatgtctaa  
 attttaggtgacttgacagagaatctgttctgtaataaaagcaagATGGTATCGAAACTCCTTCTACATCGTCT  
GATGAAGCAAATGCTACTGCAGATGAAAGgtgattcctaaggagaca

## Curriculum Vitae

**Name:** Ying Wang

**Post-secondary** Northwest University

**Education and** Xi'an, Shaanxi, China

**Degrees:** 2002-2006 Bachelor of Science, Biotechnology

The University of Western Ontario

London, Ontario, Canada

2013-2015 Master of Science, Cellular and Molecular Biology

**Honours and** Western Graduate Research Scholarship

**Awards:** 2013-2015

Nominated for the best Teaching Assistant award

2014

**Related Work** Teaching Assistant

**Experience** The University of Western Ontario

2013-2015

Research Participant

Joint program between Key Laboratory of Resource Biology and Biotechnology in Western China and Key Laboratory of the Ministry of Education for Medicinal Resources and Natural Pharmaceutical Chemistry, Shaanxi, China

2006-2010

**Publications:**

**Wang Y.**, Wang Z., Amyot L., Tian L., Gruber M.Y. , Hannoufa A. (2014) Ectopic expression of *miR156* represses nodulation and causes morphological and developmental changes in *Lotus japonicus*. *Mol. Genet Genomics*. 290:471-484.

**Wang Y.**, Hua W, Wang J, Hannoufa A, Xu Z, Wang Z. (2013) Deep sequencing of *Lotus corniculatus* L. reveals key enzymes and potential transcription factors related to the flavonoid biosynthesis pathway. *Mol. Genet Genomics*. 288: 131-139.

He M., **Wang Y.**, Hua W., Zhang Y., Wang Z. (2012) *De novo* sequencing of *Hypericum perforatum* transcriptome to identify potential genes involved in the biosynthesis of active metabolites. *PLoS One*. 7:e42081

**Abstract and Posters in Canadian and International Conferences:**

**Wang Y.**, Amyot L., Xu Z. Q., Tian L. N. and Hannoufa A. MicroRNA156 regulates plant development and nodulation in *Lotus japonicus*. *The Canadian Society of Plant Biologists – Eastern Regional Meeting 2013, University of Toronto Mississauga*.

**Wang Y.**, Amyot L., Xu Z. Q., Tian L. N. and Hannoufa A. Two homologous RNA-binding proteins play different roles in carotenoid biosynthesis and stress adaptation in *Lotus japonicus*. *The Phytochemical Society of North America 2012, University of Western Ontario*.